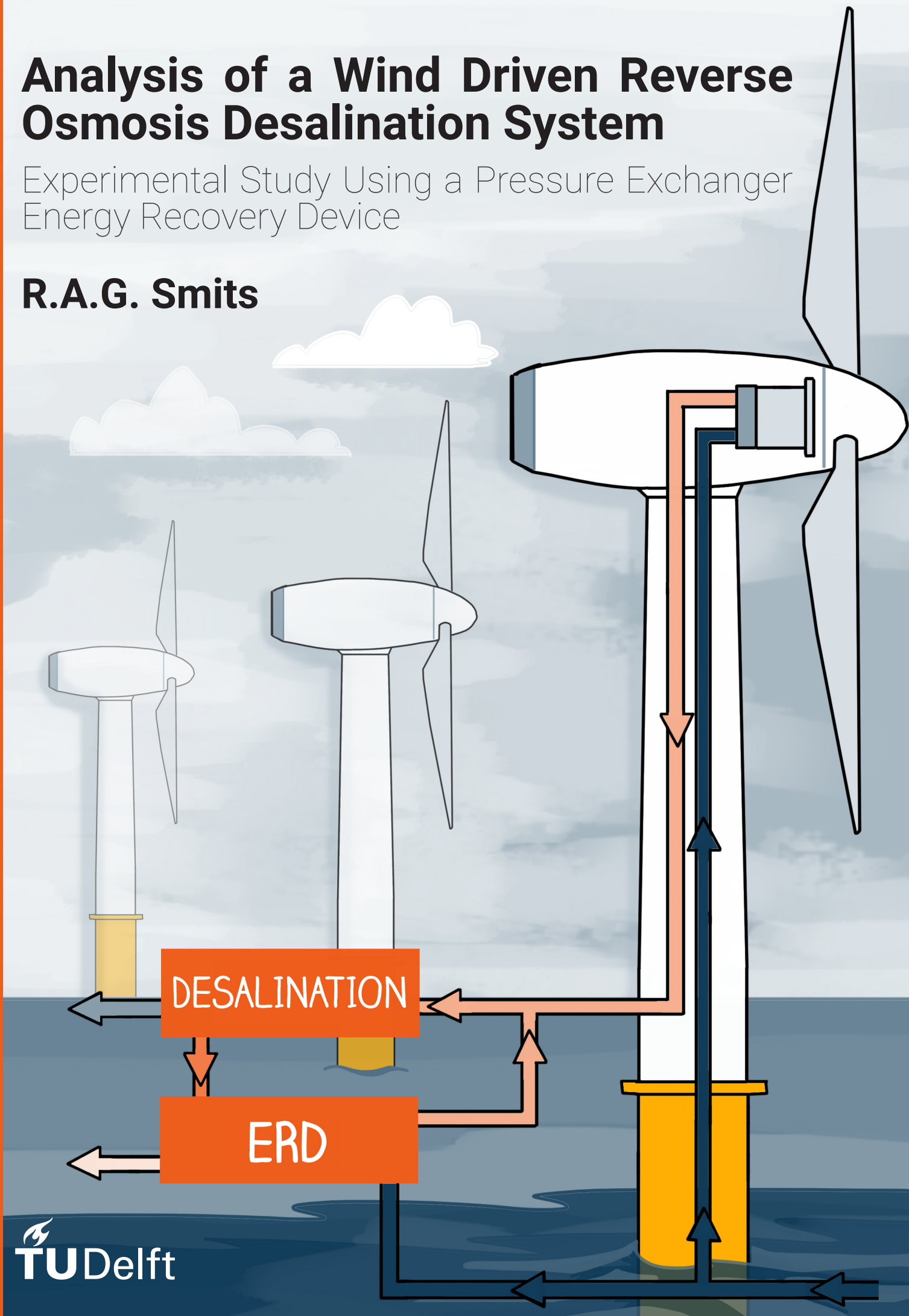


# Analysis of a Wind Driven Reverse Osmosis Desalination System

Experimental Study Using a Pressure Exchanger Energy Recovery Device

R.A.G. Smits





# Analysis of a Wind Driven Reverse Osmosis Desalination System

Experimental Study Using a Pressure Exchanger Energy Recovery Device

by

**R.A.G. Smits**

in partial fulfilment of the requirements for the degree of

**Master of Science**

at the Delft University of Technology,  
to be defended publicly on Wednesday April 17, 2019 at 17:00 PM.

Student number: 4155548  
Project duration: January 15, 2018 - April 17, 2019  
Thesis committee: Prof. dr. A. Metrikine, TU Delft, Chairman  
Dr. ir. A. Jarquin Laguna, TU Delft, Daily supervisor  
Ir. R. Jorritsma, DOT B.V., Daily supervisor  
Dr. ir. F. Pisanò, TU Delft, External Committee member

*This thesis is confidential and cannot be made public until April 17, 2024.*





# Abstract

*R.A.G. Smits  
Delft, April 2019*

With a fast growing world population, the lack of fresh water is one of the world's biggest future concerns. Water stress can lead to conflicts, holds back economic growth and has a major impact on human health. Nowadays, more and more countries that lack fresh water sources are using the saline water from the oceans and desalinate it to produce fresh water. The most common way to do this is by the means of Reverse Osmosis (RO). However, one of the biggest negative aspects of desalination is its high energy consumption, mostly provided by fossil fuels. Therefore, a more sustainable solution using renewable energy sources to power a RO system is necessary.

Delft Offshore Turbine (DOT) is currently developing a hydraulic drive train wind turbine that converts the aerodynamic power captured from the wind into hydraulic power. With a positive displacement pump, a high pressure water stream is created for centralised electricity production using a spear valve and a Pelton wheel. Using this hydraulic turbine for the purpose of fresh water production with RO can be a well fitted combination. Using wind as an energy source for desalination purposes, however, creates some major challenges, one of which is dealing with the inconsistency of wind. For varying wind speeds, a hydraulic wind turbine is controlled by regulating system pressure hence the pump torque with the spear valve. With a RO system with ERD, it is researched how to regulate the flows and pressures for a stable operation.

In this thesis, the combination of the hydraulic wind turbine with a Reverse Osmosis system with an Pressure Exchanger Energy Recovery Device (ERD) is being analysed in more detail. For this, first a numerical model is developed and an experimental test setup is designed, constructed and used to validate the numerical model results and verify the working principle of the ERD, as its behaviour in a inconsistent desalination process was not known. With the model, the RO system with the ERD is modelled to predict the systems' behaviour under variable inputs of both the high pressure pump (HPP) and the ERD as well as to investigate in which way the ERD influences the permeate production performance. The analysis shows a large positive influence on the amount of produced permeate when using an ERD in the RO system. In addition, the power consumption of the RO process can be reduced by up to 80%. A varying input provided by the high pressure pump, for example as a results of varying wind speeds, does not seem to (negatively) affect the efficiency of permeate production. A varying rotational speed of the ERD resulted in a slight variation in the feed pressure at the membranes inlet hence the pressure at the HPP discharge side. However, this limited influence is considered not enough to effectively affect and control the high pressure pumps' torque. The results obtained from the experimental tests confirmed the model results, showing that the modelled behaviour of the RO system with the ERD was accurate.

Second, a numerical model was developed for the design of a small scale wind driven reverse osmosis system with an ERD. From this, a analysis regarding turbine stability and operating regions for water production was done. This showed that for the wind turbine to operate in a stable operating region, it seems that the use of an ERD affects the system in such a way that water production can only be realised at fairly high wind speeds. To optimally make use of the hydraulic wind turbine and operate at the highest possible aerodynamic efficiency, a combination of electricity production at low wind speeds and water production with an ERD at wind speeds that are sufficient, can be interesting. Future research into a combination of electricity production with desalination is required.



# Acknowledgements

This thesis concludes my academic career at Delft University of Technology and is the result of hard work for more than a year. The combination of acquiring theoretical knowledge relating new topics like Reverse Osmosis, Energy Recovery Devices and the DOT hydraulic drive train wind turbine with gaining hands-on experience by designing, constructing and operating an experimental test setup has been a great learning experience for me. Getting the opportunity to work with high-end equipment like the iSave Energy Recovery Device (ERD) for this research felt like a ones in a lifetime experience. Here, I would like to thank the people that helped and supported me during this thesis.

First, I would like to thank my university supervisor Antonio Jarquin Laguna who guided me during this thesis. His knowledge and interest in the subject lead to interesting and helpful discussions. I also want to thank Reinder Jorritsma for supervising and steering me and for giving me the opportunity to graduate on such a nice project at DOT. Finally, I would like to thank Prof. dr. A. Metrikine for chairing my graduation committee.

Secondly, I like to thank the thank Alejandro, Deborah and Roberto for their effort with commissioning and operating the MicRODOT experimental setup. Without their help, I would not have been able to get such nice results. I would like to thank the entire team of DOT for their inspiration and experience. Thanks to Jacob, Gerrit and Tom for their help with constructing and installing the MicRODOT. Jan van der Tempel, thanks for making it possible to work with these innovative and high-end equipment at such an interesting and innovative company. A special thanks to Sebastiaan for the help and laughs during the entire length of this thesis, but especially during the design-, construction- and operating phase of the MicRODOT experimental setup. I also want to thank all personal from DOB-academy for creating a great working environment at the academy.

Last, but not least, I want to express my sincerest gratitude to my family and friends, and to my parents and brother in particular for their endless support and unconditional love during the entire length of my study in Delft. This would not have been possible without you! A special thanks to Lotte, for always believing in me and supporting me with anything I do. On top of that, the beautiful cover of this thesis could not have been realised without your creativity. Jeroen and Roos, thanks for all your help, your door was always open and I could always count on you.



# Table of Contents

<b>List of Figures</b>	<b>xi</b>
<b>List of Tables</b>	<b>xiii</b>
<b>1 Introduction</b>	<b>1</b>
1.1 Problem Introduction . . . . .	1
1.1.1 History of Desalination . . . . .	1
1.1.2 Desalination using Renewable Energy Sources. . . . .	2
1.2 Delft Offshore Turbine (DOT) . . . . .	3
1.3 Problem Definition . . . . .	4
1.4 Thesis Objectives . . . . .	4
1.5 Approach . . . . .	5
1.6 Report Structure . . . . .	5
<b>2 Reverse Osmosis (RO) and the Energy Recovery Device (ERD)</b>	<b>7</b>
2.1 Fundamental Information RO. . . . .	7
2.2 Spiral Wound Membrane . . . . .	8
2.3 Membrane Performance . . . . .	9
2.4 Energy Recovery Device (ERD) . . . . .	11
2.4.1 ERD Classifications . . . . .	11
2.4.2 Pressure Exchanger ERD . . . . .	12
2.4.3 Losses of a Pressure Exchanger ERD . . . . .	14
<b>3 Hydraulic Drive Train Wind Turbine</b>	<b>15</b>
3.1 Wind Turbine - General Working Principle . . . . .	15
3.2 Hydraulic Wind Turbine . . . . .	17
3.3 Hydraulic Wind Turbine with RO and an ERD. . . . .	19
<b>4 Numerical Model on Reverse Osmosis with an ERD</b>	<b>21</b>
4.1 Reverse Osmosis Membrane . . . . .	21
4.2 Energy Balance around Gate Valve . . . . .	23
4.3 Pressure Exchanger Energy Recovery Device . . . . .	24
4.4 Reverse Osmosis System . . . . .	26
4.4.1 Reverse Osmosis without an ERD . . . . .	26
4.4.2 Reverse Osmosis with an ERD . . . . .	27
4.5 Model Results . . . . .	28
4.5.1 Varying HPP RPM - Comparison of a System with and without ERD . . . . .	28
4.5.2 Varying ERD RPM . . . . .	31
4.6 Concluding remarks . . . . .	33
<b>5 Experimental Tests on Reverse Osmosis with an ERD</b>	<b>35</b>
5.1 Test Setup Overview. . . . .	35
5.2 Components . . . . .	36
5.2.1 High Pressure Pump . . . . .	36
5.2.2 Reverse Osmosis System . . . . .	36
5.2.3 Auxiliary Components . . . . .	38
5.2.4 Sensors . . . . .	39
5.2.5 Data Logging. . . . .	39

5.3	Test Setup Working Principle . . . . .	40
5.4	Experimental Test Results . . . . .	40
5.4.1	RO Membrane Permeability Coefficient . . . . .	41
5.4.2	Varying HPP RPM - Experimental Results and Model Validation . . . . .	42
5.4.3	Varying ERD RPM - Experimental Results and Model Validation . . . . .	45
5.4.4	Influence of Salinity . . . . .	47
5.5	Concluding Remarks . . . . .	48
<b>6</b>	<b>Wind Driven Reverse Osmosis with an ERD</b>	<b>49</b>
6.1	Wind Turbine Design . . . . .	49
6.2	Wind Driven RO - System Stability . . . . .	52
6.3	Wind Driven RO - Result Analysis . . . . .	52
6.4	Recommendations for System Improvement . . . . .	56
<b>7</b>	<b>Conclusions and Recommendations</b>	<b>59</b>
7.1	Conclusions. . . . .	59
7.2	Recommendations and Future Work . . . . .	61
	<b>Bibliography</b>	<b>63</b>
<b>A</b>	<b>Hydraulic diagram and component list</b>	<b>65</b>
<b>B</b>	<b>Wind driven Seawater Reverse Osmosis - Input parameters</b>	<b>69</b>
<b>C</b>	<b>Experimental test setup - Main components</b>	<b>71</b>
C.1	MicRODOT Experimental setup - Components . . . . .	71
C.1.1	High Pressure Pump and Electric motor . . . . .	71
C.1.2	Reverse Osmosis system . . . . .	72
C.1.3	Energy Recovery Device . . . . .	72
C.1.4	Boost Pumps. . . . .	73
C.1.5	Filters . . . . .	73
C.1.6	Sensors . . . . .	73
C.1.7	Concentrate Valve . . . . .	74
C.2	Test Plan . . . . .	74
C.3	Determination of Volumetric Efficiency. . . . .	77
C.4	Visualisation MicRODOT Test Setup . . . . .	78
<b>D</b>	<b>Energy Recovery Devices - Elaborate information</b>	<b>81</b>
D.1	Francis Turbine . . . . .	81
D.2	Pelton Wheel . . . . .	81
D.3	Turbocharger/Hydraulic Pressure Booster . . . . .	82
D.4	DWEER . . . . .	83
D.5	Pressure Exchanger (PX) . . . . .	83
<b>E</b>	<b>Technical Data and Performance Sheets</b>	<b>85</b>
<b>F</b>	<b>Electrical Wiring Diagram</b>	<b>97</b>

# Nomenclature

The next list describes the acronyms and symbols used in this document

## Acronyms

CAPEX	Capital Expenditure
DOT	Delft Offshore Turbine
ERD	Energy Recovery Device
HP	High Pressure
HPP	High Pressure Pump
LCOW	Levelized cost of water
LP	Low Pressure
NDP	Net Driving Pressure
OPEX	Operational Expenditure
PPM	Parts Per Million
PX	Pressure Exchanger
RO	Reverse Osmosis
RPM	Rotations Per Minute
SWRO	Seawater Reverse Osmosis
TDS	Total Dissolved Solids
tsr	Tip Speed Ratio

## Symbols

$\alpha$	Total damping
$\Delta\Pi$	Osmotic Pressure Difference
$\Delta$	Difference
$\delta$	Effective concentration constant
$\dot{m}$	Mass flow rate
$\eta$	Efficiency
$\gamma$	Recovery rate
$\lambda$	Tip speed ratio
$\omega$	Rotational speed
$\rho$	Density
$\tau$	Torque

<i>A</i>	Area
<i>a</i>	Effective concentration weighting coefficient
<i>B</i>	Damping
<i>C</i>	Concentration, Coefficient
<i>C<sub>p</sub></i>	Power Coefficient
<i>C<sub>t</sub></i>	Torque Coefficient
<i>e<sub>v</sub></i>	Valve resistance
<i>eff</i>	Effective
<i>J</i>	Flux, Mass moment of Inertia
<i>K<sub>w</sub></i>	Permeability constant
<i>L</i>	Leakage
<i>M</i>	Volumetric mixing ratio
<i>n</i>	Ratio
<i>OF</i>	Overflush
<i>p</i>	Pressure
<i>Q</i>	Flow rate
<i>R</i>	Salt rejection, Radius
<i>S</i>	Displacement
<i>SP</i>	Salt Passage
<i>T</i>	Temperature
<i>t</i>	Time
<i>U<sub>rel</sub></i>	Relative wind speed
<i>V</i>	Volume
<i>v</i>	Flow velocity, Wind speed

# List of Figures

1.1	Projected growth of desalination market [2]. . . . .	2
1.2	The Delft Offshore Turbine (DOT) hydraulic drive train wind turbine principle [5]. . . . .	3
1.3	Thesis report structure . . . . .	6
2.1	Left: Osmosis Principle (2.1a), Right: Reverse Osmosis principle (2.1b) [6]. . . . .	7
2.2	Schematic showing the configuration of the RO membrane system. . . . .	8
2.3	RO membrane inside working principle [9]. . . . .	8
2.4	Percentage of NaCl passing through a membrane [10]. . . . .	9
2.5	Recovery effect on hydrostatic pressure and concentrate osmotic pressure (Total Dissolved Solids (TDS): 34,000 mg/L) [10]. . . . .	10
2.6	Top Left:increasing concentration(2.6a), Top Right:increasing pressure (2.6b) , Bottom Left:increasing recovery(2.6c) , Bottom right: increasing temperature(2.6d) [11]. . . . .	11
2.7	Example of a setup with a Class I Pressure Exchanger ERD. . . . .	12
2.8	iSave Pressure exchanger Energy Recovery Device working principle [17]. . . . .	12
2.9	iSave 21 Plus Energy Recovery Device as it just arrived at DOT B.V. . . . .	14
3.1	Ideal power curve of a wind turbine [20]. . . . .	15
3.2	Optimal aerodynamic performance, following a quadratic relation between aerodynamic torque and the angular velocity of the rotor, denoted by the dashed line [21]. . . . .	17
3.3	Schematic overview of a hydraulic drive train. . . . .	17
3.4	Cross section of a spear valve [22]. . . . .	18
3.5	Schematic overview of a hydraulic drive train that includes an Reverse Osmosis system with an ERD. . . . .	19
3.6	Impression of what a future setup might look like. Note that this thesis does not focus on implementing the spear valve and Pelton Turbine. . . . .	19
4.1	Simplified Reverse Osmosis desalination system for modelling. . . . .	23
4.2	Simplistic visualisation of the ingoing and outgoing flows of an ERD. . . . .	24
4.3	Distinguished flows of a pressure exchanger ERD, used to determine mixing (VM), leakage (L) and overflush (OF). . . . .	25
4.4	Simplistic overview of a Reverse Osmosis system for modelling, including ERD. . . . .	26
4.5	Results for varying HPP RPM . . . . .	30
4.6	The ratio between permeate productions decreases for increasing recovery rate. . . . .	30
4.7	Osmotic pressure variation with changing ERD rotational speed for $C_f = 600PPM$ (left) and $C_f = 32000PPM$ (right). . . . .	32
4.8	Total system pressure variation with changing ERD rotational speed for $C_f = 600PPM$ (left) and $C_f = 32000PPM$ (right). . . . .	33
5.1	Overview of the MicRODOT test setup. . . . .	36
5.2	The high pressure pump (left) representing the wind turbine, connected to an electric motor using a ROTEX coupling. . . . .	37
5.3	The iSave ERD as it is installed in the MicRODOT test setup. . . . .	37
5.4	The RO setup, showing 4 membranes installed in pressure vessel in a parallel configuration. . . . .	37
5.5	The setup has two boost pumps. The left boost pump is the large pump, feeding the ERD. The right pump feeds the High Pressure pump. . . . .	38
5.6	Cintropur 10 $\mu m$ filter(left) and EWP-USA 3 $\mu m$ filter (right). . . . .	38
5.7	The electrical cabinet, containing the electrics and control hardware. . . . .	39
5.8	Schematic overview showing sensor locations. . . . .	40
5.9	Experimental results, used to determine permeability coefficient of the membrane. . . . .	41

5.10	Permeability coefficient. . . . .	42
5.11	Comparison of experimentally obtained pressures with numerical model prediction. . . . .	43
5.12	Permeate flow comparison between model and experimental results. . . . .	44
5.13	Permeate flow comparison between model and experimental results. . . . .	44
5.14	Comparison of experimentally obtained flow rates with numerical model prediction. . . . .	45
5.15	Permeate flow comparison for varying ERD speeds. . . . .	46
6.1	Torque and power coefficient of the DOT500 wind turbine. . . . .	49
6.2	Aerodynamic torque over angular velocity. . . . .	51
6.3	Linearisation of the aerodynamic torque results in a term of the rotor proportional to $\omega_r$ . . . . .	53
6.4	$\alpha$ can be found by a summation of the $B_r$ and $B_{HPP1}$ . . . . .	54
6.5	Tip speed ratio over wind speed. . . . .	54
6.6	Power coefficient over wind speed. . . . .	55
6.7	Permeate production over wind speed. . . . .	56
6.8	Producing permeate without ERD at low wind speeds using a variable valve in the concentrate line can make the wind driven RO system more efficient. . . . .	57
6.9	A combination of electricity production and water production can be interesting to optimally use the wind turbine. . . . .	57
A.1	Hydraulic Diagram of the MicRODOT experimental test setup (page 1) . . . . .	66
A.2	Hydraulic Diagram of the MicRODOT experimental test setup, RO membrane arrangement(page 1) . . . . .	67
C.1	Determination of the volumetric efficiency of the High Pressure pump for different flows and pressures . . . . .	77
C.1	Determination of the volumetric efficiency of the High Pressure pump for different flows and pressures . . . . .	78
C.2	The three water tanks shown in the figure are the permeate tank (green, left), the concentrate tank (black, middle) and the feed water tank (white, right). . . . .	78
C.3	A close up of the setup, clearly showing the filters, boost pumps and ERD . . . . .	79
C.4	. . . . .	79
C.4	. . . . .	80
D.1	Francis turbine with Generator [16] . . . . .	81
D.2	Pelton wheel working principle . . . . .	82
D.3	Turbocharger working principle [34] . . . . .	82
D.4	DWEER working principle [35] . . . . .	83
D.5	Pressure exchanger (PX) working principle [17] . . . . .	84
D.6	Efficiencies of Energy Recovery Devices [16] . . . . .	84

# List of Tables

1.1	Major stocks of water on earth [1]	1
1.2	Energy data of desalination techniques [2]	2
3.1	Torque balances and influence on turbine angular velocity	18
4.1	Input parameters permeate comparison	29
4.2	Input parameters Power comparison	31
4.3	Power per produced unit of permeate at 10% recovery rate	31
4.4	Input parameters variable ERD	32
5.1	Test parameters for determining the permeability coefficient	41
5.2	Permeability coefficients	42
5.3	Test parameters - Varying HPP RPM	42
5.4	Obtained experimental results for varying HPP rpm	44
5.5	Test parameters - Varying ERD RPM.	45
5.6	Obtained experimental results for varying ERD rpm	46
A.1	Component list	68
B.1	Input parameters for wind turbine design	69
C.1	High pressure pump - Janus M30.	71
C.2	Electric motor - Elsto.	71
C.3	RO membranes - DOW FILMTEC	72
C.4	Pressure Vessel - Eurotrol.	72
C.5	ERD - iSave-21 Plus.	72
C.6	Boost Pumps	73
C.7	Filters	73
C.8	Flow sensors	73
C.9	Pressure sensors	74
C.10	Temperature sensor	74
C.11	Test plan for tests having constant rotational speed of the ERD while varying the rotational speed of the HPP	75
C.12	Test plan for tests having constant rotational speed of the HPP while varying the rotational speed of the ERD	76



# Introduction

The purpose of this chapter is to introduce the project, beginning with a problem introduction, then the principle of Delft Offshore Turbine (DOT) and the problem definition. Finally, the thesis objective and the approach will be explained, and the structure of this thesis is given.

## 1.1. Problem Introduction

### 1.1.1. History of Desalination

Approximately three quarters of the earth is covered by water, of which only 2.5% is fresh water [1]. Much of this fresh water can be found in glaciers and permanent snow, as can be seen in Table 1.1, only a small part is usable to meet the freshwater demands. With a growing world population, the lack of drinking water is becoming one of the biggest concerns in the future. Water stress can lead to conflicts, it holds back economic growth and has a large impact on the health of millions of people. As the demands for freshwater grows, new ways of producing freshwater are necessary to supply the need. One way of producing fresh water is by using the saline waters, such as brackish groundwater or seawater. By desalinating the water from these water sources, freshwater can be produced.

Table 1.1: Major stocks of water on earth [1]

Location	Amount ( $\cdot 10^6 km^3$ )	Percentage of World Water
Ocean	1338.0	96.5
Glaciers and permanent snow	24.1	1.74
Groundwater (brackish or saline)	12.9	0.94
Groundwater (fresh)	10.5	0.76
Ground ice/permafrost	0.30	0.022
Freshwater lakes	0.091	0.007
Freshwater stream channels	0.002	0.0002
<b>Total</b>	<b>1385.893</b>	<b>100</b>

According to Lattemann et al. [2], the worldwide installed desalination capacity is increasing fast. Since 2006, the worldwide capacity grew with an average rate of 12 percent per year. According to some analysis, the installed capacity grew from  $64Mm^3$  per day in 2010 to  $98Mm^3$  per day in 2015, as can also be seen in Figure 1.1. Of the total desalinated water, the majority comes from seawater sources, namely 63%. A total of 19% originates from brackish water sources and only 5% comes from waste water sources.

Since desalinating became an interesting solution for producing fresh water, the Gulf countries have been the leaders when it comes to installed capacity (Figure 1.1). Around 48% of the global desalination production takes place in the Middle east, mainly in the Gulf Country states. Since the beginning of the desalination industry in the early 1960s, gradual changes took place. Nowadays, desalination plants grow in size rapidly. Due to the growing activity, and the growing number of plants worldwide, concerns about the negative impact

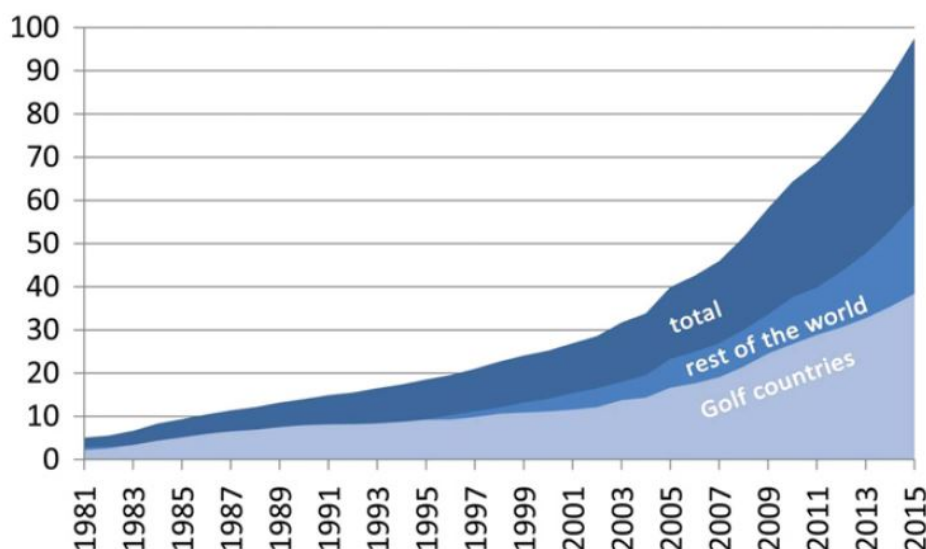


Figure 1.1: Projected growth of desalination market [2].

on the environment are being raised. One of the biggest negative aspect of desalination is its high energy consumption (see Table 1.2). The energy needed mostly comes from fossil fuels, and the main environmental concern with this is the emission of air pollutants, like greenhouse gasses, that are produced when fossil fuels are used for electricity generation, since they have a large impact on climate change.

Table 1.2: Energy data of desalination techniques [2]

	<b>Reverse Osmosis (RO)</b>	<b>Multistage flash (MSF)</b>	<b>Multi-effect distillation (MED)</b>
Operating Temperature	Below 45°C	Below 120°C	Below 70°C
Main energy source	Electrical energy	Steam (heat)	Steam (heat)
Thermal energy demand	None	250-330 kJ/kg	145-390 kJ/kg
Electrical energy demand	2.5-7 kWh/m <sup>3</sup>	3-5 kWh/m <sup>3</sup>	1.5-2.5 kWh/m <sup>3</sup>

### 1.1.2. Desalination using Renewable Energy Sources

Over the past decades, a significant increase in research has been done for using renewable energy sources as energy input for desalination processes, like wind or solar power. Most countries suffering from shortage of fresh water sources have a large amount of renewable energy sources, like countries in the Middle-East or Africa, that have a significant potential of solar power. Several small scale desalination plants driven by solar power have been installed, mainly in remote and off-grid areas. Unfortunately, scaling up to large scale plants is obstructed by technological-economic challenges, such as the lack of specialized manpower to technological limitations.

Some large-scale plants that are driven by renewable energy sources have been realised in the past couple of years, like the desalination plant in Perth, Australia, that is producing fresh water since 2006 and is powered by an 80 MW wind farm [3]. However, these plants are also connected to the grid because the desalination techniques used require continuous energy supply to provide a stable water production and operation. Renewable energy sources like solar and wind fluctuate during the day. For example, due to clouds the intensity of solar energy changes and due to constant difference in wind speed, the power output of a wind turbine is dynamic, especially when the so called rated wind speed is not reached (explained in more detail in Chapter 3).

Inconsistency of renewable energy sources is one of the main drawbacks of using renewable energy. Another drawback is the fact that the energy from renewable sources is first converted into electrical energy before it is used to operate the seawater Reverse Osmosis (SWRO) systems. Due to this extra conversion step, transmission losses are induced, which leads to a decrease in efficiency. On top of that, the system requires more

components to be able to operate, making the system less reliable. In fact, the gearboxes used in conventional wind turbines cause up to 59% of the total failures of the turbine, leading to a lot of downtime and large economic losses. [4]

The high energy consumption of Reverse Osmosis is mainly due to the need for high pressures to desalinate (sea)water. To make the desalination process more efficient, energy is being recovered from the concentrate (waste) stream, by using Energy Recovery Devices, or ERDs. The need for high pressurised water using a system with few components can be fulfilled by using the DOT Hydraulic Drive train wind turbine principle as an energy source. Combining this with an pressure exchanger ERD for an efficient Reverse Osmosis process leads to the topic of this thesis.

## 1.2. Delft Offshore Turbine (DOT)

Delft Offshore Turbine, or DOT in short, was first launched as a project by the Delft University. The project focused on the development of technical solutions to make offshore wind energy a commercially competitive source of energy. A different approach of energy production from wind to electricity was used, by using the potential of fluid power transmission for offshore wind farms with centralised electricity production, using seawater as hydraulic fluid. A simplistic overview of this principle can be seen in Figure 1.2.

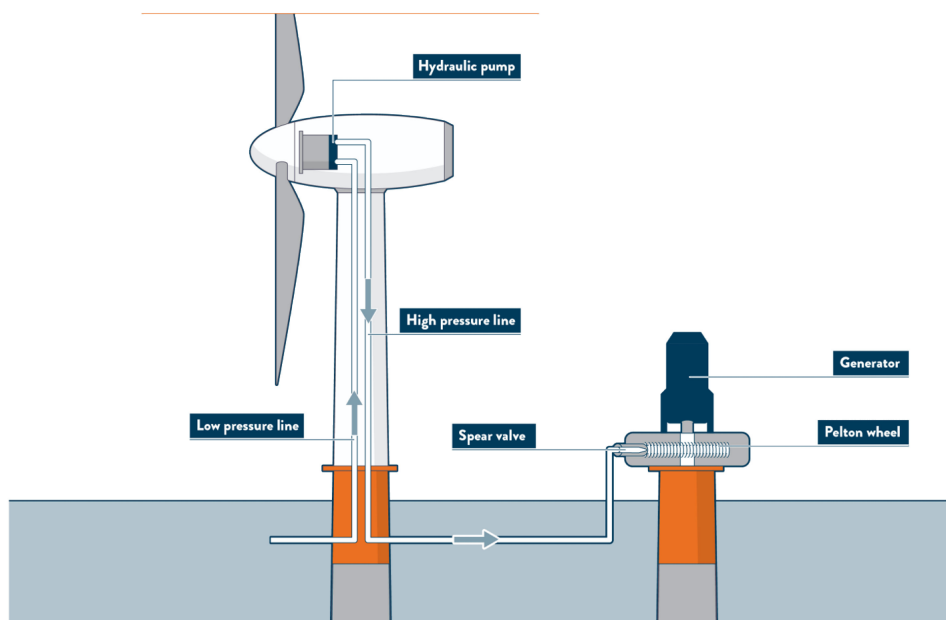


Figure 1.2: The Delft Offshore Turbine (DOT) hydraulic drive train wind turbine principle [5].

Wind energy is converted into hydraulic energy by using a positive displacement pump (hydraulic pump) that is installed in the nacelle of the wind turbine. The rotational motion of the turbine is used to pressurise a low pressure inlet seawater line. A spear valve, installed at the end of the line, is used to control the rotational speed of the wind turbine. Varying wind speeds (below the rated wind speed of the turbine) cause varying rotor torques. This causes variations in the rotational speed of the rotor if no (adaptive) counter torque is produced. The spear valve works as a resistance; by closing or opening the spear valve, the pressure in the high pressure line can be controlled and in that way the hydraulic pump will be able to give a proper counter torque to control the wind turbine. The hydraulic energy produced by the hydraulic pump is converted back into mechanical energy by using the spear valve and a Pelton turbine. The Pelton turbine is attached to a generator, which will produce electrical energy.

The main advantage of using a hydraulic drive train compared to a conventional drive train using a gearbox is the fact that conversion losses and friction losses are limited. By not using a gearbox, having a large chance of failure [4], the system can be made more reliable and less vulnerable for failures, meaning less maintenance is

required. On top of that, the entire wind turbine can be designed lighter and less expensive, since a hydraulic pump weighs much less than a gearbox and a generator. Therefore, the nacelle of the wind turbine becomes lighter and thus the wind turbine tower and foundation can be designed simpler hence less expensive, allowing for better scalability. Where most hydraulic systems work with oil due to its high viscosity, in this drive train water is used. Water is known to leak faster, especially at higher pressures, but due to its non-toxicity and high availability (at offshore locations), water is chosen as a medium for the DOT wind turbine.

A full-scale test of the DOT500, a 500kW wind turbine, was done at the Maasvlakte II in the Netherlands in 2016. The test setup included an oil loop between the turbine rotor and the water pump. During these tests, a control strategy of the wind turbine was derived, using only the rotor speed as an input. The ability to optimally capture wind of the wind turbine through control of the hydraulic pressure was demonstrated. The working principle of both the conventional wind turbine as well as the hydraulic drive train wind turbine will be elaborated in more detail in Chapter 3.

### 1.3. Problem Definition

With fresh water scarcity as one of the biggest global problems, the desalination industry is a rapidly growing industry. Nevertheless, one of the biggest negative aspects of it is its high energy consumption and impact on climate change. This leads to a growing demand for sustainable solutions. Using conventional wind turbines as an energy source causes new challenges and problems; several extra energy conversion steps are necessary. On top of that, more (vulnerable) components requiring maintenance are needed, like a gearbox, making the system less reliable. Due to the use of seawater as an hydraulic fluid and the lack of these high-maintenance components, the DOT hydraulic drive train wind turbine as an energy source for Reverse Osmosis has a large potential for tackling these problems. Implementing an Energy Recovery Device (ERD) can make the system more efficient, but this is yet to be affirmed. The fluctuating nature of wind, however, can negatively affect the systems flows and pressure and it is not known whether this influences the performance of a Reverse Osmosis system with an Isobaric ERD. On top of that, the influence of the ERD on the stability and performance of a wind driven RO-system is yet to be determined.

### 1.4. Thesis Objectives

This thesis focuses on fresh water production using Reverse Osmosis in combination with a hydraulic turbine. The aim of this study is to investigate the combination of Reverse Osmosis with the hydraulic drive train wind turbine, using a pressure exchanger Energy Recovery Device (ERD). In particular, this study focuses on the influence of the ERD on the systems' flows and pressures and the difference with a system that does not include an ERD. This will be investigated using both a numerical model and an experimental test setup.

The above-mentioned leads to the following research question:

#### **What is the influence of a wind driven Reverse Osmosis desalination system with an Energy Recovery Device on the performance and stability of a hydraulic wind turbine?**

To answer the research question, several sub questions are stated:

1. *What is the difference in performance of a desalination system with and without ERD?*
2. *How do different high pressure pump inputs and ERD settings influence flow rates and pressures of the desalination system?*
3. *In which way does the RO system with an ERD affect the rotational speed stability and controllability of the wind turbine?*

## 1.5. Approach

By answering each sub question, an answer to the main research question can be given. To be able to get the answers, a certain approach has to be determined. This approach is shortly stated below:

- *Literature study:* During this phase, fundamental information regarding Reverse Osmosis, energy recovery and the hydraulic turbine is acquired. A design for combining the DOT hydraulic drive train turbine with a Reverse Osmosis - ERD system will be made.
- *Numerical model:* A model, containing the governing equations for Reverse Osmosis with an ERD, is created to predict the behaviour of a RO system with ERD for varying loads and settings. On top of that, in the model, the RO-system will be coupled to an arbitrary hydraulic wind turbine to investigate the stability and performance of a coupled wind driven RO-system.
- *Experimental testing:* A small scale experimental test setup is designed, constructed and used to investigate the behaviour of the RO system with ERD. It is analysed in what way varying ERD settings affect system parameters, like flows and pressures.
- *Result analysing:* The results from the experiments will be compared to the theoretical results as acquired through the model. This comparison will be discussed and concluded.

The scope of this thesis focuses on the influence of the Isobaric Energy Recovery Device on a desalination system driven by an hydraulic wind turbine, as stated before. Both the numerical model and the experimental tests cover the steady state reactions and interaction between RO-system, ERD and wind turbine (hydraulic pump) and do not include any dynamic interaction between the systems. Electricity production and spear valve interaction are shortly elaborated on but are not incorporated in the model and tests.

## 1.6. Report Structure

Taking the aforementioned approach in mind, a report structure is determined as shown in the figure below. This structure is presented as a flowchart and includes the main steps that are taken in each chapter.

Chapter 1 introduces the topic of the thesis and state the problem definition and thesis objective.

In Chapter 2, fundamental information about Reverse Osmosis and the Energy Recovery Device is given. Chapter 3 gives insight in the working principles of an (hydraulic) wind turbine.

In chapter 4, the fundamental equations regarding Reverse Osmosis with an ERD are given. Moreover, model results concerning the differences between a system with and without ERD are given. In Chapter 5, the experimental setup, the conducted tests and the obtained results is elaborated on.

In Chapter 6, the coupling of an hydraulic wind turbine with a Reverse Osmosis system is made an a simplified system design is discussed. The thesis ends with Chapter 7, in which a conclusion is drawn and recommendations for future studies are given.

## Literature Study

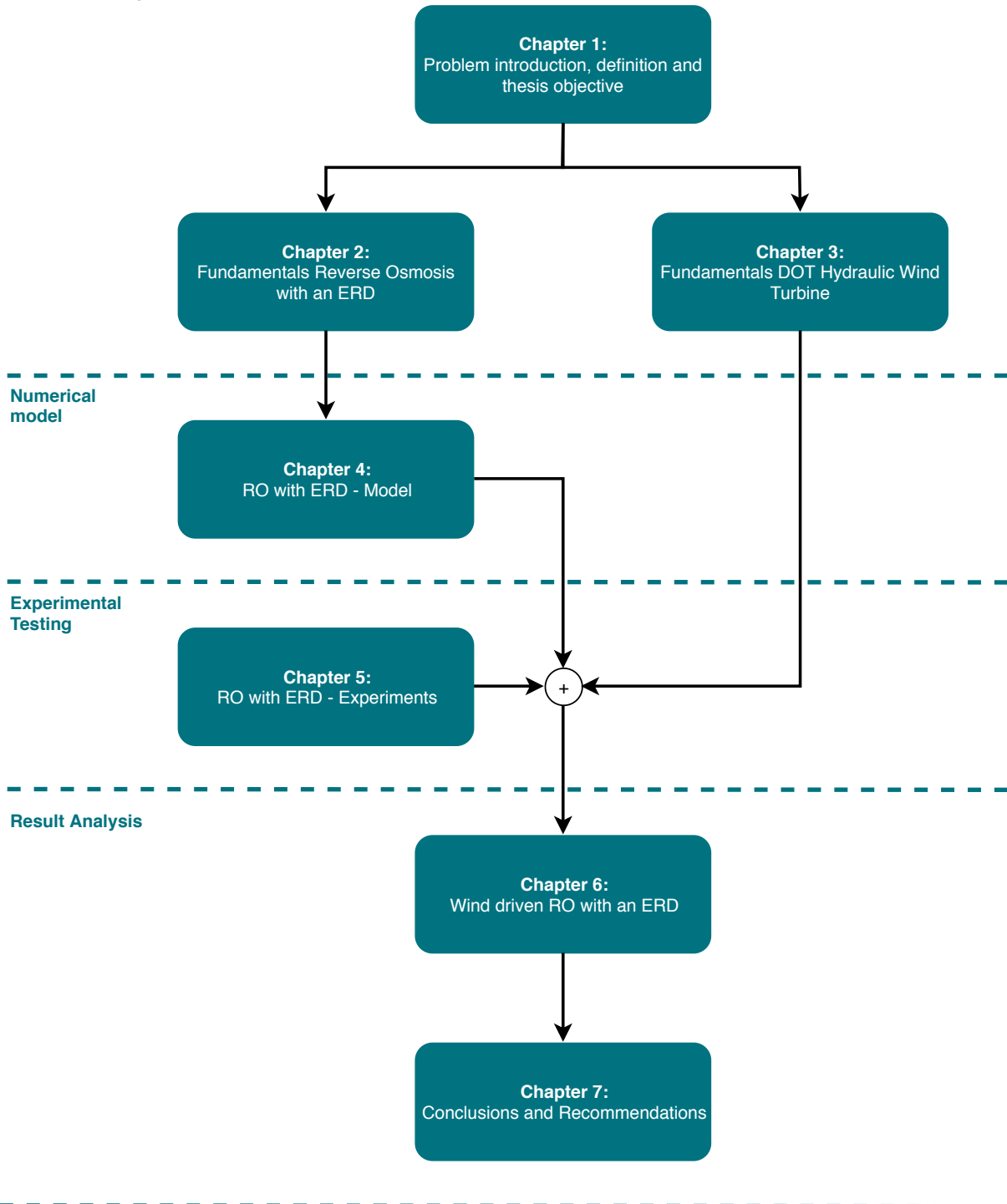


Figure 1.3: Thesis report structure

## Reverse Osmosis (RO) and the Energy Recovery Device (ERD)

This chapter provides theoretical information about Reverse Osmosis (RO) and the Energy Recovery Device (ERD). The importance is to understand the limitations of RO to be able to develop a reliable and efficient system. First, fundamental information about RO and membranes is given. After that, the Energy Recovery Device working principle is elaborated on.

### 2.1. Fundamental Information RO

For the production of fresh water by desalinating salt water numerous technologies are currently being applied. The earliest commercial plants mostly used thermal evaporation or distillation of seawater [1]. Since the beginning of the 1970s, RO techniques are being used most often, reducing the costs of water production by desalinating. [1]

Osmosis is the process where a weaker saline solution will tend to migrate through a semi-permeable membrane to a strong saline solution. The salt water stream and a fresh water stream are separated by the semi-permeable membrane (see Figure 2.1a). This membrane allows certain atoms or molecules to pass through, depending on the size of these atoms or molecules.

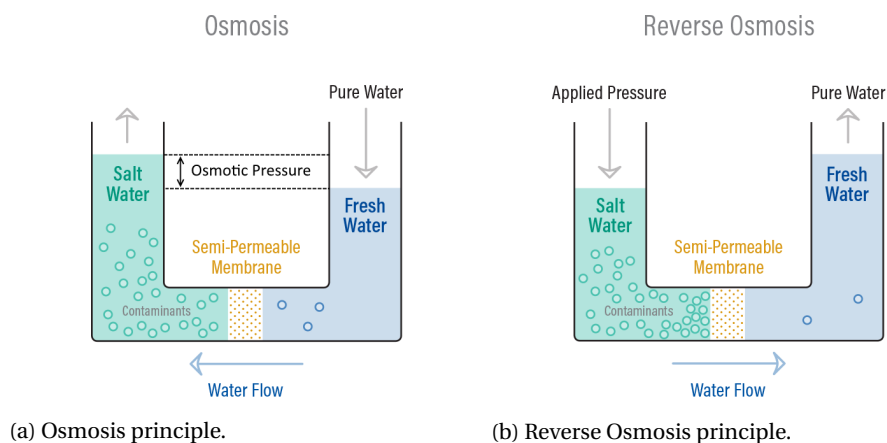


Figure 2.1: Left: Osmosis Principle (2.1a), Right: Reverse Osmosis principle (2.1b) [6].

Reverse Osmosis is this process but in reverse. Whereas osmosis occurs without the need of external energy, for RO energy (pressure) needs to be applied to the saline part to overcome the so called osmotic pressure (see Figure 2.1b). Typical values for osmotic pressures of seawater lie around 25 to 30 bars. When producing pressures higher than the osmotic pressure, water is being desalinated. Typical feed pressures in seawater applications necessary to overcome the osmotic pressure and to optimally desalinate the seawater lie in the

range from 60 to 80 bar [7].

The semi-permeable membrane that is used in RO processes allows water to flow through, but most of the dissolved salt, organics, bacteria and pyrogens are not able to pass through and will end up in the reject stream [8]. This is the stream of water that did not manage to pass through the membrane. The polymer material that is used in RO-membranes makes it possible to reject particles up to  $10^{-10}$  meters [7]. The common RO desalination techniques make use of cross-flow filtration using spiral wound membranes [9], see Section 2.2. Figure 2.2 simplistically shows this cross-flow principle where feed water is pumped through the membrane. Having forced the saline water through the membrane, two outlet streams are created. One is called the permeate (or fresh) water stream which is a low pressure flow and contains little to no salts and contaminants. The second one is the reject stream, or concentrate. This is a high pressure flow containing all contaminants that were not able to pass through the RO-membrane. The permeate is considered to be the product of desalination.

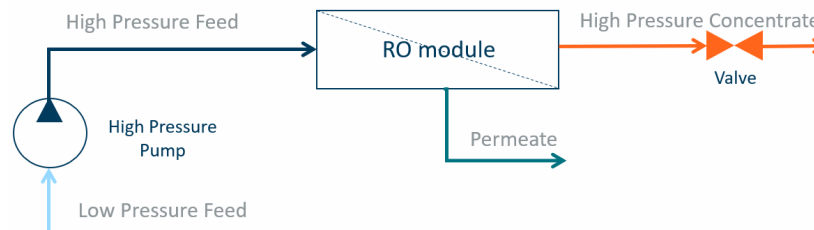


Figure 2.2: Schematic showing the configuration of the RO membrane system.

## 2.2. Spiral Wound Membrane

The working principle of the spiral wound membrane is explained using Figure 2.3. Spiral wound membranes are loaded into pressure vessels during operation. Feed water is forced through the feed spacers (by applying pressures higher than the osmotic pressure). To be able to achieve this high pressure, a certain flow resistance, or back pressure, has to be created on the back side of the RO membrane. This is done using a throttling valve, which is placed in the concentrate outlet, as depicted in Figure 2.2. By throttling this valve, the back pressure can be adjusted according to what is necessary. When not having a valve, no pressure can be built up and the feed water will just flow through the membrane, from the feed inlet side directly to the concentrate outlet side. When the system operates at a high pressure, permeate passes through the semi-permeable membrane into so called permeate channels. In a spiral direction, the permeate flows to the centre pipe of the membrane, where all the permeate is collected and is then transported to the end of the membrane at atmospheric pressure. The feed water becomes more saline when flowing through the membrane, at the end so called concentrate water (high pressure brine) remains and exits the membrane via another channel.

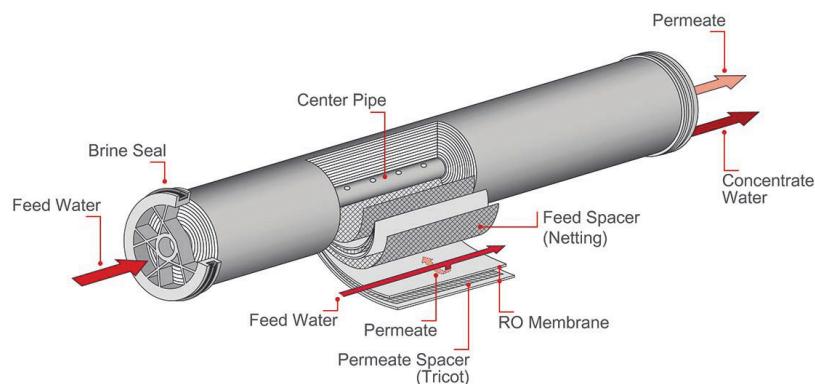


Figure 2.3: RO membrane inside working principle [9].

## 2.3. Membrane Performance

Recovery ratios of RO vary from 35% to 85%. This means that up to 85% permeate water can be obtained from the feed water stream. The ratios depend on the composition of the feed water, salinity, pre-treatment and concentrate disposal options. Typically, recovery ratios of around 30% to 50% are achieved in Seawater Reverse Osmosis (SWRO) installations [10]. The permeate, or product, usually has around 98% to 99.8% of the dissolved salts (NaCl) removed from it. This is clearly shown in Figure 2.4. At very low salinities, a relatively high salt passage can be seen. However, as the feed waters' salinity increases beyond a certain point, it rapidly decreases. From a salinity between 500 mg/L and 1000 mg/L, the salt passage gradually increases again. The figure shows tests with five different RO elements all having different specifications.

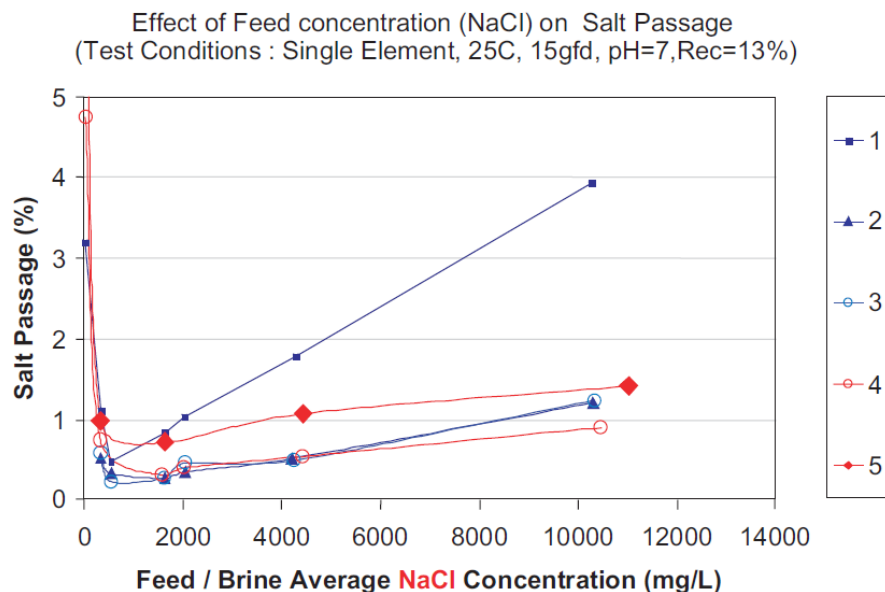


Figure 2.4: Percentage of NaCl passing through a membrane [10].

To increase recovery ratios, an increase in both feed pressure and permeate flow rate (or flux) is required. With an increasing permeate flux, the permeate salinity decreases [7] due to the increase in dilution. However, this means the concentrate stream becomes more concentrated, leading to an increase of the local osmotic pressure (as can be seen in the example in Figure 2.5) and salinity at the membrane surface, which can lead to an increase of salt precipitation and fouling (solution or a particle deposited on the membrane surface), leading to a degraded membrane performance. To avoid build-up of contaminants, cross flow filtration allows water to sweep away contaminants build up. On top of that, it allows for sufficient turbulence to keep the membrane surface clean. Temperature increase of the feed water also has influence on the salt permeability. At temperatures below 30°C, an increase in feed water temperature results in a lower feed pressure needed to operate the system. However, further increase in temperature leads to an increase in osmotic pressure which can affect the power consumption of the RO system. Figure 2.6 shows the influence of four of the most important characteristics on the membrane performance [11], which is pictured as permeate flux and salt rejection in this figure.

RO systems usually operate constantly at a constant production rate. The performance of RO systems is affected by numerous factors and system settings. Figure 2.6 shows the influence of several parameters on the RO performance [11]:

In Figure 2.6a, the influence of an increase in feed water concentration is shown, assuming that the feed pressure is constant. As can be seen, an increasing concentration results in a decrease in permeate flux. As the permeate flux decreases, so will the salt rejection. This phenomena can be explained by looking at the

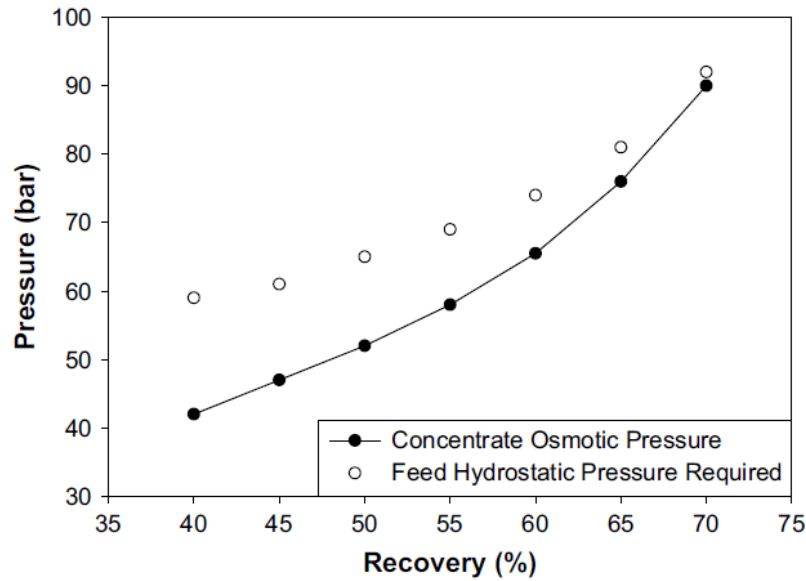


Figure 2.5: Recovery effect on hydrostatic pressure and concentrate osmotic pressure (Total Dissolved Solids (TDS): 34,000 mg/L) [10].

equation for the permeate concentration  $C_p$ , given by Bergman [11]:

$$C_p = \frac{K_s C_f}{K_w \Delta P + \Delta \pi \left( \frac{2-2\gamma}{2\gamma} \right) + K_s} \quad (2.1)$$

Here,  $K_s$  is the solute mass transfer coefficient,  $C_f$  the concentration of the feed water,  $K_w$  the membranes permeability coefficient,  $\Delta p$  the pressure difference over the membrane,  $\Delta \pi$  the osmotic pressure and  $\gamma$  the recovery rate.

This equations shows that an increase in feed water concentration results in an increase in permeate concentration, which leads to a decrease in permeate flux and vice versa. From Equation 2.1, it can also be seen that as the recovery increases or decreases, the permeate concentration increases or decreases respectively, which can also be seen in Figure 2.6c.

The osmotic pressure  $\Delta \pi$  can be defined as follows:

$$\Delta \pi = \delta C_{eff} (T + 273) \quad (2.2)$$

In this equation,  $\delta$  is a constant relating effective concentration to osmotic pressure,  $C_{eff}$  is the effective average concentration at the membrane surface and  $T$  is the water temperature in °C. In Chapter 4 this equation will be elaborated in more detail. As can be seen from the given equation, the osmotic pressure is a function temperature. An increase in temperature results in an increase in osmotic pressure. Combining this with Equation 2.1, an increase in temperature thus results in a decrease in permeate concentration, which leads to an increase in permeate flux, which is shown in Figure 2.6d. At last, as pressure increases, the permeate concentration decreases; as pressure decreases, the permeate concentration increases. This can be seen in Figure 2.6b.

When combining RO with wind energy, constant feed pressures can not be guaranteed due to the varying nature of wind. As can be seen in Figure 2.6, varying pressures would result in varying permeate flux. To keep the permeate flux constant (maximal), a solution for this effect should be thought of.

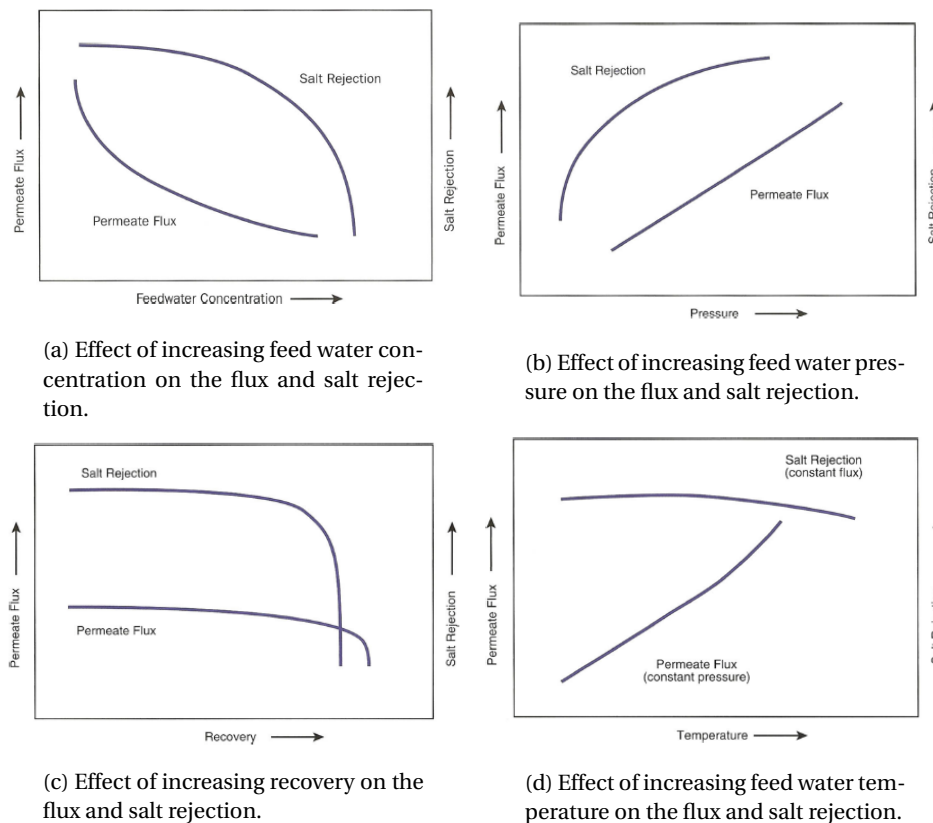


Figure 2.6: Top Left: increasing concentration (2.6a), Top Right: increasing pressure (2.6b), Bottom Left: increasing recovery (2.6c), Bottom right: increasing temperature (2.6d) [11].

## 2.4. Energy Recovery Device (ERD)

Nowadays, desalination processes have become standardised. One of the reasons RO systems have become more efficient is that Energy Recovery Devices (ERD) are used in the desalination process. In this section, fundamental information about Energy Recovery Devices will be given. On top of that, it is explained which ERD is most efficient and will be used for the experimental part of this thesis.

An Energy Recover Device is important for a seawater Reverse Osmosis (SWRO) system. An ERD helps to reduce the systems power consumption per produced volume of permeate (and thus costs), and depending on which type of ERD is used, this reduction can be up to 60 percent [12]. The basic principle of an ERD is to recover energy from the high pressure concentrate stream [7]. A typical pressure drop over the RO membranes (pressure difference between the feed stream and the concentrate stream) is around 1.5 to 2 bar [12], meaning the pressure in the concentrate stream will be nearly as high as the inlet pressure hence a potential energy is still stored in this stream.

### 2.4.1. ERD Classifications

Energy Recovery Devices can be divided into two general classes [13]. The first class (Class I) defines devices that use hydraulic power to cause a positive displacement within the recovery device, such that the energy is converted from hydraulic energy to hydraulic energy in one step. Figure 2.7 shows this principle [14].

Class II defines devices that use hydraulic energy to first convert it to mechanical energy and then back to hydraulic energy. This can be done by using a Pelton turbine (mechanical) and a generator to produce power, and then use this power to power a pump (hydraulic). Transferring hydraulic energy at once is more efficient than secondary transference. Therefore, the hydraulic energy transfer efficiency of Class I is higher than that of Class II [15].

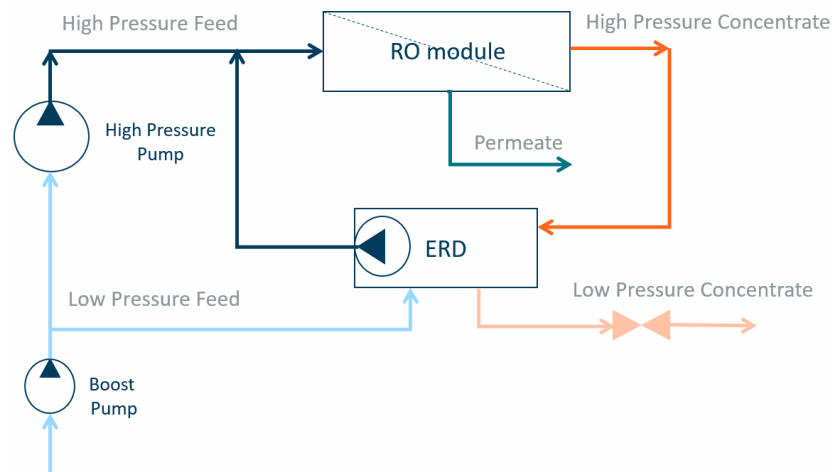


Figure 2.7: Example of a setup with a Class I Pressure Exchanger ERD.

Within each class, different types of ERDs can be distinguished, some of which are more suitable to be used in larger scale RO systems and some that are mostly used in small scale systems. In this section, the ERD chosen to work with during this thesis is elaborated in more detail. The choice for this ERD will be explained and the working principle of this ERD is elaborated in more detail. Please refer to Appendix D for an elaboration of all types of Energy Recovery Devices.

#### 2.4.2. Pressure Exchanger ERD

The most efficient and widely used ERD nowadays, that is also categorised by Class I, is the Pressure Exchanger Energy Recovery Device, also known as PX or Isobaric ERD. As Class I defines, this ERD transfers hydraulic energy to hydraulic energy directly. This is done by the use of a rotating piston, first designed by Energy Recovery Inc [16]. The working principle is explained by the use of Figure 2.8.

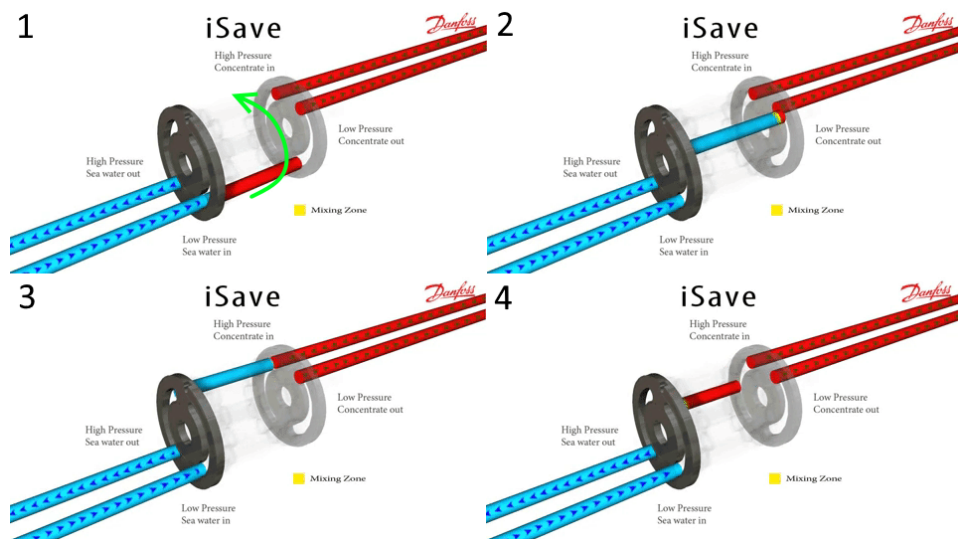


Figure 2.8: iSave Pressure exchanger Energy Recovery Device working principle [17].

1. The rotor (depicted as the grey cylinder) rotates in the direction as shown by the green arrow. This is done using an electric motor. Depending on the flow velocity of the concentrate flow, the rotational speed is chosen. The rotor consists of several chambers. While rotating, a chamber is filled with low pressure feed water, provided by a boost pump. This water replaces the low pressure concentrate wa-

ter that was in the chamber. Mostly, an abundant amount of feed water is provided to make sure all concentrate water is cleared from the chamber.

2. While rotating, the chamber is fully filled with low pressure feed water.
3. The high pressure concentrate pushes out the low pressure feed, directly converting the hydraulic energy of the concentrate water to the feed water. In this way, the low pressure feed becomes a high pressure feed stream. This feed stream will feed the RO membranes.
4. All the feed water is pushed out of the chamber and the chamber now fully contains low pressure concentrate water. Now we are back to step one where the cycle repeats.

Since there is no physical barrier between the feed water and the concentrate, a small part of the concentrate will mix with the feed water, leading to a slight increase in salt concentration of the high pressure feed water stream. This mixing can be (mostly) accounted for by supplying more low pressure feed water than there is concentrate water. The performance of the pressure exchanger can be determined by its energy transfer efficiency and the degree of mixing. The efficiency of the PX ERD can be seen as the ratio of the total energy output by the device to the total energy input (in a percentage). The rotational speed can be up to approximately 1500 rounds per minute (RPM), depending on the length of the rotor and the flow rate of the concentrate.

Pressure Exchanger ERDs are mostly used in medium to large scale desalination systems, since it is most efficient to use at high concentrate flows. Nowadays however, more and more small scale PX ERDs are being developed, meaning they can compete with, for example, turbocharger ERDs in small scale operations.

As being the most efficient Energy Recovery Device, which can nowadays be used in mostly all size of RO systems, and taking in mind the potential plan for DOT to use it for a larger scale (pilot) setup, the Isobaric Pressure Exchanger ERD is chosen to be used for the experimental test setup. The model of ERD is the Danfoss iSave 21 Plus Energy Recovery Device (iSave 21) [18].

The iSave 21 is an ERD that can operate at concentrate flow rates varying between  $6 \frac{m^3}{hr}$  at a rotational speed of 500 RPM, and  $21 \frac{m^3}{hr}$  at a rotational speed of 1500RPM. The rotational speed of the ERD is actively controlled using an electric motor. A positive displacement pump is directly attached to the same shaft of the motor and pressure exchanger. This pump is used to recirculate the flow in the ERD setup and overcomes the pressure difference between the inlet of the membranes and the outlet of high pressure feed stream of the ERD. The high pressure (HP) flow rates are linearly dependent on the RPM. The rotational speed of the ERD only influences the HP flow rates, the low pressure (LP) flow rates can only be influenced by changing the rotational speed of the feed pump. The recovery rate of the RO membranes can be influenced by changing the RPM of both the ERD and the High Pressure Pump. In Figure 2.7, all flows can be distinguished. Figure 2.9 presents the iSave 21 Plus is shown.

One of the main characteristics of a desalination system that makes use of an iSave Energy Recovery Device is the fact that the permeate flow rate is nearly identical to the feed flow rate provided by the high pressure pump. A small part of the flow provided by the high pressure pump is used to lubricate the ERD, also referred to as leakage and is a percentage of the high pressure flow rate of the ERD. A typical leakage percentage lies around 1%, according to Bergman [11]. The rest of the flow coming from the high pressure pump can be turned into permeate regardless the recovery rate of the system, until system limits are reached, like the maximum allowed feed flow rates of the membranes. In comparison: for a system that does not make use of an ERD, the amount of feed flow that can be converted into permeate depends only on the recovery rate. The relation between recovery rate, leakage flow and permeate production for a system with and without ERD is given by Equation 2.3 and is based on findings by Stover [19]:

$$\frac{Q_{p,ERD}}{Q_{p,noERD}} = \frac{1}{(1 - (1 - L)(1 - \gamma))} \quad (2.3)$$

Here,  $Q_{p,ERD}$  is the permeate flow rate for a system with isobaric ERD and  $Q_{p,noERD}$  the permeate flow rate for a system without ERD.  $\gamma$  is the recovery rate and L the leakage percentage of the ERD. From the equation can be seen that a higher recovery rate results in a smaller ratio, and thus a smaller difference between the

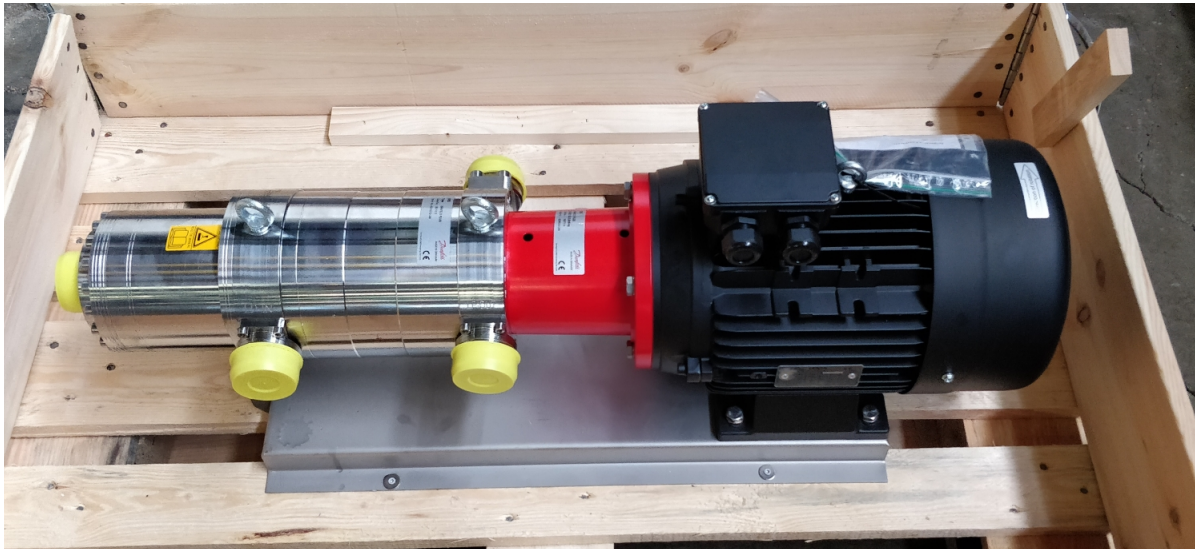


Figure 2.9: iSave 21 Plus Energy Recovery Device as it just arrived at DOT B.V.

two systems.

The implementation of the iSave 21 in a RO-model will be further elaborated Chapter 4, where the governing equations are given and the model is discussed. Chapter 5 shows the ERD in the MicRODOT experimental test setup.

### 2.4.3. Losses of a Pressure Exchanger ERD

In the case of using a pressure exchanger as ERD, hydraulic losses are the most important thing to take into account since this affects the efficiency. These losses include mixing, leakage, overflush and differential head [16]. Of each loss, a short explanation is given below:

- **Mixing:** Contamination of the high pressure feed seawater by the concentrate stream, prior to the seawater entering the membranes. The higher the mixing rate, the greater the power consumption of the high pressure pump, since the concentration of the feed water increases and thus the Osmotic Pressure. A typical mixing rate is less than 2.5% .
- **Leakage:** The direct discharge of high pressure concentrate to the low pressure concentrate stream. To compensate this, the high pressure pump must produce a higher flow and thus consume more power. A typical leakage rate lies around 1%.
- **Overflush:** The direct discharge of the seawater feed stream from the low pressure feed line directly to the low pressure concentrate line. This is mainly done to remove remaining brine from the ERD before filling it with feed water again.
- **Differential head:** A high-pressure differential results from a pressure drop between the reject stream and the feed outlet stream, meaning the high pressure pump has to account for this pressure difference. This differential head can cause at both the high and low pressure side. A low-pressure differential happens when the pressure difference between the feed inlet and the brine outlet is too high. In this case, the feed pump needs to supply a higher pressure and will thus consume more energy.

## Hydraulic Drive Train Wind Turbine

As this thesis describes the combination of the DOT hydraulic drive train wind turbine with Reverse Osmosis, it is necessary to have an understanding of all sub-systems. In this chapter, first the working principle of a general wind turbine is explained. After that, the hydraulic drive train wind turbine will be elaborated and a link to combining it with a Reverse Osmosis system will be made.

### 3.1. Wind Turbine - General Working Principle

By extracting power from the wind, a wind turbine is able to produce electricity. The amount of power extracted depends on several aspects, of which the size, geometry and environmental wind conditions are the most influential. A wind turbine rotor converts wind energy into kinetic energy in the form of torque and angular velocity. By using a gearbox, attached to the rotor via a shaft, this torque is decreased and the rotational speed is increased. Attaching the gearbox to a generator, this rotation can be converted into electricity, which is then transported using the grid.

Each turbine has its own shaped power curve. Figure 3.1 shows the ideal power curve shape of an arbitrary horizontal-axis, variable speed, pitch controlled wind turbine. The three regions shown in the figure have different objectives. Below the cut-in wind speed, the turbine will not rotate, since it is not cost-effective to keep it running. In region 1, between the cut-in wind speed ( $v_{ci}$ ) and  $v_2$ , the wind turbine operates at maximum efficiency. At wind speed  $v_2$ , where the nominal rotation speed is reached, the optimal tip speed ratio ( $\lambda$ ) and the corresponding maximum power coefficient ( $C_P$ ) is reached. In region 2, between  $v_2$  and the rated wind speed  $v_{rated}$ , the nominal power output is achieved by increasing the rotor torque. In region 3, from the rated wind speed until the cut-out speed ( $v_{co}$ ), the power is kept constant. This is done by keeping

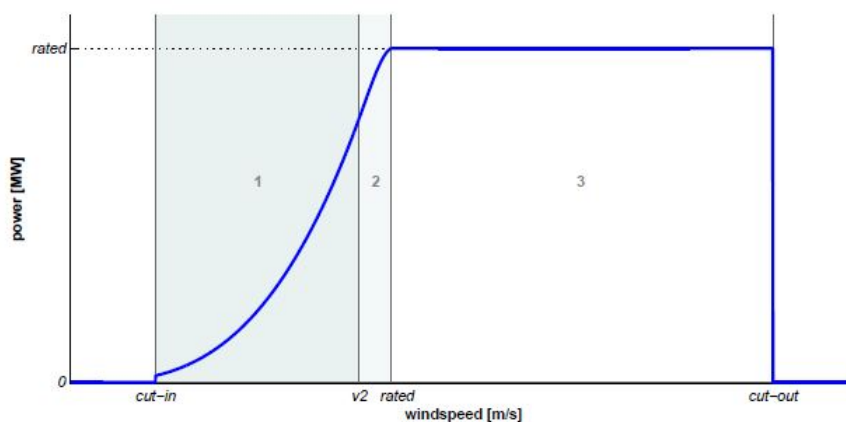


Figure 3.1: Ideal power curve of a wind turbine [20].

the rotational speed and torque constant by pitching the turbine blades. After reaching the cut-out wind speed, the turbine is shut down, mainly to prevent structural damage.

To be able to determine the power curve of a horizontal axis wind turbine, the power that the turbine extracts from the wind has to be calculated [21], starting with the equations for determining the tip speed ratio,  $\lambda$ , of the wind turbine, as can be seen in Equation (3.1). The tip speed ratio is defined as the ratio between the speed of the rotor blade tip and the free relative stream wind speed,  $U_{rel}$ .

$$\lambda = \frac{\omega_r R}{U_{rel}}, \quad (3.1)$$

Here,  $\omega_r$  is the angular velocity of the wind turbine and  $R$  the radius of the turbine. The aerodynamic power and torque of the turbine can be determined as follows:

$$P_{aero} = C_P \frac{1}{2} \rho_{air} \pi R^2 U_{rel}^3 \quad (3.2)$$

$$\tau_{aero} = C_\tau \frac{1}{2} \rho_{air} \pi R^3 U_{rel}^2 \quad (3.3)$$

where  $\rho_{air}$  is the density of the air,  $C_P$  is the power coefficient and  $C_\tau$  the torque coefficient of the turbine.

The expression for the power coefficient is defined as follows:

$$C_P = \frac{P_{aero}}{P_{wind}} = \frac{\tau_{rotor} \omega_r}{\frac{1}{2} \rho_{air} \pi R^2 U_{rel}^3} \quad (3.4)$$

The expression for the torque coefficient is defined as follows:

$$C_\tau = \frac{\tau_{aero}}{\frac{1}{2} \rho_{air} \pi R^3 U_{rel}^2} \quad (3.5)$$

Combining Equation (3.1), (3.4) and (3.5) gives the following relation between  $C_P$  and  $C_\tau$ :

$$C_t = \frac{C_p}{\lambda} \quad (3.6)$$

To be able to find the optimal static relationship between the aerodynamic torque as a function of the rotor speed [21], Equations (3.1) and (3.6) can be inserted into Equation (3.3):

$$\tau_{aero} = K_1 \omega_r^2 \quad (3.7)$$

where,

$$K_1 = \frac{C_{P,max}}{\lambda_{P,max}^3} \frac{1}{2} \rho_{air} \pi R^5 \quad (3.8)$$

In Figure 3.2, the theoretical optimal performance for different wind speeds and rotational speeds can be found as described by Equation 3.7. In this figure, the intersection point between the dashed line, which represents  $C_{P,max}$ , and the lines denoting the torque per wind speed is the optimal point of performance for the turbine at that wind speed.

To be able to produce electricity, a generator is used. In the nacelle of most conventional wind turbines, the generator is connected to the rotor via shafts and a gearbox. The aerodynamic torque on the rotor, as described by Equation 3.3, should be in an equilibrium with the torque from the generator. Whereas the aerodynamic torque is a function of the angular velocity of the rotor, the generator torque is expressed as a function of the angular velocity of the generator  $\omega_{gen}$  and a transmission ratio of the gearbox  $G$  [21]. The definition for the generator torque is as follows:

$$\tau_{gen} = K_2 \omega_{gen}^2 \quad (3.9)$$

$$K_2 = \frac{C_{P,max}}{G^3 \lambda_{P,max}^3} \frac{1}{2} \rho_{air} \pi R^5 \quad (3.10)$$

In these equations, it is assumed that the shaft is rigid.

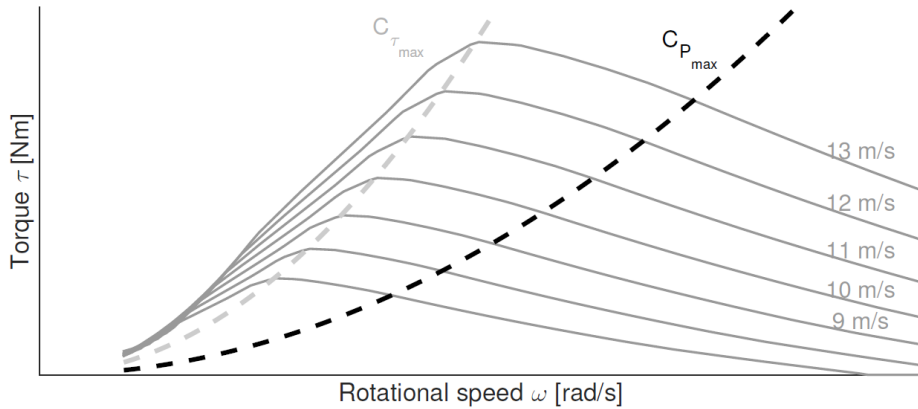


Figure 3.2: Optimal aerodynamic performance, following a quadratic relation between aerodynamic torque and the angular velocity of the rotor, denoted by the dashed line [21].

### 3.2. Hydraulic Wind Turbine

As explained in Subsection 1.1.2, the gearbox of an conventional wind turbine is the part that is most prone to breaking [4]. Excluding a gearbox from the drive train would both simplify and reduce maintenance. As mentioned in Section 1.2, using a hydraulics drive train would have many benefits. This section will provide insight in the working principle of the hydraulic drive train.

A hydraulic drive train wind turbine makes use of a positive displacement pump in the nacelle. A schematic overview of such a drive train is given in Figure 3.3. In order to operate safely and extract power from the wind as efficient as possible, the speed of the rotor has to be controlled. Since the rotor torque is determined by the wind speed, which is an environmental parameter and can not be influenced, the angular velocity below rated wind speeds has to be regulated by applying a counter torque. For a wind turbine that uses a hydraulic drive train, the counter torque is given by a (positive displacement) hydraulic pump. In the case of the DOT principle, a nozzle is located in the high pressure line of the pump. By opening or closing this nozzle, the pressures can be affected hence the torque of the pump can be controlled. The equations for balance between the rotor torque,  $\tau_{rotor}$ , and the pump torque,  $\tau_{pump}$  is described by Equation 3.11 [20]:

$$J_t \dot{\omega}_r = \tau_{rotor} - \tau_{pump} \tag{3.11}$$

Here,  $J_t$  is the total combined mass moments of inertia of the aerodynamic rotor and the pump.  $\omega_r$  is the rotational speed of the rotor. By influencing the pump torque, the rotor speed can be adjusted. The rate of how fast the speed can be adjusted is determined by the total inertia of the system. From Equation 3.11, the influences of the torque values on the turbines rotor speed can be determined, as can be seen in Table 3.1.

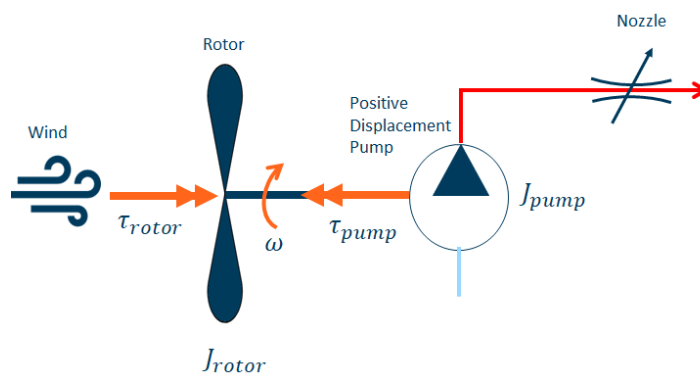


Figure 3.3: Schematic overview of a hydraulic drive train.

As explained in Section 3.1, a wind turbine operates in different regions. Below the rated wind speed, a vari-

Table 3.1: Torque balances and influence on turbine angular velocity

$\tau_{rotor} > \tau_{pump}$	$\omega_r \uparrow$
$\tau_{rotor} < \tau_{pump}$	$\omega_r \downarrow$
$\tau_{rotor} = \tau_{pump}$	$\omega_r$ constant

ation in wind speed will result in an variation in rotor torque. Above the rated wind speed, this variation is accounted for by pitching the blades. To prevent the turbine from constantly accelerating with increasing wind speeds below the rated wind speed, the pump torque is (actively) controlled to give proper counter torque. By controlling the counter torque, the turbine is able to operate at its highest aerodynamic efficiency. The relation between the pump torque and the rotor speed is as follows:

$$\tau_{pump} = \frac{Q_{pump} \Delta p_{pump}}{\omega_r} \quad (3.12)$$

Here,  $\Delta p_{pump}$  is the pressure difference over the pump. Assuming the discharge pressure to be significantly higher than the inlet pressure, this pressure difference is taken to be equal to the discharge pressure of the pump. The DOT hydraulic drive train uses a spear valve as a nozzle to influence this pressure. Such a valve is depicted in Figure 3.4. At a given rotational speed, the positive displacement pump provides a certain flow. Theoretically, this flow changes proportionally with rotational speed, regardless the pressure it operates at. A slight increase in internal leakage for increasing pressure, however, prevents it from being truly linear. The flow provided by the pump flows through the spear valve. The relation between the pressure and the flow going through the spear valve  $Q_{SV}$  is given by Equation 3.13 [22]. Assuming one spear valve is used,  $Q_{SV}$  is equal to  $Q_{pump}$ .

$$Q_{SV}^2 = \frac{2 \Delta p_{SV} C_d^2 A_{SV}^2}{\rho_{water}} \quad (3.13)$$

Where  $\Delta p_{SV}$  is the pressure drop across the spear valve,  $A_{SV}$  is the effective area of the spear valve,  $C_d$  is the discharge coefficient and  $\rho_{water}$  is the density of the medium, in this case water.  $A_{SV}$  can be changed by changing the spear valves' position  $S$ , as can be seen in Figure 3.4. Assuming that the pressure at the outlet of the valve is atmospheric,  $\Delta p_{SV}$  is equal to the pressure at the pump side of the nozzle and thus it can be said that  $\Delta p_{SV}$  is equal to  $\Delta p_{pump}$ . Rewriting Equation 3.13 using this relation will give Equation 3.14

$$\Delta p_{pump} = \frac{1}{2} \frac{Q_{SV}^2 \rho_{water}}{C_d^2 A_{SV}^2} \quad (3.14)$$

where  $A_{SV} = \pi \frac{D_{nz}^2}{4}$

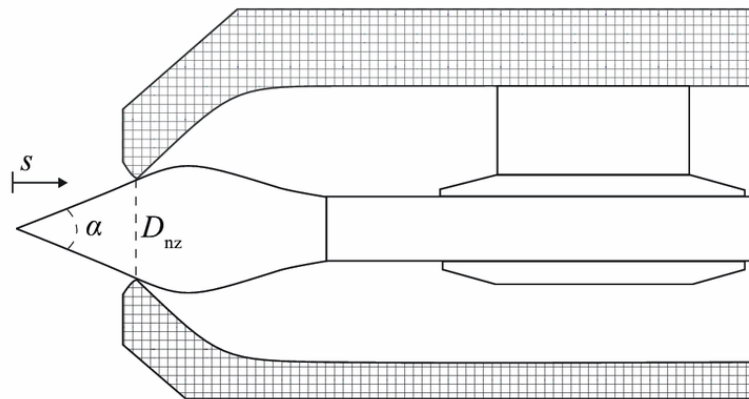


Figure 3.4: Cross section of a spear valve [22].

The spear valve area is the only parameter that can be directly influenced by changing the spear valves position, denoted as  $S$  in Figure 3.4. Opening the spear valve, and thus increasing the area, would result in a decrease in pressure. Closing the spear valve would results in an increase in pressure.

### 3.3. Hydraulic Wind Turbine with RO and an ERD

In this section, the combination of the DOT hydraulic drive train wind turbine with Reverse Osmosis will be shortly explained based on theory previously presented. As aforementioned, the output of a hydraulic drive train in a wind turbine is a high pressurised (HP) flow, and in the case for DOT, the used medium is seawater. Besides using this HP flow to produce electricity by the means of a spear valve and Pelton turbine, using the flow for desalination can be a very interesting and a well suited combination. As explained in Section 3.2, the spear valve is used to both control the turbine as well as produce electricity by jetting the high pressure flow via the valve on a Pelton turbine. For this thesis, focus will be on replacing the spear valve with an RO + ERD system, as schematically shown in the figure below. It will be researched how the RO+ERD system influences the system's flows and pressures and whether the system can be actively controlled and can operate stable without the use of a spear valve. This is shown schematically in Figure 3.5, where  $Q_f$ ,  $Q_p$  and  $Q_c$  refer to the feed, permeate and concentrate flow respectively.

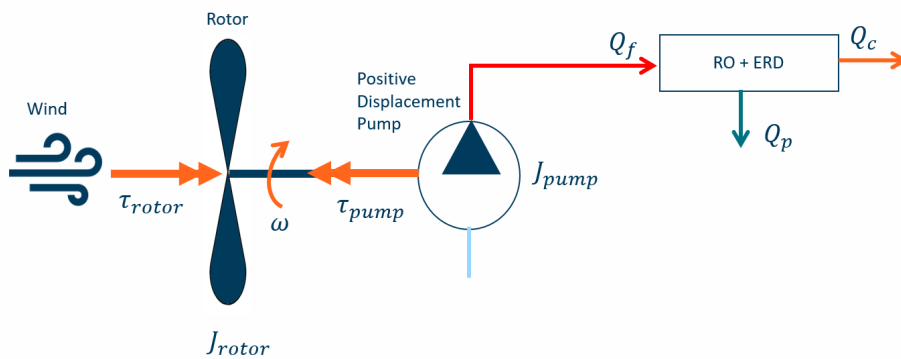


Figure 3.5: Schematic overview of a hydraulic drive train that includes an Reverse Osmosis system with an ERD.

The following chapters will elaborate on all subsystem required to combine the hydraulic turbine with a Reverse Osmosis system, both by giving fundamental information as well as describing the governing equations. In Chapter 6, the total setup combination will be explained into more detail and modelled results will be shown. Figure 3.6 gives an impression of what wind driven reverse osmosis system can look like. In the figure a combination of Seawater Reverse Osmosis with electricity production is shown, although the spear valve and Pelton turbine will not be discussed and analysed in this research.

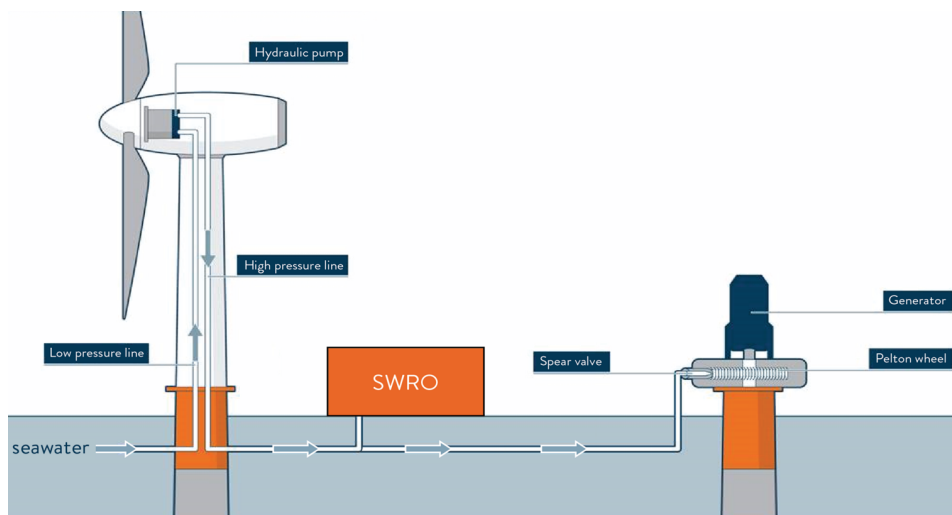


Figure 3.6: Impression of what a future setup might look like. Note that this thesis does not focus on implementing the spear valve and Pelton Turbine.



# 4

## Numerical Model on Reverse Osmosis with an ERD

In this chapter, first the fundamental equations for Reverse Osmosis and the Energy Recovery Device will be elaborated. Then, a combination of RO with an ERD will be given and a comparison of a system with and without ERD will be shown, using a numerical model. These model results will be compared to the results obtained from the experimental tests shown in Chapter 5. In Chapter 6, the implementation of a hydraulic drive train wind turbine in the desalination process will be modelled and elaborated by equations and results.

### 4.1. Reverse Osmosis Membrane

This section will discuss the theory of Reverse Osmosis and the governing equations used. To start with, there is a mass balance across the RO membrane. This equation is given in (4.1)

$$\dot{m}_f = \dot{m}_c + \dot{m}_p, \quad (4.1)$$

where  $\dot{m}_f$ ,  $\dot{m}_c$  and  $\dot{m}_p$  are the mass flow rates of respectively the feed, concentrate and permeate flows. The equation for conservation of mass can be rewritten as equation (4.2).

$$v_f A_f \rho = v_c A_c \rho + v_p A_p \rho, \quad (4.2)$$

Here,  $v$  is the flow velocity and  $A$  is the piping area for the feed, concentrate and permeate streams. Since it is assumed that fluids are incompressible, the density remains constant at higher pressures. Therefore, there is no change in density  $\rho$  over the membrane, and thus equation (4.2) can be rewritten as (4.3).

$$v_f A_f = v_c A_c + v_p A_p, \quad (4.3)$$

Each term of  $vA$  is equal to the volumetric flow rates of each stream, given in (4.4).

$$Q_f = Q_c + Q_p \quad (4.4)$$

The water flux through the membrane [11],  $J_w$ , can be determined as shown in equation (4.5). It is expressed as  $\frac{kg}{m^2s}$ , or units of mass flow per area per time, in this case seconds.

$$J_w = K_w(\Delta p - \Delta \Pi) = \frac{v_p A_p \rho}{A_m} \quad (4.5)$$

In here,  $\Delta p$  is the hydrostatic pressure difference over the membrane and  $\Delta \Pi$  the osmotic pressure difference.  $K_w$  is the permeability coefficient of the membrane and  $A_m$  the area of the membrane. The term  $\Delta p - \Delta \Pi$  is called the net driving pressure, or *NDP*. The net driving pressure is the actual driving pressure available to force the water through the membrane.

The permeability (or mass transfer) coefficient  $K_w$  can be written as follows:

$$K_w = \frac{c_w u_w D_w S_w}{lRT} \quad (4.6)$$

Here,  $c_w$  is the water mole concentration,  $u_w$  the partial molar volume of water,  $D_w$  the water diffusion coefficient,  $S_w$  the water solubility,  $l$  the thickness of the membrane,  $R$  the ideal gas constant and  $T$  the temperature of water. Mostly, the permeability coefficient is determined experimentally, since it is generally influenced by the type of membrane used.

When knowing the flow rates of each stream, it is possible to determine the permeate recovery rate,  $\gamma$ , as follows from equation (4.7);

$$\gamma = \frac{Q_p}{Q_f} \cdot 100\% \quad (4.7)$$

The permeate stream always has a certain amount of salts and solids dissolved (Total Dissolved Solids, or TDS). The salt passage through the membrane,  $SP$  can be calculated, using the concentration of both the feed stream,  $C_f$  and the permeate stream,  $C_p$ . This calculation is shown in equation (4.8)

$$SP = \frac{C_p}{C_f} \cdot 100\%, \quad (4.8)$$

and from this, the salt rejection,  $R$ , can be easily determined (4.9):

$$R = \left(1 - \frac{C_p}{C_f}\right) \cdot 100\% \quad (4.9)$$

Just as for the water flux, the dissolved solute (or salt) flux through the membrane,  $J_s$ , can also be derived. This derivation is shown in equation (4.10).

$$J_s = K_s(C_m - C_p) \quad (4.10)$$

In this equation,  $K_s$  is the salt permeability coefficient of the membrane and  $C_m$  the concentration at the membrane surface.  $C_m$  is equal to the average concentration of the feed stream and the concentrate stream, or  $\frac{C_f + C_c}{2}$ . The salt permeability coefficient can be found as follows:

$$K_s = \frac{Q_p C_p}{A_m \Delta C} \quad (4.11)$$

In this equation,  $\Delta C$  is the concentration differential, which is given in (4.12):

$$\Delta C = (C_m - C_p) = \frac{C_f + C_c}{2} - C_p \quad (4.12)$$

Using equation (4.11), equation (4.10) can be rewritten into equation (4.13):

$$J_s = \frac{Q_p C_p}{A_m} \quad (4.13)$$

## 4.2. Energy Balance around Gate Valve

Bartman et al. [23] developed a fundamental model that represents a Reverse Osmosis desalination system. This model is based on an mass-equilibrium around the entire system and an energy balance taken around the gate valve in the concentrate stream. The gate valve creates a back pressure, such that the desalination process can take place. Figure 4.1 shows this simplified system for modelling.

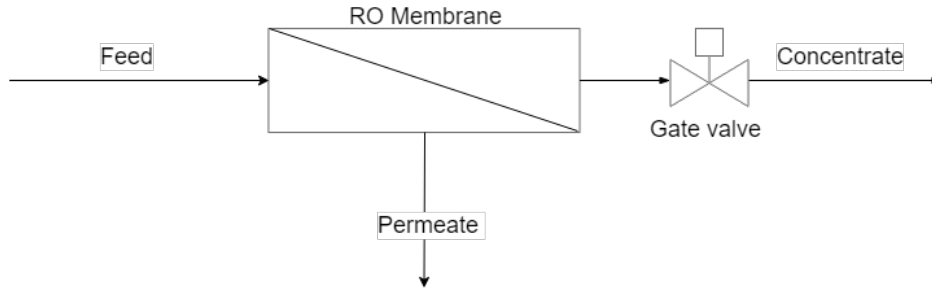


Figure 4.1: Simplified Reverse Osmosis desalination system for modelling.

This subsection will only cover the balance around the gate valve. When knowing all equations for each subsystem, the total system will be elaborated. For the energy balance around the gate valve, the following equation (4.14) is used:

$$\frac{d}{dt}(E_{k,tot} + E_{p,tot}) = -\Delta\left(\frac{1}{2}\frac{\bar{v}^3}{\bar{v}} + E_p + \frac{p}{\rho}\right)\dot{m} + W_m - E_v \quad (4.14)$$

In this equation, the left-hand side represents the change in kinetic energy over the valve over time. On the right-hand side, the following parameters can be distinguished:  $\bar{v}$  is the averaged flow velocity in the pipe,  $E_p$  is the potential energy due to difference in height,  $\dot{m}$  is the mass flow rate of the stream,  $\rho$  is the density of the fluid,  $W_m$  represents the work done on the system and  $E_v$  represents the losses due to friction.

To be able to simplify this equation, several assumptions will be made:

- The height difference between the inlet and the outlet of the valve is null, meaning  $E_p = 0$  and the height of the system itself is negligible, so also  $E_{p,tot} = 0$
- The flow velocity of both the inlet and the outlet is equal, so  $\Delta\bar{v} = 0$
- The used fluid is in-compressible, meaning  $\rho_{in} = \rho_{out}$ .
- Density does not change with changing salinity
- There is no external work done on the system, so  $W_m = 0$

Using these assumptions, equation (4.14) can be written as follows:

$$\frac{d}{dt}E_{k,tot} = -\frac{\Delta p}{\rho}\dot{m} - E_v, \quad (4.15)$$

The friction losses due to the valve,  $E_v$  can be approximated by using the following equation:

$$E_v = \frac{1}{2}e_{vc}\dot{m}v^2 \quad (4.16)$$

Here,  $e_v$  is the friction losses factor, which is a coefficient that represents the valve resistance to the flow going through it.  $e_v$  depends on the valve used and its characteristics. The total kinetic energy  $E_{k,tot}$  is the integral of the kinetic energy over the total systems volume,  $\frac{1}{2}\dot{m}v^2$ , or  $\frac{1}{2}\rho Vv^2$ . This leads to the following equations for the balance around the gate valve:

$$\rho V \frac{dv}{dt} = -\frac{\Delta p}{\rho}\dot{m} - \frac{1}{2}e_v\dot{m}v^2, \quad (4.17)$$

In this formula,  $e_v$  has not been determined yet. As explained earlier,  $e_v$  is the valve resistance coefficient, and it is related to the valve coefficient (or so called concept of valve)  $C_v$  for a valve in a water system, and can be found in equation (4.18). Here,  $A$  is the area of the piping in which the valve is installed.

$$C_v = \frac{A}{\sqrt{\frac{1}{2}\rho e_v}} \quad (4.18)$$

The valve coefficient is depending on both the type of the valve as well as the valves opening position. This relation can be expressed empirically based on the following Equation 4.19:

$$C_v = \mu O_v - \phi \quad (4.19)$$

In this equation,  $\mu$  and  $\phi$  are both constants that are depending on the type of the valve and must be determined experimentally.  $O_v$  is the valves opening position in percentages. By combining both equation (4.18) and (4.19), the valve resistance coefficient  $e_{vc}$  can be found:

$$e_v = \frac{2}{\rho} \left( \frac{A}{\mu O_v - \phi} \right)^2 \quad (4.20)$$

### 4.3. Pressure Exchanger Energy Recovery Device

In this section, the governing equations for the Isobaric Energy Recovery Device (ERD) will be discussed. A mass balance around the ERD will be elaborated as well as definitions for the phenomena volumetric mixing (VM), overflush (OF) and leakage (L) that occur when using an ERD as explained in Subsection 2.4.3 of Chapter 2.

As can be seen in Figure 4.2, where an ERD is simplistically shown, the ERD has two in-going and two outgoing flows. This is also explained in Subsection 2.4.2. In the figure,  $Q_{f,LP,ERD}$  represents the low pressure seawater feed stream going into the ERD,  $Q_{f,ERD}$  refers to the pressure feed stream exiting the ERD.  $Q_c$  is the high pressure concentrate stream and  $Q_{c,LP,ERD}$  is the low pressure concentrate stream.

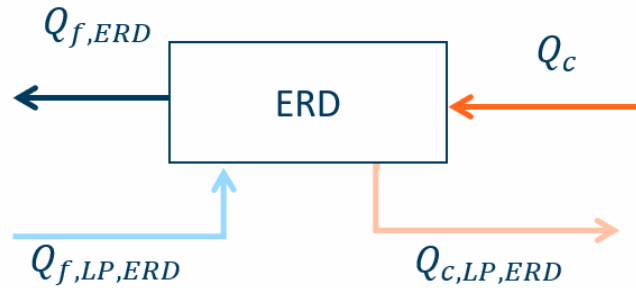


Figure 4.2: Simplistic visualisation of the ingoing and outgoing flows of an ERD.

From Figure 4.2, the mass balance around the ERD can be obtained, given by Equation 4.21. For this mass balance, it is assumed that the density of each stream is equal and an increase in concentration does not affect the density, therefore it can be said that the mass balance can be expressed as a balance of flows.

$$Q_{f,LP,ERD} + Q_{c,LP,ERD} = Q_{f,ERD} + Q_c \quad (4.21)$$

Within the ERD, the energy from the concentrate is transferred directly to the seawater stream, without the use of a physical barrier. This mechanism allows for some mixing of concentrate into the seawater (VM). Another term that has to be accounted for is leakage (L), which occurs at the seals of the isobaric chambers. First, an expression for the mixing rate is determined. For this, the ERD is divided into two parts, as can be seen in Figure 4.3.

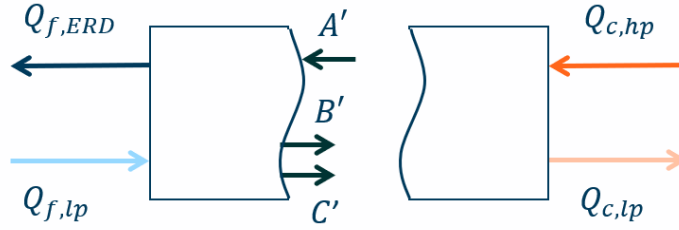


Figure 4.3: Distinguished flows of a pressure exchanger ERD, used to determine mixing (VM), leakage (L) and overflush (OF).

The mass balance around the left end of the ERD can be written as follows in equations (4.22), as described by Stover and Gorenflo in [24]. Figure 4.3 is used to distinguish the flows in and around the ERD.

$$Q_{f,lp}C_{f,lp} + Q_{A'}C_{A'} = Q_{f,ERD}C_{f,ERD} + Q_{B'}C_{B'} + Q_{C'}C_{C'} \quad (4.22)$$

In this equation,  $C_x$  is the concentration of each stream  $x$  and  $Q$  is the flow rate of each stream. Here,  $C_{f,ERD} = C_{A'}$  and  $C_{f,lp} = C_{B'} = C_{C'}$ .

A way to reduce this mixing phenomena is to supply excess seawater to clear the chambers of the rotary pressure exchanger, as explained Section 2.4. This is called overflush. Overflush (OF) is defined by the ratio between the ingoing and outgoing feed water streams, and can be written as follows:

$$OF = \frac{Q_{f,lp} - Q_{f,ERD}}{Q_{f,ERD}} \quad (4.23)$$

and  $Q_{C'}$  can be determined as well:

$$Q_{C'} = Q_{f,lp} - Q_{f,ERD} = OF(Q_{f,ERD}) \quad (4.24)$$

The mixing flow  $Q_M$  is the flow that contains the feed water and includes a small amount of concentrate water, and is defined as  $Q_M = Q_{A'} = Q_{B'}$ . Knowing this, inserting it in Equation 4.21 gives the following relation for the volumetric mixing:

$$\frac{Q_M}{Q_{f,ERD}} = VM = \frac{C_{f,ERD} - C_{f,lp}}{C_{c,hp} - C_{f,lp}} \quad (4.25)$$

The leakage of the ERD can be defined by the difference between the ingoing high pressure concentrate stream  $Q_{c,hp}$  and the outgoing high pressure feed stream  $Q_{f,ERD}$  as can be seen in equation (4.26):

$$L = \frac{Q_{c,hp} - Q_{f,ERD}}{Q_{c,hp}} \quad (4.26)$$

As explained by Stover and Andrews [25], there is no Equation established that determines the efficiency of isobaric Pressure Exchanger ERDs. Based on experimental data and data provided by several manufacturers, the overall efficiency of the isobaric ERD is determined to be between 90 and 97%.

## 4.4. Reverse Osmosis System

Now that the equations and balances for each subsystem are known, they can be combined to end up with the governing equations for a Seawater Reverse Osmosis system with an ERD. An overview of the system is shown in Figure 4.4.

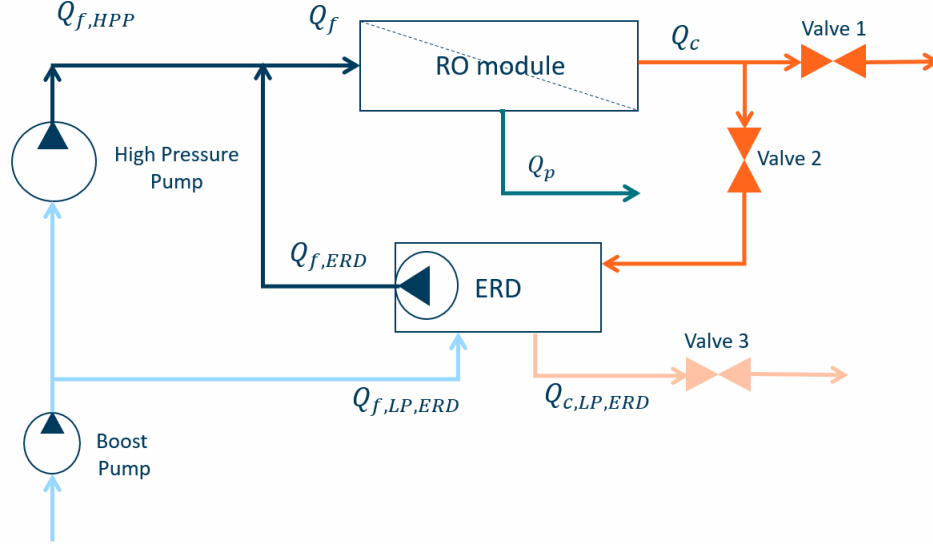


Figure 4.4: Simplistic overview of a Reverse Osmosis system for modelling, including ERD.

In the figure, the three subsystems treated in the previous sections can be distinguished. The figure shows a setup that can be used both with and without ERD. When fully closing valve 2 and 3 while valve 1 is open, the system can be seen as a desalination system without ERD. Valve 1 is in this case the concentrate valve, used to deliver back pressure for the membranes. When fully closing valve 1 while valve 2 is fully opened, the system can be considered as a desalination system with an ERD. Valve 3 is used to prevent cavitation from occurring in the ERD and it is set in such a way that a minimum required pressure is realised at the low pressure concentrate outlet.

### 4.4.1. Reverse Osmosis without an ERD

Substitution of Equations 4.1 and 4.3 in Equation 4.17 results in the following equation:

$$\rho V \frac{dv_c}{dt} = p_{sys} A_c - \frac{1}{2} \rho A_c e_{vc} v_c^2, \quad (4.27)$$

In here,  $V$  is the systems volume and  $e_{vc}$  the valve resistance of the valve in the concentrate stream.  $A_c$  is the area of the concentrate piping, in which the valve is placed

To obtain the expression for the system pressure, the flow velocity of the permeate flow must be calculated, given in Equation 4.28, which is also show by Bartman et al. [23]. To obtain Equation 4.28, Equation 4.5 is used, where the pressure drop over the membrane is considered negligible, such that the pressure of the concentrate stream is equal to the pressure of the feed stream. Therefore,  $\Delta p$  is equal to  $p_{sys}$ :

$$v_p = \frac{A_m K_w}{\rho A_p} (p_{sys} - \Delta \Pi) \quad (4.28)$$

Here,  $p_{sys}$  represents the pressure of the system. From which follows equation (4.29) when also using (4.3) to account for the term  $A_p v_p$ :

$$p_{sys} = \frac{\rho(A_f v_f - A_c v_c)}{A_m K_w} + \Delta \Pi \quad (4.29)$$

The osmotic pressure,  $\Delta\Pi$ , can be computed using the following equation (4.30):

$$\Delta\Pi = \delta C_{eff}(T + 273) \quad (4.30)$$

Where  $\delta$  is a constant relating effective concentration to osmotic pressure,  $C_{eff}$  is the effective average concentration at the membrane surface and  $T$  is the water temperature in °C.  $C_{eff}$  can be obtained using the following equation:

$$C_{eff} = C_f \left( a + (1 - a) \left( (1 - R) + R \frac{v_f}{v_c} \right) \right) \quad (4.31)$$

In here,  $C_f$  is the concentration of the feed stream, or the total dissolved solids in the feed (TDS),  $R$  is the salt rejection of the used membrane as determined in Equation 4.9 and  $a$  is an effective concentration weighting coefficient. A typical value for  $a$  is 0.5 [23], such that Equation 4.31 can be rewritten into Equation 4.32:

$$C_{eff} = \frac{1}{2} C_f + \frac{1}{2} C_f \left( (1 - R) + R \frac{v_f}{v_c} \right) \quad (4.32)$$

Now that all terms of  $p_{sys}$  are known, Equation (4.27) can be rewritten, where  $p_{sys}$  will be filled in, which results in the governing equation for the RO system, Equation 4.33. Note that this equation focuses on desalination without an ERD using the balance around the gate valve.

$$\frac{dv_c}{dt} = \frac{A_c(A_f v_f - A_c v_c)}{A_m K_w V} + \frac{\Delta\Pi A_c}{\rho V} - \frac{1}{2} \frac{A_c e_{vc} v_c^2}{V} \quad (4.33)$$

#### 4.4.2. Reverse Osmosis with an ERD

Equation 4.29 is shown as a function of the feed and concentrate areas and flow velocities. Using expression 4.3 and 4.4, this equation can be written in terms of the permeate flow rate:

$$p_{sys} = \frac{\rho Q_p}{A_m K_w} + \Delta\Pi \quad (4.34)$$

The permeate flow rate,  $Q_p$ , is related to the flow coming from the high pressure pump as follows from Equation (4.35) Stover [19]:

$$Q_{f,HPP} = Q_p \frac{1 - (1 - L)(1 - \gamma(Q_{f,HPP}))}{\gamma(Q_{f,HPP})}, \quad (4.35)$$

where  $\gamma$  is the recovery rate as determined by Equation (4.7) and  $Q_{f,HPP}$  is the flow coming from the high pressure pump.

The total feed flow  $Q_f$  for the membranes is a summation of two flows, as can be seen in Figure 4.4. First, there is a flow coming directly from the high pressure pump,  $Q_{f,HPP}$ . Second, there is a feed flow coming from the ERD,  $Q_{f,ERD}$ . Due to aforementioned losses like mixing, leakage and overflush in the ERD system, the size of the low pressure feed flow  $Q_{f,lp,ERD}$  is higher than the the outgoing high pressure feed flow  $Q_{f,ERD}$  to overcome these losses.

The mass balance in front of the membranes is given by the following Equation:

$$\dot{m}_f = \dot{m}_{f,hpp} + \dot{m}_{f,ERD} \quad (4.36)$$

As explained in Section 4.1, it is assumed that fluids are incompressible and thus the density is not influenced by pressure. Equation 4.36 can be rewritten such that a flow balance is given:

$$Q_f = Q_{f,hpp} + Q_{f,ERD} \quad (4.37)$$

The influence of using an ERD on the feed concentration can be determined.  $C_{f,ERD}$  is defined using Equation 4.22 and 4.25:

$$C_f = \frac{Q_{f,hpp} C_{f,hpp} + Q_{f,ERD} C_{f,ERD}}{Q_f} \quad (4.38)$$

## 4.5. Model Results

The numerical model discussed in this section is designed based on the components and settings used in the experimental setup, which will be elaborated in Chapter 5. In this way, a comparison between model and tests results is most reliable. The model will thus make use of the characteristics of the iSave-21 ERD, the Hydroton Janus M30 Hydraulic pump and four DOW FILMTECH SW30-4040 membranes, placed in a parallel configuration. The permeability coefficient of these membranes is obtained experimentally and compared to results obtained using ROSA 9, a program for Reverse Osmosis System Analysis. A more detailed explanation about the obtainment of this coefficient can be found in Subsection 5.4.1. As the experimental tests have been conducted without the use of salt water, the feed concentration is relatively low. A similar value for the concentration is used in the model.

The high pressure pump is a positive displacement pump, the provided high pressure feed flow rate is linear proportional to its rotational speed (as can be seen in Appendix E). Using the experimental tests, the volumetric efficiency for the hydraulic pump is determined empirically based on rotational speed and pressure of the pump. The volumetric efficiency accounts for leakage losses. In Appendix C, the determination of this efficiency is found. The relation is shown in Equation 4.39:

$$Q_{f,HPP} = \omega_{HPP} V_p \eta_{hydr} \quad (4.39)$$

Here,  $\omega_{hpp}$  is the angular velocity of the pump in  $rad/s$ ,  $V_p$  the volumetric displacement in  $m^3/rad$  and  $\eta_{hydr}$  the volumetric efficiency.

The hydraulic power supplied by the pump is a function of the flow rate and the systems pressure. This is stated in Equation 4.40. The shaft power, or mechanical power, of the pump, describing the power of the rotating pumps shaft, is given by Equation 4.41 and is defined by the torque ( $\tau_{HPP}$ ) on the shaft and the angular velocity of the pump ( $\omega_{HPP}$ ).

$$P_{hydr} = Q_{f,HPP} p_{sys} \quad (4.40)$$

$$P_{shaft} = \tau_{HPP} \omega_{HPP} \quad (4.41)$$

### 4.5.1. Varying HPP RPM - Comparison of a System with and without ERD

As explained in Subsection 2.4.2, one of the characteristics of an RO system using an Isobaric Pressure Exchanger ERD is that the flow rate coming from the high pressure pump is nearly equal to the amount of permeate produced. The leakage (or lubrication) flow of the ERD accounts for the difference. Using a typical leakage rate of 1% for the iSave ERD (Appendix E), a comparison between the two systems with and without ERD is made based upon the relation permeate production per high pressure feed flow rate and rotational speed. For this, the rotational speed of the ERD is taken such that the flow rate is constant at  $7 m^3/hr$ . The relation for flow at different angular velocities can be found in Appendix E, at the specification section of the iSave ERD.

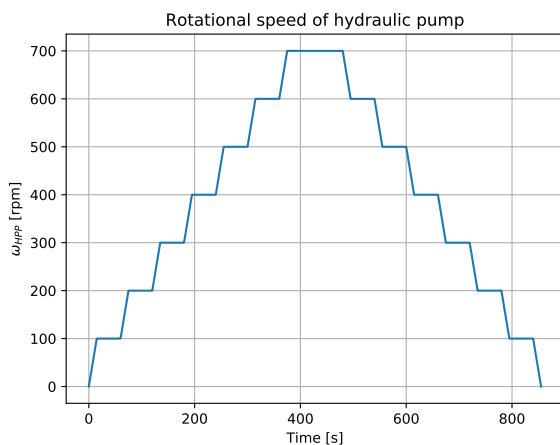
### Permeate production

In Figures 4.5a, 4.5b and 4.5c, a comparison between the two systems is made. In Table 4.1, the input parameters are shown.

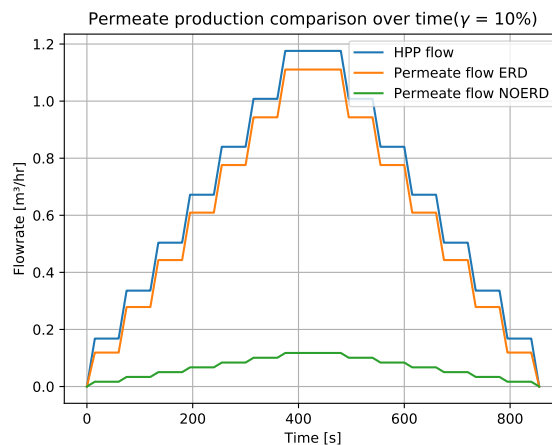
Table 4.1: Input parameters permeate comparison

Parameter	Value	Units
$\omega_{HPP}$	0-700	RPM
$V_p$	$3.5e^{-5}$	$m^3/rev$
$Q_{ERD}$	7	$m^3/hr$
$\gamma$	10	%
$L$	1	%
$n_{mem}$	4	-
$A_m$	7.34	$m^2$
$\delta$	0.2641	Pa/ppm K
$a$	0.5	-
$K_w$	$3.43e^{-9}$	s/m
$R$	0.993	-
$C_f$	600	ppm
$T_{water}$	10	$^{\circ}C$

The rotational speed of the high pressure pump is increased over time following a step function. According to Equation 4.39, this results in a delivered flow that directly follows this curve. This RPM step function is shown in Figure 4.5a. The permeate productions for both systems do follow this step response too, as Figure 4.5b. From the Figures 4.5b, where the permeate production over time is shown, and 4.5c where the permeate production per rotational speed can be seen, it can be observed that the use of an ERD has a large influence on the amount of permeate produced compared to a system that does include one. The difference between the HPP flow and the permeate flow with ERD as seen in the figure is caused by the leakage flow of the ERD. When including an ERD that has a constant rotational speed in a system having a high pressure pump rotating at variable speeds, it should be noted that no constant recovery rate can be obtained. The recovery rate is defined as the ratio between permeate flow and membrane feed flow, as Equation 4.7 shows. Using Equations 4.37 and 4.7, it is seen that the rotational speed (and thus flow) of the ERD should vary to keep the ratio and recovery rate constant at varying hydraulic pump speeds. At the used constant ERD RPM, the recovery rate at highest permeate production lies rate around 13%.



(a) The RPM of hydraulic pump follows a step-response.



(b) The permeate production for a system with a recovery rate of 10% follows the HPP step response.

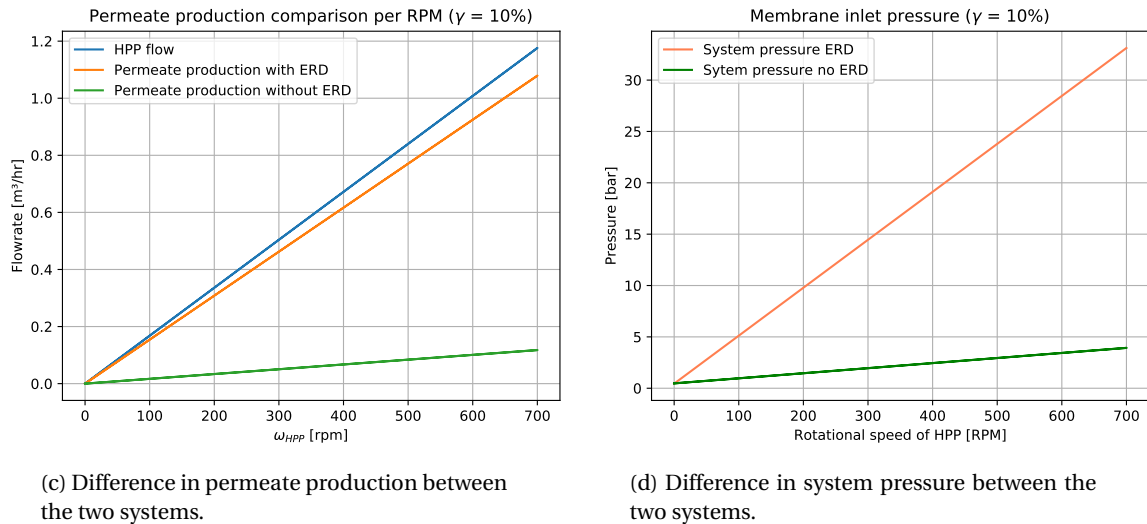


Figure 4.5: Results for varying HPP RPM

In Section 2.4 Equation 2.3, the comparison of permeate production between the two systems is given by a ratio  $\frac{Q_{p,ERD}}{Q_{p,noERD}}$ , where  $Q_{p,ERD}$  refers to the permeate flow rate for a system with ERD and  $Q_{p,noERD}$  to a system without ERD. For different leakages percentages, the ratio over recovery rate is shown in Figure 4.6.

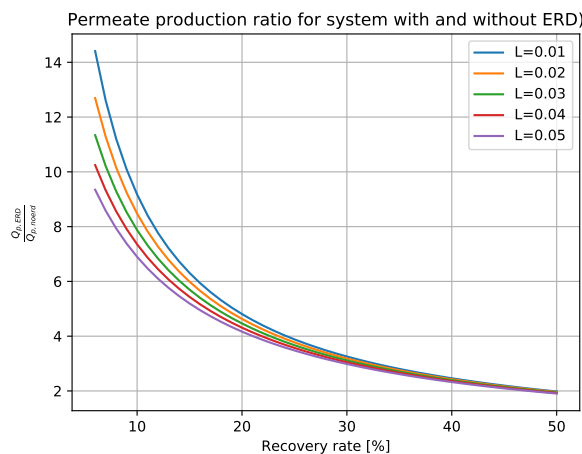


Figure 4.6: The ratio between permeate productions decreases for increasing recovery rate.

From Figure 4.6, it can be concluded that a system with ERD produces a multiple amount of permeate water compared to a system without ERD. Even if both systems have a recovery rate of 50% when using the same high pressure pump (size), the system with ERD can produce up to twice the amount of permeate.

#### Power consumption per produced permeate

Using the obtained results regarding permeate production, the relation for power consumption per produced unit volume of permeate can be determined. This is done using Equations 4.40 and 4.41 as well as the technical data of some of the simulated components (Appendix E). The power consumption is based on the obtained maximum values of produced permeate as shown in Figure 4.5b. This is done such that the obtained values can be compared to reference cases, since for these cases the power consumption is determined based on a constant maximum permeate production rate. A concentration of 32000 PPM is used to simulate the use of seawater.

Table 4.2: Input parameters Power comparison

Parameter	Value	Units
$\omega_{HPP}$	700	RPM
$\omega_{ERD}$	700	RPM
$C_f$	32000	ppm
$\gamma$	10	%

The results between the two systems are presented in Table 4.3. For the determination of the power consumption for a system with an ERD, the power consumption of the ERD is determined. This is done by using the pressure drop measured across the membranes and the (average) pressure drop over the Isobaric pressure exchanger. This is the total differential pressure that the positive displacement pump of the ERD needs to add to the system. A system using an ERD would use 18% of the power that is needed to produce the same amount of permeate without an ERD, according to the numerical model. For the calculations, the power used by auxiliary components like feed pumps and sensors is not considered. In the table, reference values are shown. For both systems, the obtained model values lie in the same order of magnitude. Probable differences might be the use of different component characteristics (like different hydraulic pumps) and the inclusion of auxiliary components.

Table 4.3: Power per produced unit of permeate at 10% recovery rate

	Value	Units
Power consumption system with ERD (model)	3.01	kWh/m <sup>3</sup>
Power consumption system with ERD (iSave Selection Tool, Danfoss)	3.23	kWh/m <sup>3</sup>
Power consumption system without ERD (model)	16.6	kWh/m <sup>3</sup>
Power consumption system without ERD (ROSA [26])	18.62	kWh/m <sup>3</sup>

#### 4.5.2. Varying ERD RPM

Aforementioned in Section 3.2, the hydraulic wind turbine control is based on influencing pressures in the system which affects the torque of the hydraulic pump. This is done to counteract the rotor torque during varying wind speeds, especially in the region below the rated wind speed. In the original design of the hydraulic drive train, influencing this pressure is done using a spear valve in the high pressure line, since that is the only parameter that can be controlled. The combination of the hydraulic wind turbine with Reverse Osmosis and an ERD will result in another parameter that can be controlled; the rotational speed of the ERD. In this subsection, the influence of varying the speed of the ERD on the pressure of the system is investigated.

Looking at Equations 4.30 and 4.32, the velocities of the feed and concentrate flows influence the effective concentration and the osmotic pressure. Using that the feed and concentrate line both have similar areas, Equation 4.32 is rewritten as function of flow rates. Using that the feed flow is a summation of the flow provided by the ERD and the flow provided by the high pressure pump and the relation between concentrate flow and ERD feed flow (Equation 4.26, the following equation (4.42) for the effective concentration  $C_{eff}$  is obtained:

$$C_{eff} = \frac{1}{2}C_f + \frac{1}{2}C_f \left( (1-R) + R \frac{Q_{f,HPP} + Q_{f,ERD}}{\frac{Q_{f,ERD}}{1-L}} \right) \quad (4.42)$$

As the high pressure feed flow of the ERD directly follows the rotational speed, according to the above mentioned equations this influences the effective concentration and osmotic pressure. Combining this result with Equation 4.34, the results shown in Figure 4.7 are obtained. For this, the parameters shown in Table 4.4 are used.

Table 4.4: Input parameters variable ERD

Parameter	Value	Units
$\omega_{HPP}$	700	RPM
$V_p$	$3.5e^{-5}$	$m^3/rev$
$\omega_{ERD}$	500-1000	RPM
$Q_{ERD}$	6-13.6	$m^3/hr$
$L$	1	%
$n_{mem}$	4	-
$A_m$	7.34	$m^2$
$\delta$	0.2641	Pa/ppm K
$a$	0.5	-
$K_w$	$3.02e^{-9}$	s/m
$R$	0.993	-
$C_f$	600 and 32000	ppm
$T_{water}$	10 and 25	$^{\circ}C$

In Figure 4.7, two curves are plotted; one for the case in which the feed concentration is similar to the concentration of the water used at the experimental setup (600 PPM, Figure 4.7a) and one for the case in which seawater is used as a medium (32000 PPM, Figure 4.7b). There is a clear difference in the magnitude of the osmotic pressures between both cases, however in both cases it can be seen that the variation of ERD speed does not influence the osmotic pressure significantly. For the seawater case, the maximum difference is 1.42 bar.

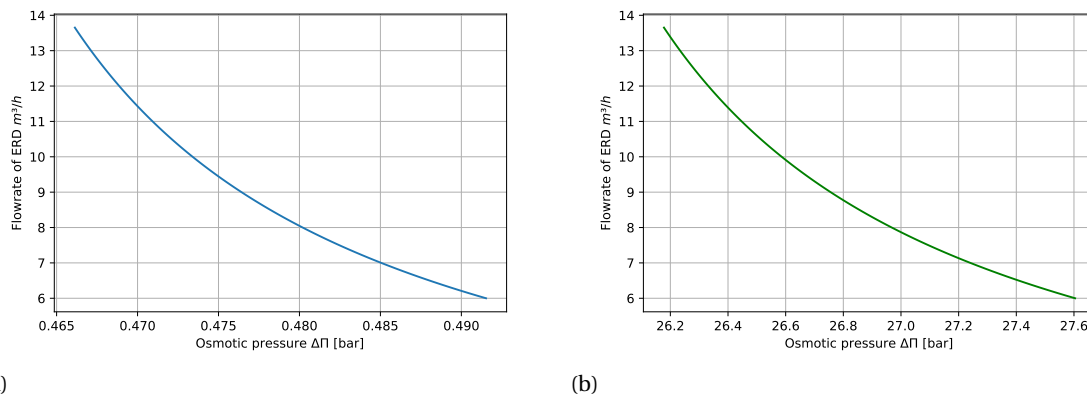


Figure 4.7: Osmotic pressure variation with changing ERD rotational speed for  $C_f = 600$  PPM (left) and  $C_f = 32000$  PPM (right).

Besides having an influence on the osmotic pressure, varying the rotational speed of the ERD influences the recovery rate of the system. This conclusion can be drawn when combining Equations 4.35 and 4.37 and rewrite it for  $\gamma$ . This results in an varying permeate production and this will slightly influence the first term of Equation 4.34. The total system pressure per rotational speed of the ERD for both concentrations is presented in Figure 4.8. Note that in both cases, the maximum ERD speed is chosen at 1000 RPM. This is done to prevent that the total feed flow delivered by both high pressure pump and ERD does exceed the maximum allowed feed flow of the 4 membranes used in the experimental setup, such that realistic values are obtained. The model results for the case with 600 PPM will be compared to the obtained results from the experimental tests, since these tests are done with water having such an amount of particles dissolved.

From the numerically obtained results shown in Figure 4.8, it can be seen that a varying rotational speed of the ERD has a small influence on the total systems' pressures. For the case in which water with a salt concentration of 600 PPM is used, the maximum influence of the ERD on the pressure is approximately 2.5 bar. In case of more saline waters, the ERD is able to affect the pressure by roughly 3.5 bar. As the pump torque is linearly related to the pressure, it can be said that the effect of changing the rotational speed of the

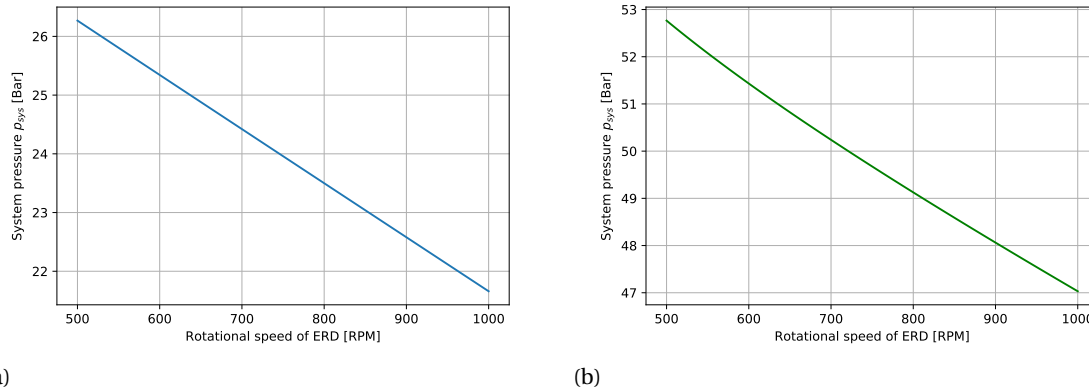


Figure 4.8: Total system pressure variation with changing ERD rotational speed for  $C_f = 600PPM$  (left) and  $C_f = 32000PPM$  (right).

ERD on the pump torque  $\tau_{pump}$  is limited. To be able to draw conclusions regarding torque controllability using the ERD, the experimental results shown in Chapter 5 will be used to validate the numerically obtained results.

## 4.6. Concluding remarks

In this chapter, insight in the working principle of a Reverse Osmosis with an ERD has been given. The obtained results will be compared to experimental tests in the Chapter 5. The results will also be used to combine the system with a theoretical hydraulic wind turbine in Chapter 6.

According to theoretical data and the numerical model, permeate production is linearly related to the high pressure pump rotational speed and flow rate. The amount of produced permeate using an ERD is significantly higher compared to a system that does not include an ERD. Assuming a theoretical maximum possible recovery rate of 50%, nowadays a recovery rate for (large) RO plants, the minimal ratio  $\frac{Q_{p,ERD}}{Q_{p,noERD}}$  equals roughly 2, and increases for decreasing recovery rates. For a recovery rate of 10%, which is approximately the maximum recovery rate of the experimental setup and the used rate for the numerical model, the difference in power consumption is determined to quantify the performance of both desalination systems. For a RO system with ERD, the power consumption for producing a unit volume of permeate is approximately 18% of the power needed to produce the same amount of permeate without an ERD. This matches with results obtained from literature.

Varying the rotational speed of the ERD seems to influence the systems pressure, but does not have a significant effect. A large variation in rotation speed of the ERD results in a computed pressure difference of maximally 3.5 bar. Hence the pump torque is not influenced much. The experimental test results are required to validate these results before conclusions can be drawn.



# Experimental Tests on Reverse Osmosis with an ERD

The numerical model, as discussed in Chapter 4, is based on theoretical data and assumptions. As a result of this, a difference in obtained results between the model and the physical world is likely to exist. Therefore, an experimental test setup is designed to validate the obtained model results. Reverse Osmosis is a well known technology, for systems without an ERD the results are straightforward and the technology is proven. Supper [27] provided results showing the behaviour of an RO system without ERD on varying inputs, both obtained numerically and experimentally. Therefore, the experiments done in this thesis only focus on the system with an ERD. In this chapter, first the test setup concept and design will be discussed. Secondly, the tests are elaborated on. The setup is designed to test the behaviour of the system for varying high pressure pump rotational speeds as well as varying angular velocities of the chosen Energy Recovery Device. These results will be compared to the numerically obtained results to draw conclusions. More detailed information about each of the used components, the test plan describing the tests carried out and images of the test setup can be found in Appendix C.

## 5.1. Test Setup Overview

The purpose of the experimental test setup is to determine the influence of an Energy Recovery Device on the permeate production and on the RO-systems flows and pressures. Also, the extent to which varying rotational speeds of the HPP will affect the production rate of permeate is evaluated. The test setup is named MicRODOT, which is based on the acronyms Micro (or small), RO (Reverse Osmosis), and DOT (referring to the name of the company Delft Offshore Turbine). A preliminary design of the MicRODOT setup was done before the start of this thesis, meaning multiple components were already chosen and purchased. These components are considered and taken into account for the design of the test setup. A selection of circumstances prevented testing with salt water during the course of this thesis. However, for future testing, it is known that components are going to be in contact with seawater and therefore need to be corrosion resistant.

The MicRODOT setup is designed in such a way that it can be used for multiple different projects. The design was done considering two configurations; one for water production with an ERD and one for centralised electricity production using two spear valves and a Pelton Turbine. Via a network of hoses and valves, the water coming from the hydraulic high pressure pump is transported. By using manual valves, flows are directed in such a way the setup can be used for both configurations. In Appendix A, a detailed hydraulic diagram of the total setup is shown. Note that for future studies, it is possible to also use the setup for simultaneous water and electricity production. The use of the spear valve and Pelton turbine is outside the scope of the experiments and this thesis.

The wind turbine is represented using a combination of an electric motor and a hydraulic pump. With a rotor model, a theoretical wind field can be used to simulate the wind turbine. For the experiments done, however, the electric motor is controlled manually. By measuring the pressure after the hydraulic pump, the torque on the rotor can be calculated. Since the theoretical wind turbine rotor speed and torques are different from

the experimental setup speed and torque, a scaling ratio has to be applied, as is also done in the numerical model. This will be discussed in Chapter 6.

Figure 5.1 shows an overview of the MicRODOT test setup. In there, the three main components are numbered; 1 denotes the high pressure pump, 2 is the iSave Energy Recovery Device and 3 denotes the RO-membrane configuration. In Section 5.2, the components and their functions are elaborated in more detail.



Figure 5.1: Overview of the MicRODOT test setup.

## 5.2. Components

In this section, the components used in the MicRODOT test setup are briefly discussed. In Appendix E, a more detailed description and specifications of each component are given.

### 5.2.1. High Pressure Pump

The setup consists of three main components, starting with the high pressure pump connected to a electric motor, shown in Figure 5.2. The pump-motor combination is used to simulate the DOT wind turbine. The DOT concept requires a positive displacement pump to easily produce high pressure flows, wherefore the test setup makes use of such a type of pump as well. The high pressure pump used is a bidirectional axial piston pump being able to provide a flow of up to  $3.6 \text{ m}^3/\text{hr}$  at a maximum rotational speed of 1500 RPM, assuming a minimal volumetric efficiency of 70% at low RPMs, based on the efficiency map made in Appendix C. The pump is able to provide larger flows at higher speeds, but the speed of this system is limited by the maximum rotational speed of the electric motor, which is 1500 RPM.

### 5.2.2. Reverse Osmosis System

The Reverse Osmosis system contains two main components; the Energy Recovery Device and the RO membranes. The Energy Recovery Device used is the iSave 21 Isobaric Energy Recovery Device, as is explained in Section 2.4 and shown in Figure 5.3 as it is installed in the MicRODOT setup. The iSave can be used in setups having concentrate flows of minimally  $6 \text{ m}^3/\text{hr}$ . A minimum of four DOW FILMTEC SW30-4040 membranes are required (hence installed) in a parallel configuration to meet these flow specifications, This configuration is shown in Figure 5.4. According to the membranes' specifications (Appendix E), each membrane has a feed flow limit of  $3.6 \text{ m}^3/\text{hr}$ . Considering their approximate recovery rate of 8 to 10%, a maximum total theoretical concentrate flow rate of around  $13 \text{ m}^3/\text{hr}$  can be realised. A maximum permeate flow rate of around  $1.3 \text{ m}^3/\text{hr}$  is possible using this configuration. Due to the lower maximum flow rate of the boost pump that provides feed water for the ERD ( $8.4 \text{ m}^3/\text{h}$ ), the maximum flow rate of the ERD is limited to that maximum flow and therefore both the maximum concentrate and permeate flow rates of the total system are lower than the maximum flows of the RO membrane configuration.

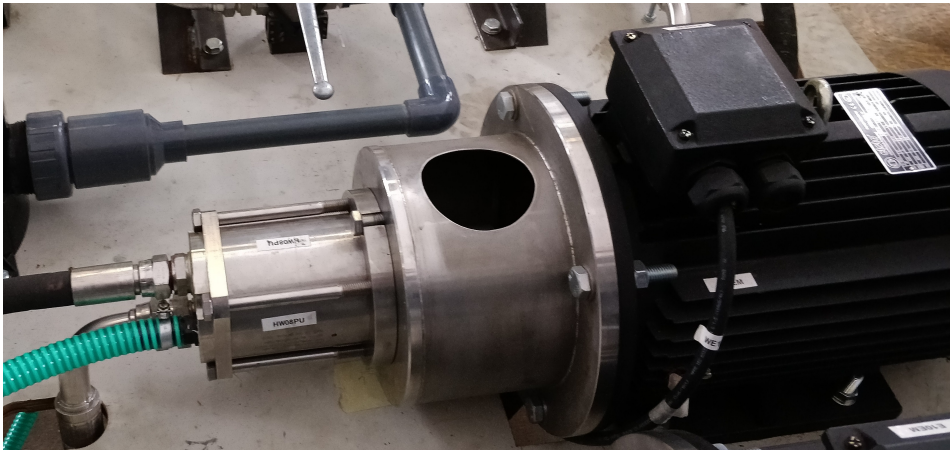


Figure 5.2: The high pressure pump (left) representing the wind turbine, connected to an electric motor using a ROTEX coupling.



Figure 5.3: The iSave ERD as it is installed in the MicRODOT test setup.



Figure 5.4: The RO setup, showing 4 membranes installed in pressure vessel in a parallel configuration.

### 5.2.3. Auxiliary Components

#### Boost Pumps

To feed the high pressure pump and the iSave ERD, two centrifugal boost pumps are used. Due to the design of the system and the RO-systems characteristics, the iSave ERD requires a significantly higher feed flow. Therefore, two different pump are used. One being able to provide up to  $8.4 \text{ m}^3/h$ , feeding the ERD and one having a maximum flow of  $3 \text{ m}^3/h$ , feeding the high pressure pump. The inlet pressure of the high pressure pumps requires to be 3 bar, this to provide sufficient inlet of the pump chambers.



Figure 5.5: The setup has two boost pumps. The left boost pump is the large pump, feeding the ERD. The right pump feeds the High Pressure pump.



Figure 5.6: Cintropur  $10 \mu\text{m}$  filter(left) and EWP-USA  $3 \mu\text{m}$  filter (right).

#### Water Filters

To maintain a safe and proper operation, the ERD and the hydraulic pump both have a limit in allowable particle sizes flowing through. For the ERD, the dictated particle size is  $3 \mu\text{m}$ , for the hydraulic pump this is  $10 \mu\text{m}$ . To achieve that, in both feed lines a filter is installed.

#### Hydraulic Components

In Figure 5.1, a large network of hoses and piping can be seen, where different types of hoses can be distinguished. For water lines at atmospheric pressures, green suction hoses are used. The low pressure system design contains a small amount of PVC piping, which is manufactured in-house. Most of the network however, both low and high pressure, is made of black pressure hoses, designed and manufactured by an external certified company and able to withstand pressures up to 100 bar, far beyond the maximum allowable pressure of most components.

To prevent that pressures exceed components pressure limits, pressure relief valves are installed both in the low and high pressure lines for safe operation. Possible causes of a sudden increase in pressure are i.e. clogged filters. Since people operate the system, wrongly closed valves due to inattention might also be a cause. A second measure for safe operation is an electrical valve installed in the high pressure line. In case of an emergency stop, this valve will instantly open such that pressure can be released from the system.

### Electrical System

To power and control the MicRODOT setup, an electrical cabinet is specially designed for this setup. All components in the setup are controlled by a Programmable Logic Controller, or PLC. The motors and pump are controlled by a Variable Frequency Drive (VFD), one for each. The PLC reads out the signals input coming from the sensors, the VFD received these signals from the sensors and in that way can control the specific component. In Appendix F, the design of the electrical cabinet and the electrical wiring diagram can be found.



Figure 5.7: The electrical cabinet, containing the electrics and control hardware.

#### 5.2.4. Sensors

To obtain results from the setup, several flow, pressure and temperature sensors are being used. In Section 5.4 below, a schematic overview is shown in which all sensors are denoted. The flow sensors are used to determine the important flow rates; the input flow of the hydraulic pump, the input flow of the ERD and the permeate flow. For economic reasons, it is chosen to only use flow meters in the low pressure lines, since they are significantly cheaper. Given the high pressure flows are functions of the low pressure input and output flows and the leakages of the pumps are measured and/or known, the high pressure flow rates can be determined.

The pressure sensors are installed in both the low and high pressure lines and are used for both system security and obtaining test results. As aforementioned, the system makes use of hardware to prevent a pressure overload. By constantly monitoring the pressure in the control software, an emergency stop can be triggered in case of such an overload. The temperature sensors are used to monitor temperature changes of the water. This can i.e. indicate dry running and/or overheating pumps.

#### 5.2.5. Data Logging

Data is obtained both digitally and analog. Motor rotational speeds are based on input power frequencies and the characteristics of the motor. By sending a digital signal from the software, via the PLC to the motor, the rotational speed of the motor is set. The installed sensors send an analog signal to the PLC, for each sensor in the system the sampling time is 20ms, meaning the sensors obtains 50 data points every second. Using TwinCat, the system can be controlled and sensors signals can be read. With Scopeview, the sensors signals can be logged and saved for further processing.

### 5.3. Test Setup Working Principle

The previous section described the components used in the experimental test setup. Here, in short the working principle of the setup is explained. A schematic overview of the setup is shown in Figure 5.8.

Feed water is stored in a large tank, which can hold up to  $0.7 \text{ m}^3$ . The two used boost pumps are self priming pumps, meaning they are able to suck up the water from the tank. One boost pump provides the feed flow for the positive displacement pump, while the other feeds the ERD. The high pressure pump represents the wind turbine. Its rotational speed can be adapted to simulate variations in (wind) inputs. The ERD is used to recover the energy stored in the high pressure concentrate flow from the RO process. At the inlet of the RO-module, which is the configuration containing the 4 RO membranes, the high pressure feed flow of both the high pressure pump and the ERD are combined to end up with one total feed flow for the membranes. The permeate produced by the RO membranes is shortly stored in a permeate tank. As aforementioned, the high pressure concentrate stream coming from the membranes contains a large amount of unused energy. This flow is used to pressurise the low pressure feed water stream of the ERD, which was provided by the boost pump. While the feed water becomes pressurised by the Pressure Exchanger ERD, the concentrate flow loses its hydraulic pressure, after which it is collected in a separate concentrate tank. After measuring the concentrations and salinities from both the concentrate and permeate tanks, the water of both tanks is pumped back into the feed water tank using two submersible pumps. In this way, a closed loop water system is created, such that most water is reused. On top of that, by mixing both the highly saline concentrate and the permeate with the feed water, the total salinity of the feed water remains constant.

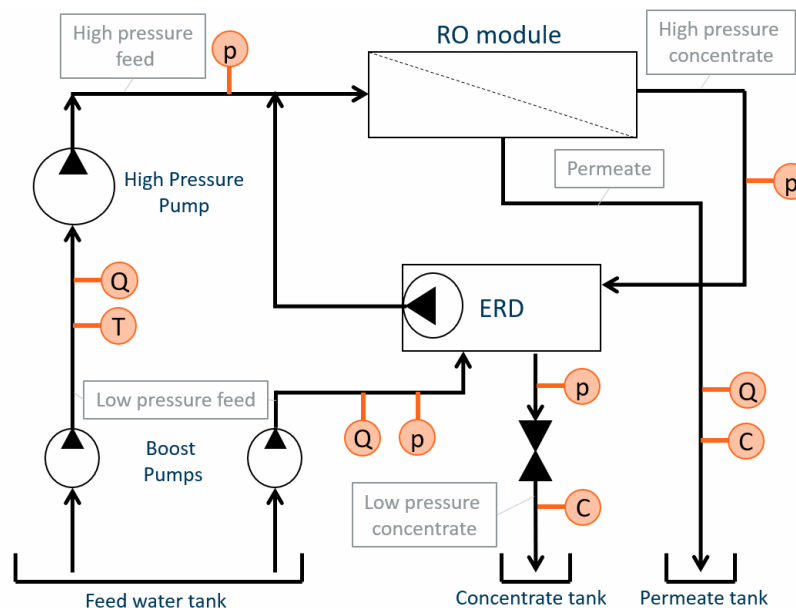


Figure 5.8: Schematic overview showing sensor locations.

### 5.4. Experimental Test Results

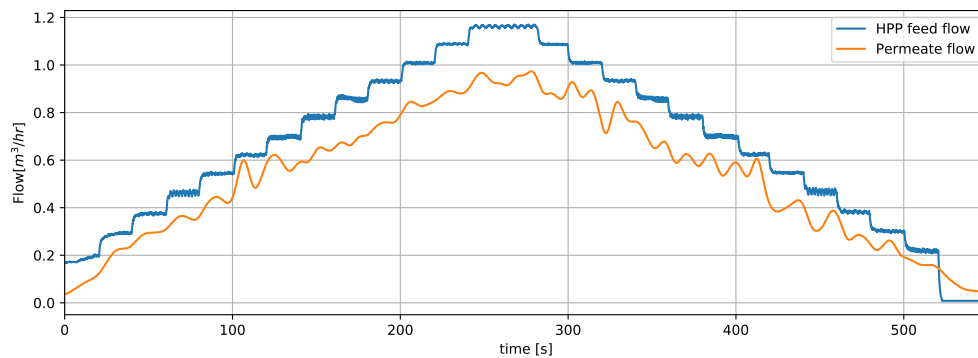
The goal of this section is to present the experimental test results and compare the results to the numerically obtained results. First, the permeability coefficient is determined. This value is used in the numerical model. Then, the steady state tests and results will be elaborated. In Figure 5.8, a schematic overview of the setup including the locations of the sensors is shown. Here,  $T$  denotes a temperature sensor,  $Q$  a flow sensor,  $p$  a pressure sensor and  $C$  the location where the salt concentration is measured. For the tests, the rotational speed of the high pressure pump and the ERD are the two variables that can be influenced. Two different types of tests will take place, the first focuses on varying the rotational speed of the high pressure pump while keeping the ERD at a constant speed, the second test type will focus on varying the rotational speed of the ERD, while having the high pressure pump rotate at a constant speed.

### 5.4.1. RO Membrane Permeability Coefficient

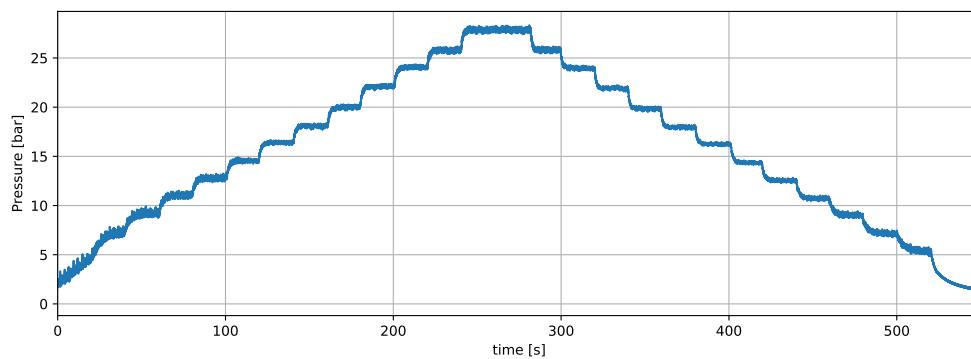
The permeability coefficient is a membrane specific coefficient and depends on the systems parameters and settings, like pressure, recovery rate, water temperature and salt concentration. The equation to determine the permeability coefficient can be found in Section 4.1, Equation 4.6. Due to the large amount of dependent variables, the coefficient is often determined and obtained experimentally. For this, use of Equation 4.29 is made. For the determination of the coefficient, fresh water with a concentration of 600 PPM is used. The value obtained using the experiments will be compared to values found in literature and to the value obtained using ROSA 9, a program used to design a Reverse Osmosis system in which the used variables like salinity, permeate production and recovery rate can be implemented [26].

Table 5.1: Test parameters for determining the permeability coefficient

Parameter	Value	Units
$\omega_{HPP,max}$	700	RPM
$\Delta\omega$	50	RPM
$\omega_{ERD}$	700	RPM
$C_f$	600	ppm
$T_{water}$	10	$^{\circ}C$



(a) Hydraulic pump and permeate flow rate.



(b) System pressure.

Figure 5.9: Experimental results, used to determine permeability coefficient of the membrane.

As can be seen from Figure 5.9a, the permeate flow rate more or less follows the step function of the high pressure pump. This results in a pressure build up in the system following this same step function. To be able to determine a representable value for  $K_w$  using the data from Figures 5.9a and 5.9, the data between  $t = 50s$  and  $t = 300s$  is used. In Figure 5.10, obtained permeability coefficient over time is shown, as well as a mean value. Due to variations of the system over time (for example small changes in concentrations/temperatures),

the coefficient over time is never a constant. However, for model calculations, a constant value is used. The obtained mean value of the permeability coefficient is  $3.43e^{-9}$  s/m. This is in the same order of magnitude compared to the values acquired using ROSA and literature, shown in Table 5.2.

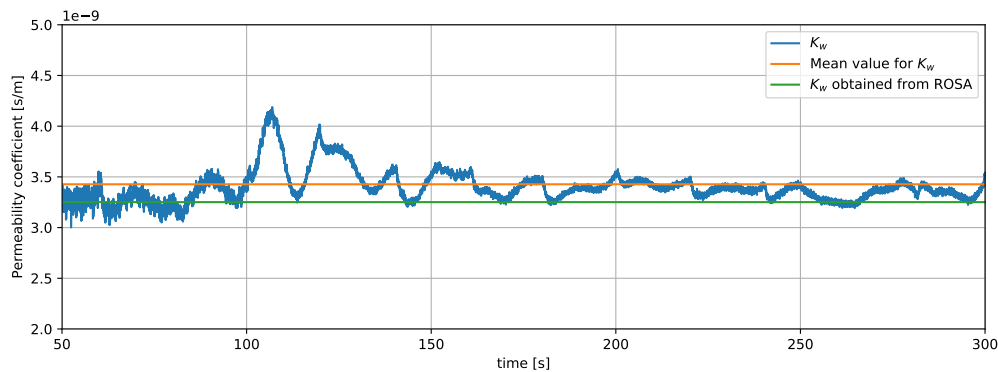


Figure 5.10: Permeability coefficient.

Table 5.2: Permeability coefficients

Source	Value	Units
Experimental tests	$3.43e^{-9}$	s/m
ROSA	$3.25e^{-9}$	s/m
Lu et al. [28]	$3.1e^{-9}$	s/m
Bartman et al. [29]	$9.7e^{-9}$	s/m

#### 5.4.2. Varying HPP RPM - Experimental Results and Model Validation

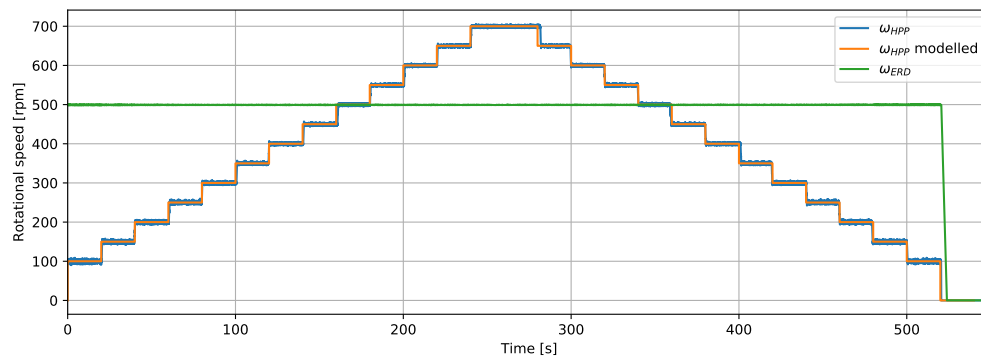
For a seawater Reverse Osmosis System with an ERD, two parameters can be controlled; the rotational speed of the hydraulic pump and the rotational speed of the ERD. Computed results of this are shown in Chapter 4. To validate these results, the following two sections describe the experimental tests in which these variables are controlled, starting with the speed of the hydraulic pump. The test parameters used are shown in Table 5.3. The parameters that will be obtained from the tests are the system pressure  $p_{sys}$  and permeate flow rate

Table 5.3: Test parameters - Varying HPP RPM

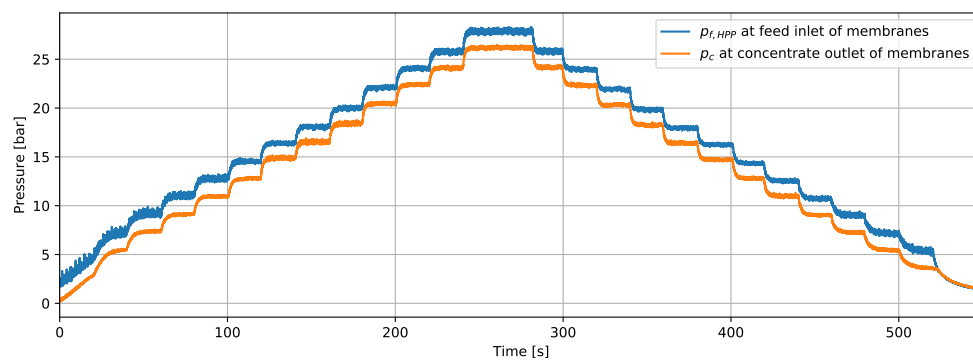
Parameter	Value	Units
$\omega_{HPP,max}$	700	RPM
$\Delta\omega$	50	RPM
$\omega_{ERD}$	500	RPM
$C_f$	600	ppm
$T_{water}$	10	$^{\circ}C$

$Q_p$ . Using these parameters, the assumed working principle of the system with ERD can be validated. In Figure 5.11, a comparison between the experiments and the part of the numerical model covering the results of the system with ERD is shown. As the RO system without an ERD is already repeatedly been studied, validation of such a system without ERD is not incorporated into this thesis.

The results depicted in the Figure 5.11 show the influence of the increasing rotational speed on the system pressure. From the numerical model, it was expected that the pressure increase would follow the same step function as the rotational speed of the hydraulic pump. From Figure 5.11a, at lower pressures, the pressure behaves a little different and does not fully follow the step response. One of the reasons for this is the fact that the used hydraulic pump is designed to perform best for rotational speeds of 500 RPM and higher. Therefore, at speeds well below this speed, the pump will not perform optimally. On top of that, at low



(a) Hydraulic pump and ERD RPM.



(b) System pressure.

Figure 5.11: Comparison of experimentally obtained pressures with numerical model prediction.

rotational speeds and pressure hardly any water leaks through the pumps seals, a higher percentage of low pressure feed water is pressurised resulting in a relatively higher pressure per RPM. At higher pressures, the leakage flow increases leading to system pressure comparable to the values obtained from the numerical model. The volumetric efficiency of the high pressure pump is determined empirically per RPM of the pump and pressure of the system, and can be found in Appendix C, Section C.3. The used assumption that water is incompressible can be verified using the figures. As the flow increases, the pressure instantly increases, with hardly any delay.

The modelled permeate flow rate is compared with the obtained tests results, as can be found in Figure 5.12. The difference in flow rate between the high pressure pump flow and the permeate production is as given by Equation 4.35. As can be seen from Figure 5.12, this approximation seems to be accurate. The produced permeate is shown as a mean value per time step. The modelled permeate production approached the mean values of the experimental test data. At both low and high feed flows, the permeate production linearly follows the feed flow, from which can be concluded that the efficiency of the membranes is not negatively influenced by different and varying feed inputs hence rotational speeds of the high pressure pump. On top of that, the graph confirms the assumptions made for the model, in which this linear relation was expected to occur. The slight difference between the obtained experimental results and the results from the numerical model are mostly a result of the nonlinearities of the RO membranes, that are not accounted for in the model. On top of that, the actual specification of the membranes can slightly vary from the theoretical values given by the manufacturer.

The relation between the rotational speed of the high pressure pump and the feed flow and permeate flow is proportional. From Equation 4.34 as well as Figure 5.11 it can be seen that this results in a linear relation between system (pump) pressure. This results in a linear relation between the rotational speed of the high pressure pump and the pump torque. In Figure 5.13 this is shown, based on the experimental data obtained.

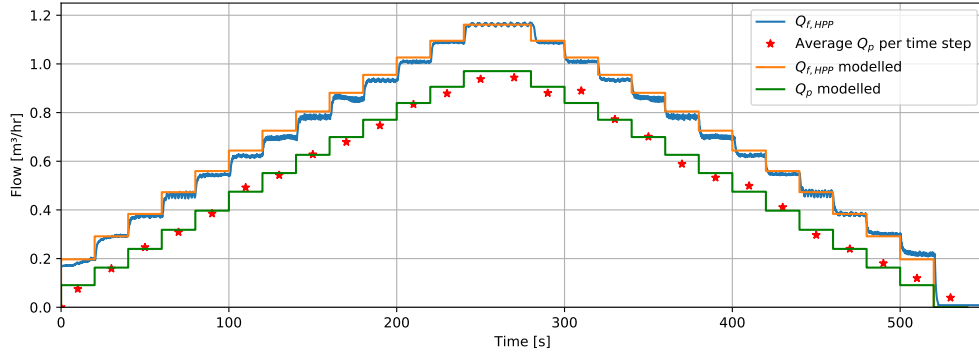


Figure 5.12: Permeate flow comparison between model and experimental results.

This will be further used in Chapter 6, in which the RO system with the ERD is combined with a hydraulic wind turbine.

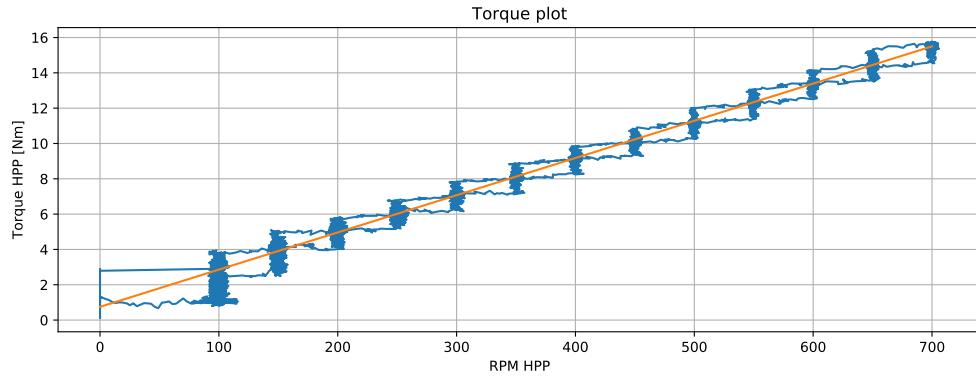


Figure 5.13: Permeate flow comparison between model and experimental results.

In Table 5.4, a comparison of the obtained results between the model and the experimental tests is numerically shown. From this table, it can be seen that the expected maximum flow rate of the high pressure pump,  $Q_{HPP,max,model}$ , matches the maximum flow rate of the tests,  $Q_{HPP,max,test}$ . The permeate flow obtained from the experiments,  $Q_{p,max,test}$ , slightly differs from the numerically determined values,  $Q_{p,max,model}$ , with a difference of around 1% between the model and experiments. This is due to the difference in the modelled leakage rate of both the ERD and the high pressure pump, for more accuracy these leakage rates have to be determined in more detail. The maximum pressure obtained from the model and the experiments is approximately 0.1 bar. From the comparisons, it is concluded that the model can obtain representative results. Using the model to simulate these kind of tests, the predicted flow rates and pressures can be accurately obtained.

Table 5.4: Obtained experimental results for varying HPP rpm

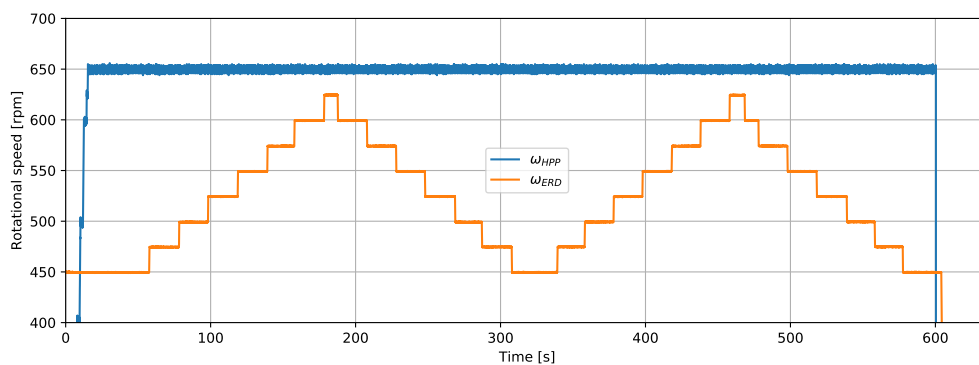
Parameter	Value	Units
$Q_{HPP,max,test}$	1.16	$m^3/h$
$Q_{p,max,test}$	0.96	$m^3/h$
$p_{sys,max,test}$	27,8	bar
$Q_{HPP,max,model}$	1.16	$m^3/h$
$Q_{p,max,model}$	0.97	$m^3/h$
$p_{sys,max,model}$	27.9	bar

### 5.4.3. Varying ERD RPM - Experimental Results and Model Validation

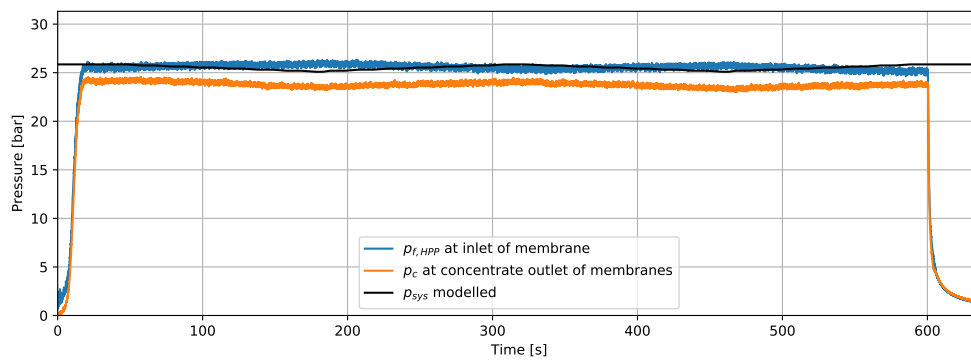
Here, the variation of the ERDs' rotational speed is discussed and its influence is shown by the means of some experiments. In Chapter 4 it is explained that the ERD influences the recovery rate of the system. On top of that, based on the model results, a slight variation in system pressure for different angular velocities is expected. This will be verified using the test results. In Figure 5.14, the results of one of the tests are shown.

Table 5.5: Test parameters - Varying ERD RPM.

Parameter	Value	Units
$\omega_{HPP}$	650	RPM
$\omega_{ERD}$	450-625	RPM
$\Delta\omega_{ERD}$	25	RPM
$C_f$	600	ppm
$T_{water}$	10	$^{\circ}C$



(a) Variation of the rotational speed of the ERD (orange) with constant pump speed (blue)



(b) System pressure for varying rotational speed.

Figure 5.14: Comparison of experimentally obtained flow rates with numerical model prediction.

An increase of ERD rotational speed result in a slight increase in system pressure at the feed inlet of the membrane, whereas it results in a small decrease of pressure at the concentrate outlet of the membrane, as can be observed from Figure 5.14b. At a rotational speed of the ERD 450 RPM, the pressure at the membranes concentrate side is close to 24 bar. As the rotation speed of the ERD increases, the pressure on the concentrate side decreases, however, the maximum drop in pressure is around 1 bar resulting in a pressure of 23 bar at 625 RPM of the ERD. Comparing the results from Figure 5.14b to the results obtained from the model, which is shown by the black line in the graph, an opposite reaction in the variation of the system pressure is observed.  $p_{sys}$  in the model refers to the inlet pressure. Where it was expected that the system pressure would decrease for increasing rotational speed of the ERD, the opposite occurs in the experimental tests. The cause of this divergence is based on an assumption made in Chapter 4, when Equation 4.28 is defined.

There, it is said that the pressure drop over the membranes can be neglected, such that  $\Delta p$  equals  $p_{sys}$ .  $\Delta p$  referred to the difference in hydraulic pressure between the concentrate flow and the permeate flow. Taking this into account, and noticing that a pressure drop over the membrane does exist as can be seen from the difference between the inlet and outlet pressure in Figure 5.14b, the results seem to fit the expectations and  $p_{sys}$  equals the pressure at the membranes' concentrate outlet. The small pressure increase at the inlet of the membranes occurs due to the increase in losses in the membrane as well as the increase in pipe friction and efficiency losses with increasing flow. This behaviour is not yet accounted for in the model.

As the rotational speed of the ERD determines the high pressure flow rate of the ERD, changing the rotational speed will result in a change in total feed flow to the membranes. According to the relations given in Equations 4.37 and 4.38, a changing ERD high pressure feed flow (and thus total feed flow) results in an alteration in feed concentration. From the model results however, hardly any change in permeate production was expected. The experimental results as given in Figure 5.15 confirmed these expectations, as the permeate flow rate over time is not visually affected.

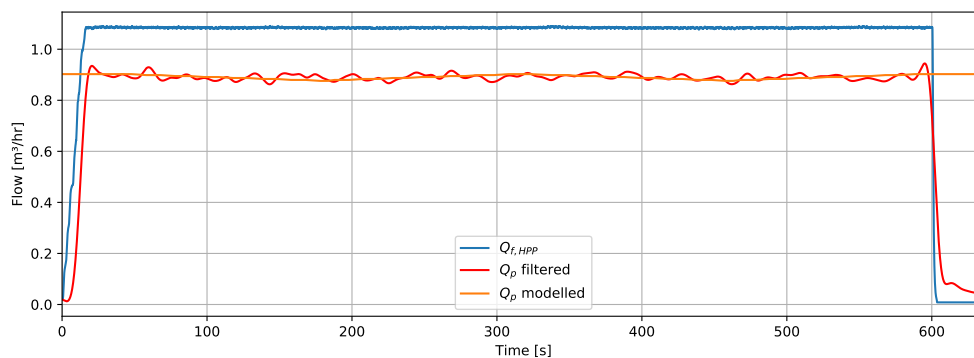


Figure 5.15: Permeate flow comparison for varying ERD speeds.

In Table 5.6, a comparison of the most important obtained results from the model and the experimental tests is numerically shown. As can be seen, the mean maximum permeate production computed by the model,  $Q_{p,mean,model}$ , and obtained from the the experimental tests,  $Q_{p,mean,tests}$ , are similar. A difference of approximately 1.1% between the two results can be distinguished. The system pressure obtained from the model differ from the experimental tests. For the results, the system pressure computed using the model,  $p_{sys,model}$ , can be best compared to the pressure of the concentrate line from the experimental tests,  $p_{cond,test}$ , since this pressure varies following the same pattern. The difference in pressure pattern is previously explained in this section. In the model, the pressure drop over the membrane was assumed to be negligible, while in fact a small pressure drop can be seen. This explains the difference in pressures. By determining the exact pressure drop of the membrane at different flows and pressures, this can be accounted for in the model to obtain better matching results.

Table 5.6: Obtained experimental results for varying ERD rpm

Parameter	Value	Units
$Q_{p,mean,test}$	0.88	$m^3/h$
$p_{sys,min,test}$	25.48	bar
$p_{sys,max,test}$	25.90	bar
$p_{conc,min,test}$	23.50	bar
$p_{conc,max,test}$	24.18	bar
$Q_{p,mean,model}$	0.89	$m^3/h$
$p_{sys,min,model}$	25.07	bar
$p_{sys,max,model}$	25.85	bar

#### 5.4.4. Influence of Salinity

As aforementioned, the tests are conducted using water with a low salt concentration of around 700 PPM (parts per million), which is approximately the same as fresh water from the tap. Due to some unforeseen circumstances, it was not possible to use salt water. In this subsection, a short explanation is given on the differences in results if (more) saline water was used. Salt water means more dissolved solids. The salt concentration (also known as Total Dissolved Solids, or TDS) of seawater is approximately 35000 PPM [12]. With more solids in the water, the higher the osmotic pressure is. This means that the minimum pressure needed to desalinate water via reverse osmosis becomes higher. As a comparison, the osmotic pressure for water with 700 PPM TDS is around 0.5 bar, whereas for water having 35000 PPM TDS the osmotic pressure lies around 25 bar.

The results obtained from the tests explained in Subsections 5.4.2 and 5.4.3 will be evaluated based on this knowledge, starting with the tests for varying rotational speeds of the high pressure pump. In these tests results, it can be seen that permeate water is immediately being produced when the high pressure pump starts rotating. At that moment, the pressure of the system is barely 2 bar, meaning the osmotic pressure is overcome. In fact, a small amount of permeate is being produced when only the ERD is rotating, since the pressure at that time is already around 1.5 bar, well above the osmotic pressure for water having 700 PPM TDS. When the water is more saline, it would be seen that permeate is not directly being produced when the high pressure pump is turned on. However, the system' pressure would rise towards the values of the osmotic pressure in a very short time, at very low rotational speeds of the pump. At that point, even at low rotational speeds and flow rates, permeate is being produced while the pressure in the system is already 25 bar. Basically, the biggest difference in results would be the operating pressure, which would shift upwards approximately with the value of the osmotic pressure. The maximum pressure of the system with the same permeate production will then lie around 60 bar. Secondly, the amount of TDS in the permeate water would be a little higher, since with increasing salinities, the salt rejection will go down. This was also explained in Section 2.3 and shown in Figure 2.6a.

For the second test discussed in Subsection 5.4.3, in which the influence of a varying rotational speed of the ERD is discussed, a small difference in pressure variation can be observed, shown in Figure 5.14b. The variation of the pressure for varying rotational speeds was explained in Section 4.5.2 and depicted in Figure 4.7 for different amounts of TDS. As concluded, a higher amount of TDS resulted in a larger variation in pressure. However, even for the highest TDS case of 32000 PPM, the pressure difference between highest and lowest system pressure will be around 3 bar, compared to 1 bar for the 700 PPM case. The total operating pressure at higher salinities is higher and lies around 60 bar, instead of 25 to 30 bar.

## 5.5. Concluding Remarks

By doing experimental tests, the working principle of the ERD as it was assumed to work was confirmed. The numerically obtained results were compared to the experimental results, showing large similarities.

First, the influence of a varying rotational speed of the high pressure pump was investigated. This showed that a variation in rotational speed, hence varying high pressure feed flows and pressures, has no significant effect on the performance and efficiency of the Reverse Osmosis system. The permeate flow rate instantly follows the increase or decrease in high pressure feed flow. This confirmed the numerical model, in which a similar effect could be observed. The test also confirmed the behaviour of the system with ERD as predicted. Since hardly any information regarding the total systems behaviour was available in literature, the modelled results had to be compared to real life tests to be verified.

Second, the rotational speed of the ERD was actively controlled, to see how a change in RPM would influence the RO system. From these experiments, a slight variation in pressure at the inlet and outlet of the membrane can be observed. This pressure change is a result of a small variation in the osmotic pressure that occurs when the rotational speed hence high pressure outlet flow of the ERD is changed. This outcome was also predicted by the numerical model. Now that it is seen that the ERD hardly affects the system pressures, a control strategy for pump (torque) control with only an ERD does not seem to be suitable. For a setup in which a hydraulic turbine is combined with Reverse Osmosis, as was discussed in Section 3.3, the RO with ERD system can not fully replace the spear valve. Future research into adding a spear valve to the RO system with an ERD in order to control the high pressure pumps' torque is necessary.

# Wind Driven Reverse Osmosis with an ERD

The combination of an Hydraulic drive train wind turbine with a Reverse Osmosis system has not been commercialised yet. Some research in combining Reverse Osmosis with sustainable (fluctuating) energy sources has been done, for example by Supper in his MSc. thesis [27]. The implementation of an ERD in research however has not been done yet. In Chapter 4, the results for a Reverse Osmosis system with an ERD are shown. These results are compared and verified in Chapter 5. In this chapter, the Seawater Reverse Osmosis (SWRO) system will be combined with the hydraulic drive train wind turbine principle. First, the model will be explained and the results will be shown, after which conclusions regarding system stability and performance can be drawn. In Appendix B the used parameters are shown.

## 6.1. Wind Turbine Design

The model from Chapter 4 is based on characteristics of the components used in the experimental setup. The system limits, regarding permeate production and system pressures are shown in that chapter as well. In this chapter, a wind turbine will be designed that is based on these limits. Besides that, turbine characteristics of the DOT500 [20] hydraulic turbine will be used. This turbine is a 500kW hydraulic redesign of a Vestas V44 600kW wind turbine [30]. In Figure 6.1 the  $C_p$  and  $C_t$  curves are given at a fixed pitch angle of the blades at  $0^\circ$ .

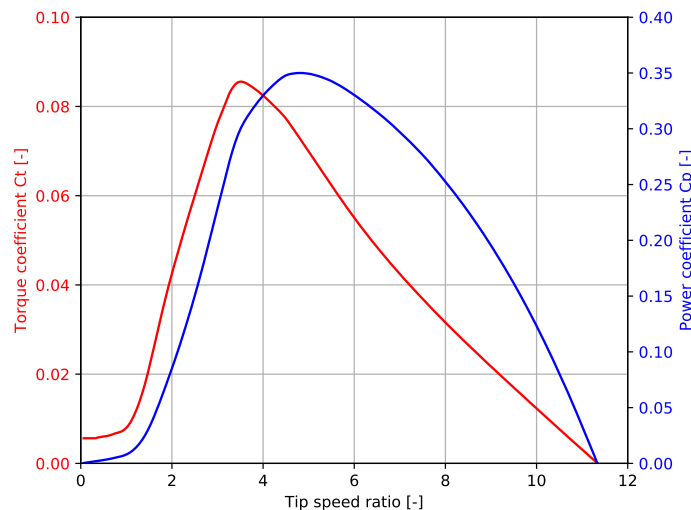


Figure 6.1: Torque and power coefficient of the DOT500 wind turbine.

The turbine design is based on the selected pump used in the experimental setup, of which the flow rate and rotational speed are known. For the setup with the ERD in place, the resulting permeate productions are now known as well as the influence of this permeate flow on the systems pressure. For a proper wind turbine design, the operating limits of both the membranes and the wind turbine should be considered as well as the

minimum pressure needed for reverse osmosis to happen; the osmotic pressure. For the used membranes, the maximum pressure is 69 bar. For the turbine, a maximum allowed tip speed  $v_{tip}$  of 80 m/s is considered [31]. For this system, the salt concentration of seawater is used, equal to 32000 PPM. For this concentration, the osmotic pressure is around 25 bar. To simplify the system model, some assumptions have been made:

- ERD Leakage ( $L$ ) neglected, thus  $Q_{HPP} = Q_p$
- $\Delta p$  across membranes = 0
- Shaft between rotor and pump is rigid
- Constant rotational speed of ERD

The most important parameter that links the Reverse Osmosis system to a hydraulic wind turbine, is the pump torque  $\tau_{HPP}$ . This torque is dependent on the flow provided by the high pressure pump at a certain rotational speed and the amount of permeate that is produced, following from Equation 3.12. To determine the maximum pump torque, the maximum allowed membrane pressure and the maximum flow rate of the hydraulic pump at which the membranes permeate limit is reached, is used. These limits, as well as all the input variables used in this model, can be found in Table B.1 in Appendix B.

The maximum allowed pump torque and maximum pump power are determined first. The torque is based on the maximum flow provided by the high pressure pump at 750 RPM and its volumetric displacement, the power can be found using the flow and the maximum allowed pressure of the membranes.

$$\tau_{HPP,max} = Q_{f,HPP,max} V_p \quad (6.1)$$

$$P_{HPP,max} = Q_{f,HPP,max} p_{mem,max} \quad (6.2)$$

The rotational speed of 750 rpm is chosen such that the provided flow of the high pressure pump is approximately similar to the maximum produced permeate flow. For this model, it is assumed that the leakage percentage of the ERD is 0, resulting in the relation  $Q_{f,HPP} = Q_p$ , as can be obtained used Equation 4.35. The maximum power of the pump is used to determine a rotor size for the wind turbine. This is done by rewriting Equation 3.2 and using characteristics of the DOT500 turbine [20]. The power and torque coefficient over the tip speed ratio of this turbine are shown in Figure 6.1 for a fixed pitch angle of 0°. The definition of the Rotor radius is given by Equation 6.3.

$$R_r = \sqrt{\frac{P_{HPP,max}}{0.5 C_{P,max} \rho_{air} \pi U_{rated}^3}} \quad (6.3)$$

Here,  $C_{P,max}$  is the maximum power coefficient,  $\rho_{air}$  is the density of air and  $U_{rated}$  is the wind turbines' rated wind speed. with this rotor radius, the maximum rotational speed of the rotor can be obtained using Equation 6.4.

$$\omega_{r,max} = \frac{v_{tip,max}}{R_r} \quad (6.4)$$

Where  $v_{tip,max}$  refers to the maximum tip speed of the wind turbines' blades, taken as 80 m/s to minimalise erosion at the blades edge. [31]. The maximum rotational speed of the rotor does not directly match the maximum possible rotational speed of the pump. To match these, a ratio is used. This ratio will be important to link the aerodynamic torque of the rotor to the torque of the pump:

$$n_{turb} = \frac{\omega_{HPP,max}}{\omega_{r,max}} \quad (6.5)$$

The torque graph of the designed wind turbine can be obtained using the wind speeds between the cut in wind speed and the rated speed:

$$\omega_r = \frac{\lambda U_{wind}}{R_r} \quad (6.6)$$

$$\tau_{aero} = \frac{1}{2\lambda^3} \rho_{air} \pi R_r^5 \omega_r^2 C_p \quad (6.7)$$

Here,  $\lambda$  is the tip speed ratio of the wind turbine. The equations mentioned above results in the torque graph shown in Figure 6.2. The parameters to determine the design are shown in Appendix B, Table B.1.

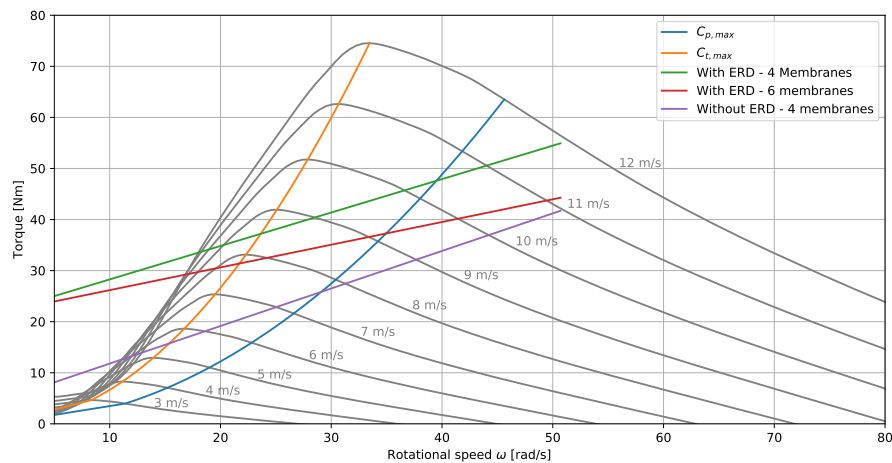


Figure 6.2: Aerodynamic torque over angular velocity.

In Figure 6.2, the aerodynamic torque lines of the horizontal axis wind turbine are shown, depicted by the grey curves. Each line represents the aerodynamic torque over rotational speed of the wind turbine at the given wind speeds. In this case, the wind speeds between the cut-in wind speed (3 m/s) and the rated wind speed (12 m/s) of the wind turbine are shown. To optimally use the wind turbines' aerodynamic power, it is tried to let the wind turbine operate at the rotational speed at which the power coefficient,  $C_p$ , is maximal. Per wind speed, this optimal point is given by the crossing of the grey lines with the blue  $C_{p,max}$  curve. The optimal torque curve is defined by a quadratic function. For a hydraulic wind turbine turbine, the spear valve is used to regulate the counter torque on the rotor to follow this curve. As a positive displacement pump is used, of which a known characteristic is that its flow rate increases linearly with increasing RPM, Equation 3.14 is used to show that the pressure - RPM relation, hence the torque - RPM relation, will also be quadratic. For this case however, the spear valve is not included, but instead the system is combined with a RO desalination system with an ERD. For such a system, it is determined that the pressure - RPM relation and pump torque - RPM relation is not quadratic, but linear. This is shown in Chapter 5, Figure 5.13.

This linear relation can also be seen in the Figure 6.2, where 3 different cases are shown. The green torque line represents the high pressure pump torque of a system using 4 membranes. This case is the base case and is based on the characteristics of the MicRODOT experimental setup. The HPP torque is determined using Equation 6.1. This torque is multiplied by the turbine ratio  $n_{turb}$ . The same is done for a system that contains 6 membranes (red line) instead of 4, whereas the permeate flow rate is similar to the base case. The purple line represents the torque for a system using 4 membranes but does not use an ERD. In all three cases, the same rotational speed variation of the high pressure pump is used and thus the feed flow from the pump is similar. At 750 RPM, the flow rate of the HPP is approximately similar to the maximum permeate flow rate of the base case (limited by the membranes). The linear relation between rotational speed and pump torque is explained in Section 5.4.

## 6.2. Wind Driven RO - System Stability

To be able to say something about the stability of the wind turbine, both with and without RO system with ERD, a system term proportional to the turbines rotational speed  $\omega_r$  has to be determined. For the total stability of the system, only the base case for RO with 4 membranes and an ERD is evaluated. With these results, a conclusion regarding the other cases can be given. As explained in Chapter 3, Section 3.2, the torque balance is a function of rotor torque and pump torque, given by Equation 3.11. A linearisation of this equation results in the following Equation 6.8 [20]:

$$J_t \dot{\omega}_r + B_r \omega_r + B_{HPP1} \omega_r + B_{HPP2} = 0 \quad (6.8)$$

Here it can be seen that the pump torque  $\tau_{HPP}$  is written as a function of two constants ( $B_{HPP1} \omega_r + B_{HPP2}$ ).  $B_{HPP1}$  is the term of the pump proportional to the rotor rotational speed  $\omega_r$ ,  $B_r$  is the term of the rotor proportional to  $\omega_r$ . The total term can be written as  $\alpha = (B_r + B_{HPP1})$ , such that Equation 6.8 can be redefined as Equation 6.9:

$$J_t \dot{\omega}_r + \alpha \omega_r + B_{HPP2} = 0 \quad (6.9)$$

First, a linearisation of the aerodynamic torque of the rotor is done, as explained by Jarquin Laguna [21]. The linearisation for the wind turbine rotor torque is given by Equation 6.10. This gives the rotor term  $B_r$ . The linearisation of the aerodynamic torque is done around its operating point ( $\bar{\omega}_r, \bar{U}$ ). Here, the bars over the variables mean 'steady-state value'. The constant  $B_r$  can be seen as a kind of damping term when taking the positive values above  $\lambda_{\tau, max}$  where  $C_t$  is a decreasing function of  $\lambda$ .

$$B_r(\bar{\omega}_r, \bar{U}) = - \left. \frac{\partial \tau_{aero}(\bar{\lambda}, \bar{U})}{\partial \bar{\omega}_r} \frac{\frac{\partial C_t}{\partial \lambda}}{\frac{C_t}{\lambda}} \right|_{\bar{\omega}_r, \bar{U}} \quad (6.10)$$

To find a solution for  $\alpha$ , a definition for  $B_{HPP1}$  has to be obtained. This is done by first rewriting the definition for the high pressure pump torque given by Equation 6.1, where Equation 6.2 and 4.34 are used. Since for this model it is taken that the leakage  $L$  of the ERD is negligible, the permeate flow rate  $Q_p$  can be taken equal to  $Q_{HPP}$ . Equation 6.11 shows the expression for the hydraulic pump torque:

$$\tau_{HPP} = V_p \eta_{vol} \Delta \Pi + \frac{V_p^2 \eta_{vol}^2 \rho_{water}}{n_{mem} A_m K_w} \omega_r \quad (6.11)$$

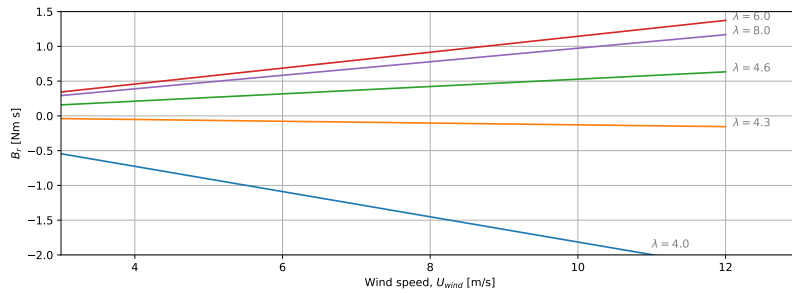
From Equation 6.11 the pump term proportional to  $\omega_r$ ,  $B_{HPP1}$ , can be obtained, given by Equation 6.12. In there, it is assumed that the rotational speed of the high pressure pump does not affect the osmotic pressure term  $\Delta \Pi$ , since its influence is negligibly small.

$$B_{HPP1} = \frac{V_p^2 \eta_{vol}^2 \rho_{water}}{n_{mem} A_m K_w} \quad (6.12)$$

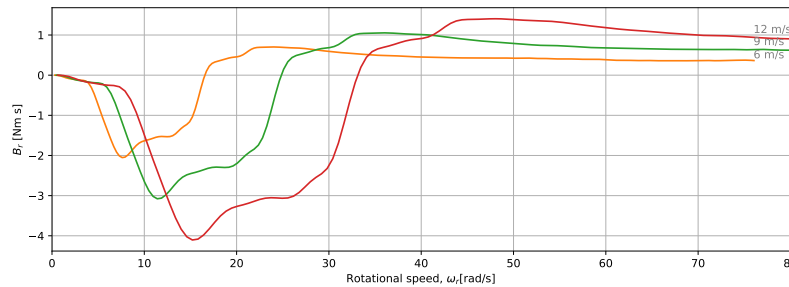
Here it can be seen that this term is a constant based on constant system parameters.

## 6.3. Wind Driven RO - Result Analysis

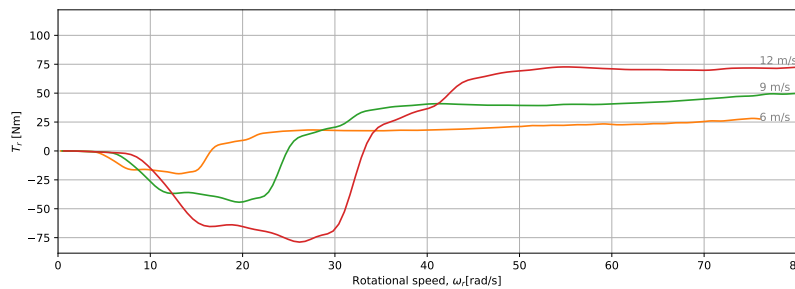
Using Equation 6.10, the stable operating region of the wind turbine is determined and shown in Figure 6.3a. There it can be observed that for tip speed ratios higher than  $\lambda_{\tau, max}$  (the value of  $\lambda$  at which  $C_t$  is max, as shown in Figure 6.1) the constant  $B_r$  is positive hence at that given tip speed the turbine operates in a stable region. In Figure 6.3b,  $B_r$  of the wind turbine is plotted as a function of the rotational speed of the rotor. In this figure, the turbine operates in a stable region for positive values of  $B_r$ . The higher the wind speed, the higher the rotational speed of the wind turbine needs to be for  $B_r$  to be positive. This rotational speed can also be found by the crossings between the  $C_{t, max}$  curve and the aerodynamic torque curves in Figure 6.2. This shows that the stable operating region of the wind turbine can be found at the right hand side of the  $C_{t, max}$ . By multiplying  $B_r$  with the rotational speed of the turbine  $\omega_r$ , a torque graph can be obtained, as shown in Figure 6.3c.



(a) Linearising aerodynamic torque gives the term  $B_r$  of the wind turbine, plotted over the wind speed for different tip speed ratios  $\lambda$ .



(b) Linearising aerodynamic torque gives the term  $B_r$  of the wind turbine, plotted over the rotational speed of the turbine for different wind speeds  $U_{wind}$ .

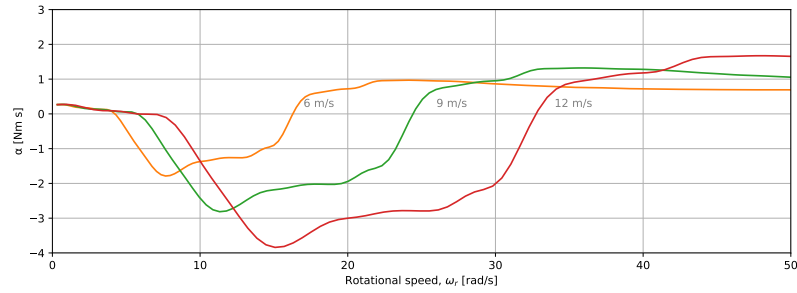


(c) Multiplying the term  $B_r$  by the turbines rotational speed results in the torque term  $T_R$ .

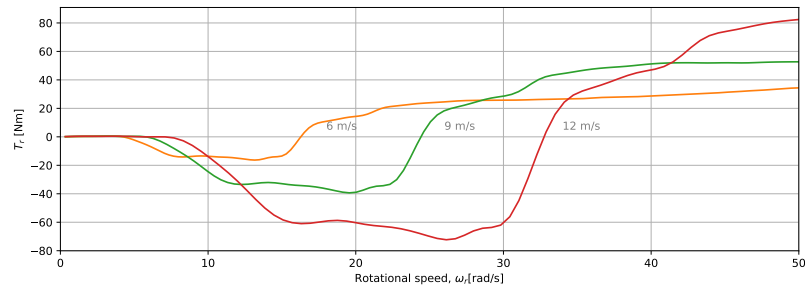
Figure 6.3: Linearisation of the aerodynamic torque results in a term of the rotor proportional to  $\omega a_r$ .

The total term proportional to  $\omega a_r$  of the system,  $\alpha$ , as aforementioned is a summation of  $B_r$  and  $B_{HPP1}$ , of which it was shown that the latter is a constant. In Figure 6.4a, the total systems term can be seen. Also from  $\alpha$ , a definition of torque can be given by multiplying it with the rotational speed of the rotor. This definition is given in Figure 6.4b.

From both Figure 6.4a and Figure 6.4b, a conclusion regarding the stable region of operation of the coupled wind turbine desalination system can be given. For the system to be defined stable,  $\alpha$  has to be mathematically positive. As Figure 6.4a shows,  $\alpha$  is positive for low rotational speeds for each given wind speed curve. Although this would implicate the system is stable, it will not operate at these low rotational speeds since the torque term of the system at those rotational speeds is equal to zero. For low wind speeds, the system is able to operate stable at relatively low rotational speeds, as is shown by the curve denoting 6 m/s. However, from fig:torquegraph it could be seen that the pump torque line for the used case (4 membranes) crosses the  $C_{t,max}$  line at a wind speed of approximately 8.5 m/s. The turbine torque at 6 m/s is not high enough to produce permeate water, since the counter torque from the pump would be too high to overcome, resulting in a constantly decelerating wind turbine in the unstable region. As for higher wind speeds, the system torque reaches the torque required for desalination, water can be produced and the system is able to operate in the stable region. As aforementioned, the results given in the figures above are based on case for



(a) The total term  $\alpha$  of the system is a summation of  $B_r$  and  $B_{HPP1}$ .



(b) By multiplying  $\alpha$  with the rotational speed of the rotor  $\omega_r$ , a torque relation can be found.

Figure 6.4:  $\alpha$  can be found by a summation of the  $B_r$  and  $B_{HPP1}$ .

4 membranes with the ERD. However, by understanding the principle of stability for this case, the stability regions for the other cases can be derived from the given results as well.

From the results mentioned in the previous paragraph, saying something about the aerodynamic efficiency at which the system operates is difficult. On top of that, a clear overview of the stable operating region and the amount of water produced at a certain wind speed is missing for each of the 3 cases. First some insight in the stable region at which water can be produced will be given. This is shown by Figure 6.5, in which the stable region is shown by as function of the tip speed ratio, where all values for  $\lambda$  above  $\lambda_{CT,max}$  are considered stable.

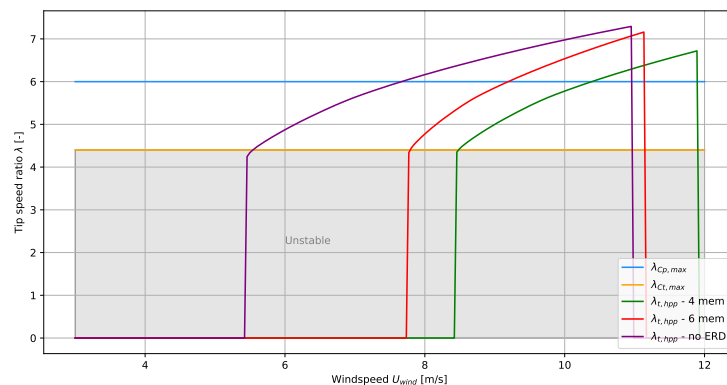


Figure 6.5: Tip speed ratio over wind speed.

Here, it can be seen that the system without ERD operates in the stable region for wind speeds of around 5.5 m/s and above. The two cases in which the ERD is included are stable at higher wind speeds, 7.7 m/s for the system with ERD and 6 membranes and 8.4 m/s for the system with ERD and 4 membranes. This difference

can be explained by the maximum system pressure of each system. The system without ERD operates at lower pressures due to its lower permeate production, this results in lower high pressure pump torques. The 6-membrane case with ERD operates at slightly lower pressures, although the permeate production is similar to the 4-membrane case, due to the higher total area of the membranes compared to the 4-membrane case. This was explained by equation 4.34.

Second, it is determined at which aerodynamic efficiency each of the three systems operates and produced permeate. As aforementioned, the optimal turbine torque curve at which the aerodynamic efficiency of the wind turbine is maximal follows a quadratic function. By following this function, the tip speed ratio of the wind turbine is constant (as seen in Figure 6.5) and the power coefficient  $C_p$  is maximal. By plotting the power coefficient of each desalination case, the aerodynamic efficiency of each system can be determined. The power coefficients can be found in Figure 6.6.

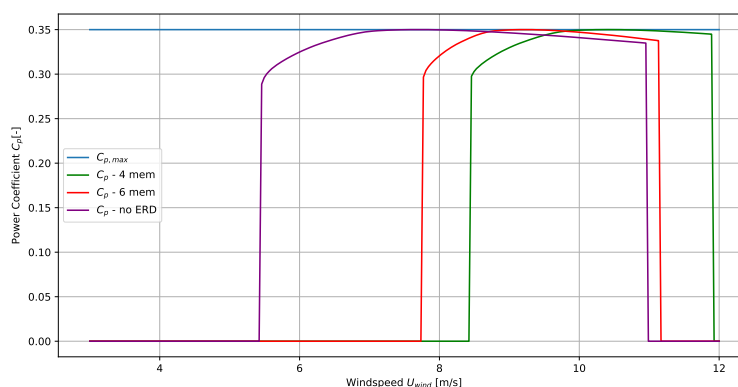


Figure 6.6: Power coefficient over wind speed.

Since the pump torque - rotational speed relation for all three cases is defined by a linear function, it is not possible to constantly operate at the highest aerodynamic efficiency hence maximal power coefficient  $C_{p,max}$ . However, from Figure 6.6 it can be seen that the system with ERD and 4 membranes operates at fairly high efficiencies at high wind speeds; an efficiency difference compared to the ideal case ( $C_{p,max}$ ) of around 1% can be seen at maximum wind speed ( $C_p$  is approximately 0.34 compared to  $C_{p,max}$  of 0.35). Although neither system can follow the quadratic function and are thus not able to operate at maximal aerodynamic efficiency (besides at the point at which the pump torque curve crosses with the  $C_{p,max}$  curve in Figure 6.2), the loss in efficiency during permeate production for each of the three systems is not significantly high. The permeate productions are given in Figure 6.7. For the system without ERD, permeate production is realised at relatively low wind speeds compared to the other two cases (the wind speed at which permeate can be produced is referred to as  $U_{p,in}$ ). However, the maximum amount of permeate that can be produced is significantly lower. The 6-membrane setup is able to start producing permeate at slightly lower wind speeds compared to the 4-membrane case. However, using more membranes while the amount of permeate is similar does mean the permeate production efficiency (per area of membrane) is lower. On top of that, the maximum permeate production is reached at lower wind speeds, hence the power coefficient when producing permeate above rated wind speeds is lower. Above rated wind speeds, for this turbine wind speeds higher than 12 m/s, the maximum amount of permeate can constantly be produced since the rotational speed of the turbine will not increase further hence the pump flow rates and systems pressures will remain constant.

From Figure 6.7, it can be seen that the maximum permeate production for the system with ERD is higher than for the system without ERD. For this system, with ERD 2.46 times the amount of permeate is being produced at maximum production rate compared to the system without ERD. As the flow rate provided by the high pressure pump is similar for both cases, and the system pressures are comparable, the power consumption per produced volume for this case differs the same ratio as the difference in permeate; 2.46. In Section 4.5.1 a ratio of approximately 5 was obtained. The difference in ratio can be explained by the used recovery rate of the system without ERD in this section. For the system without ERD, a constant valve setting was chosen

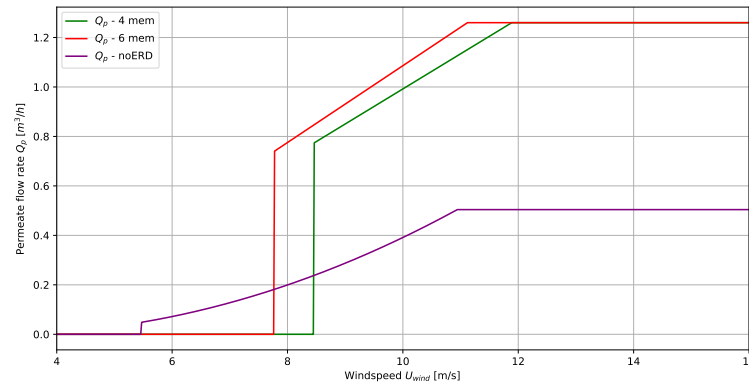


Figure 6.7: Permeate production over wind speed.

in such a way that an approximate recovery rate of 40% at maximum production (hence a a max permeate flow rate of around  $0.5 m^3/h$ ) was achieved. As the recovery rate for the model tests in Subsection 4.5.1 was close to 10%, a lower efficiency and thus higher power consumption per produced volume of permeate was obtained.

## 6.4. Recommendations for System Improvement

For neither of the latter cases, water is being produced directly from the cut-in wind speed of the wind turbine. In fact, for all three cases, a lot of aerodynamic power of the wind turbine is lost, especially at low wind speeds when no water can be produced. By combining several setups however, a larger operating range of the wind turbine can be used. If a solution was found to both produce water and operate at  $C_{p,max}$  by following the quadratic torque-rpm relation of the wind turbine, the most optimal and efficient system can be found. For this, two recommendations are given regarding system improvements. These recommendations are not proven yet and future research is required to determine the performance of each.

The case without ERD described in Section 6.3 has a fixed valve located in the concentrate stream, therefore having a linear torque-rpm relation. However, by using a variable valve in the high pressure concentrate line, this relation can become quadratic, as explained by Greco and Jarquín-Laguna [32]. With such a RO setup, permeate production can be realised at fairly low wind speeds, while the system operates at its maximal aerodynamic efficiency. By combining such a system with i.e. a system with ERD, both a more optimal use of the wind turbines' range can be used and higher permeate productions can be realised. In Figure 6.8, two examples is shown. In the graph the red line shows the pump torque for 1 case. Here, when the rotational speed of the turbine increases, water is being produced at around 5 m/s wind speeds. At that time, no ERD is being used. For increasing wind speeds an rotational speeds, the pump torque follows the  $C_{p,max}$  curve until the line crosses the green torque line and  $U_{pin}$  is reached. At that moment, the ERD is turned on and added to the system while the variable valve is being closed (the simplistic schematic overview in Figure 4.4 shows a system with which this might be possible). Now, the pump torque follows this linear line, still operating at relatively high efficiencies, as was explained in Figure 6.6 and maximum permeate rates. With this setup, the wind turbine is able to operate at its highest aerodynamic efficiency for a long time and the ERD is used to eventually produced maximum permeate. The other example is shown by the blue dashed line. For this case, the system starts producing permeate without ERD at around 4.5 m/s, from that point on, the pump torque is still following a quadratic curve, however, the turbine will not operate at its highest aerodynamic efficiency, but slightly below ( $C_p$  will lie around 0.34 instead of  $C_{p,max}$  of 0.35). Nonetheless, for this case, the ERD can be included to the system at lower wind speeds. Although the turbine is not operating most efficiently, the permeate production efficiency is higher than the latter example, since the maximum production can be realised at lower wind speeds hence more water is being produced.

In all the latter examples, only water production is taken into account. If the turbine is not able to produce permeate up to a certain wind speed however, producing electricity below that wind speed can be a second

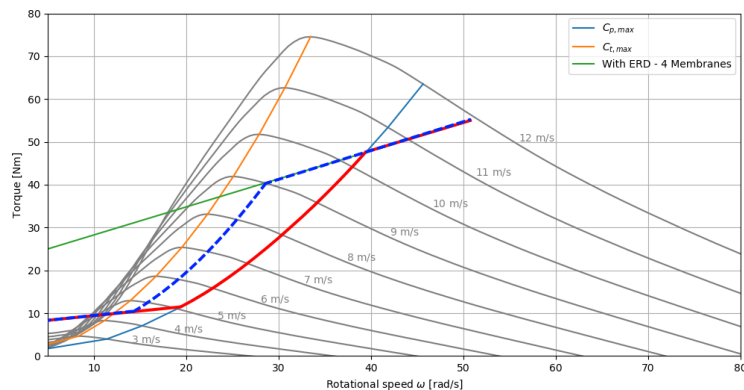


Figure 6.8: Producing permeate without ERD at low wind speeds using a variable valve in the concentrate line can make the wind driven RO system more efficient.

option to investigate and consider. Research into combining water production with electricity production using a spear valve and Pelton turbine has not been included in this thesis. However, using some assumptions this combinations is shortly elaborated on. In Figure 6.9, the torque curves for such a system are shown. As can be clearly seen does it look similar to the latter elaborated case. Using a spear valve, the quadratic torque-rotational speed relation can be obtained, as was explained in Section 3.2. From the cut-in wind speed, electricity production can be realised and for increasing wind speeds (and rotational speeds), the ideal aerodynamic torque curve can be followed while electricity production increases. At the moment that permeate production can be realised at  $U_{p,in}$ , and  $C_{p,max}$  is maximal, the system can shift towards water production, starting to follow the linear torque function. For increasing wind speeds, now only water is being produced.

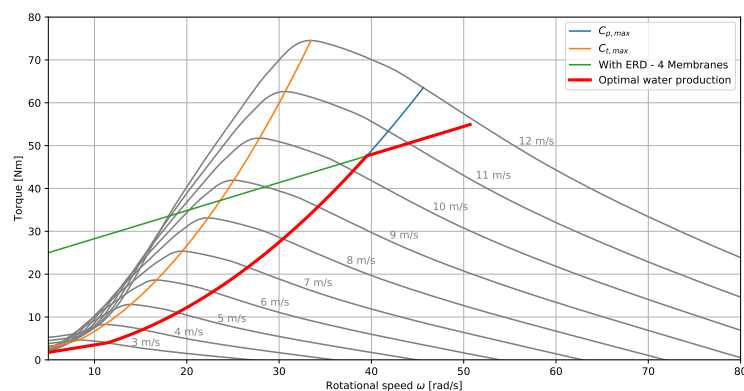


Figure 6.9: A combination of electricity production and water production can be interesting to optimally use the wind turbine.

As aforementioned, to come up with the most efficient solution, both for water production as well as a combination of both water- and electricity production, future study into the systems behaviour, efficiency, stability and performance is necessary.



# Conclusions and Recommendations

The goal of this thesis is to determine the influence of a wind driven Reverse Osmosis desalination system with an ERD on the performance and stability of a hydraulic drive train wind turbine. With this combination, the wind turbine will use its high pressurised water stream to feed the RO membranes. It was investigated how varying high pressure pump inputs influence the performance of the desalination system. Next, the effect of a varying rotational speed of the pressure exchanger ERD on the systems pressures and flows is determined and the influence of the ERD on efficiency of the desalination process was analysed. A numerical model is made of an RO system with ERD. The model is validated by means of an experimental setup. In the end, a simplified design of a wind driven RO system with an ERD was presented. With this design, the wind turbines' rotational stability and performance was analysed and discussed.

## 7.1. Conclusions

The global demand for fresh water is rapidly increasing while fresh water becomes scarcer. New sustainable solutions for the production of fresh water are required to be able to meet the futures' demands. Desalination by the means of RO with an ERD, driven by a hydraulic drive train wind turbine can be such a solution. Preliminary research into this combination showed promising results, this thesis continues on that.

Desalination by the means of RO is a well known technology to produce fresh water from saline sources. By using a pressure exchanger ERD, this process can be made more efficient and less power consuming. Comparing the system with ERD to a system without ERD showed that a significant increase in permeate production can be realised when an ERD is included in the RO system. One of the characteristics of a system with ERD is the fact that the flow rate at which permeate is being produced is nearly identical to the flow rate provided by the high pressure pump, whereas for a system without ERD this flow rate is determined by the recovery rate of the system. As for large scale setups this recovery rate lies around 50%, a system with ERD would be able to produce twice the amount of permeate. Quantifying the performance of both systems as power consumption per produced volume of permeate, a system with ERD performed substantially better. The power needed to produce one cubic meter of water with a system without ERD is roughly five times higher compared to a system with ERD.

The ERD is used to recover and reuse energy which is normally lost in the RO process. Conventional RO systems produce permeate at constant system pressures and feed flow rates. For those cases, the rotational speed of the ERD is set in such a way that maximum RO performance is achieved. For a RO system that is combined with a hydraulic wind turbine however, these pressures and flow cannot be guaranteed constant, since they depend on wind inputs on the wind turbines rotor. A comparison between constant and varying inputs showed that the membrane performance is not significantly affected by varying loads. The efficiency of permeate production at low high pressure pump inputs is similar to the efficiency seen at higher input flow rates and pressures.

The fluctuating nature of wind leads to varying inputs on the high pressure pump of the wind turbine, resulting in varying rotor torques of the the hydraulic wind turbine. To deal with this varying torque and

keep the turbine operate at its highest aerodynamic efficiency possible, a proper counter torque is required. This counter torque is provided for by the pump of the hydraulic turbine, which, in case of the hydraulic wind turbine without a RO system, can be influenced and controlled using a spear valve that can affect the system pressures. The optimal relation between rotational speed and rotor torque of a wind turbine follows a quadratic function. When using a RO system with ERD instead of a spear valve, however, it is shown that the relation between rotational speed and pump torque is linear, meaning it is not possible to operate operate at  $C_{p,max}$  only using the RO+ERD system.

By using a numerical model, the wind driven RO system with the ERD was analysed. An experimental test setup was used to validate the model results. At the beginning of this research, the exact working principle of the pressure exchanger ERD was yet unknown and hardly described by literature, especially for systems with varying input loads. Fortunately, the results obtained from the experimental tests showed very similar behaviour of the ERD and desalination system. Using the experimental setup, the predicted results of the numerical model could be confirmed. Both the model and the experiments showed that the ERD is able to affect the system pressures and flows. By varying the rotational speed of the ERD, the effective concentration can be slightly affected, leading to varying total system pressures. Nonetheless, the difference in pressure for different rotational speeds of the ERD is not significant. The effect of varying rotational speeds on the pressure as obtained from the experimental results was around 1 bar, which confirmed the model results in which similar values were obtained. Although the tests were done using fresh water, according to the model a maximum pressure difference of 3 bar will be obtained if water with a salinity compared to seawater is used. With the current test setup and results, the variation in rotational speed of the ERD did not seem to influence the amount of permeate being produced. With the results mentioned in this paragraph, it is shown that the RO system with ERD can not substantially influence and control the system pressures hence the high pressure pump torque. For a future setup, in which a hydraulic turbine is combined with a RO system with ERD, the ERD will not be able to sufficiently influence the high pressure pump torques for varying rotor torques. For this, future research into methods for active pressure and torque control when combing a RO system with ERD with a hydraulic wind turbine is required.

As an understanding of the RO system with an ERD was gained, the following step was to analyse this RO system driven and fed by a hydraulic wind turbine. For this, in a numerical model a design of a small scale wind turbine was done, using characteristics of an existing Vestas V44 wind turbine as well as limiting factors of the experimental setup, like maximum allowed pressure, rotational speeds and flow rates. The model shows the stable operating regions of a wind turbine combined with a desalination system for 3 different RO setups. For a system with 4 membranes and an ERD, referred to as the base case, the results showed that the hydraulic wind turbine is able to operate stable and start producing permeate water at relatively high wind speed (called  $U_{p_{in}}$ ) with respect to the turbines cut-in wind speed. The base case system is comparable to the experimental test setup configuration. When water is being produced, the turbine itself is able to operate at aerodynamic efficiencies close to its maximum. However, due to the linear relation between pump torque and rotational speed of the high pressure pump, it can be concluded that the turbine is never able to continuously follow the ideal aerodynamic efficiency for varying rotational speeds of the rotor, since here the torque-rpm relation follows a quadratic function. By including more membranes while keeping the permeate production similar to the base case, it is shown that permeate production can start at lower wind speeds, although this difference is not significant. Not using an ERD can result permeate production at even lower wind speeds, nonetheless the maximum permeate production rate is significantly lower.

To optimally make use of the wind turbine at maximum aerodynamic performance, a system design should be considered in which the pump torque - rotational speed relation follows a quadratic function while being able to use most of the available aerodynamic power. A possible design can be a combination of water production with electricity production via a spear valve and a Pelton turbine. In such a case, electricity can be produced below the  $U_{p_{in}}$  and water production is realised at  $U_{p_{in}}$ . Future research into combining RO with electricity production and to optimally produce permeate using the full potential of the hydraulic wind turbines, is required.

## 7.2. Recommendations and Future Work

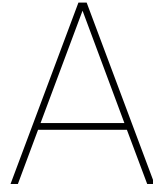
- **Model Extension:** The current model used for modelling the RO system with the ERD was based on steady states, in which the turbine - pump behaviour was not directly coupled. For future research, a dynamic model that includes coupling between the wind turbine and the RO system should be investigated. On top of that, the model should be extended to a time domain model, in which varying wind speeds over time can be implemented. In this way, the dynamic behaviour of the wind turbine with the RO desalination system can be evaluated using an ODE solver. For the system without ERD, an ODE solver was used to evaluate system response on increasing pump rotational speeds. However, the implementation of the ERD in this model has not been done yet. On top of that, a model that includes a turbine control strategy is recommended. Using the current model, operational and stability ranges could be determined, however, a control strategy for wind turbine control was not included. For this, more research into combinations of techniques for system improvement, i.e. electricity production and water production combined, is required. This recommendation for system improvement is shortly discussed in Section 6.4 as well.
- **Financial study:** Although the world is looking for renewable ways of producing water, it has to be economically attractive for people to invest in it. In this thesis, a simplistic evaluation of price per produced water is shown. However, a more detailed analysis is required to determine if a wind driven reverse osmosis system can compete with conventional desalination plants. For this, more insight in the actual power consumption per produced volume of permeate is required, as well as a total costs analysis of all required components and sub-systems. Both the Operational Expenditures (OPEX) of the wind driven RO system as well as the Capital Expenditures (CAPEX) should be analysed to be able to determine the total levelized costs of water (LCOW).
- **Long term experimental tests:** The current conducted tests with varying loads and inputs on the membranes were short term tests. However, to be able to say something about the long term impact of fluctuating flows on the membranes performance and life span, long term tests and simulations are required. At this moment, it is concluded that a variation in flow and pressure does not influence the membranes performance, however, since nearly all existing RO-desalination plants and systems produce at constant loads, no information and literature regarding long term fluctuating loads on the membrane is available.
- **MicRODOT improvement:** For future research, an improvement of the MicRODOT test setup is recommended. As the current large boost pump in the setup has a maximum flow rate of around  $8.4 \text{ m}^3/\text{h}$ , the rotational speed of the iSave ERD was limited by this flow, which resulted in a relatively small range in which the rotational speed could be varied. As shown in Appendix E, the iSave high pressure flow rate can be set between 6 and  $21 \text{ m}^3/\text{hr}$ . Having the ability to increase the low pressure feed flow towards the ERD further, a better understanding regarding the influence of the ERD can be given since its rotational speed can be varied to higher values. Second, increasing the amount of membranes in a pressure vessel will result in a desalination system with higher possible recovery rates. With this addition, the potential of the ERD can be better used and the setups performance and production rate can be better compared to existing desalination plants and applications. The most interesting setup expansion would be the addition of a small scale wind turbine to the RO system with ERD for the most reliable results.
- **Test improvement:** First, by using saline water for experimental testing, the model results as expected for higher salinities can be validated more accurately. It is expected that the system behaves in a similar manner when salt water is used, the model results showed similar behaviour regarding permeate production and flow rates, but higher system pressures. As the osmotic pressure of salt water is higher, the pressures needed for desalination will be higher and thus the experimental tests might give slightly different results compared to the numerical model. On top of that, due to the larger difference in inlet and outlet pressure of the ERD, the efficiency of the pressure exchanging mechanism will become higher, resulting in lower leakage rates and higher permeate productions. Second, the experimental tests should be conducted with a time-domain rotor model on the high pressure pump. Abrupt variation in flow rates and pressures aren't considered during the conducted tests, using a fluctuating inconsistent wind model will give better insight in the dynamic behaviour of the membranes under variable loads.

- **Spear valve implementation:** To determine optimal usage and performance of the wind driven reverse osmosis system, the implementation and use of a spear valve should be investigated. The experimental setup is designed in such a way that a spear valve can be used in a flow line parallel to the RO and ERD configuration. As was seen from the results, a control strategy is necessary since the ERD barely influences the system pressures hence pump torques and a linear relation between pump torque and rotational speed was obtained. A parallel flow line configuration, such that water is being produced at a constant rate and the pressure variation is accounted for by the spear valve should be researched.

# Bibliography

- [1] National Research Council et al. *Desalination: a national perspective*. National Academies Press, 2008.
- [2] Sabine Lattemann, Maria D Kennedy, Jan C Schippers, and Gary Amy. Global desalination situation, chapter 2, sustainability science and engineering, volume 2, issn 1871-2711. Technical report, DOI 10.1016/S1871-2711 (09) 00202-5, 2009.
- [3] Water Technology. Perth seawater desalination plant, 2018. URL <https://www.water-technology.net/projects/perth/>.
- [4] B Nivedh. Major failures in the wind turbine components and the importance of periodic inspection. *Windinsider*, 2014.
- [5] S. Mulders. Hydraulic wind turbines, 2019. URL <https://www.tudelft.nl/en/3me/departments/delft-center-for-systems-and-control/research/data-driven-control/hydraulic-wind-turbines/>.
- [6] Puretec Industrial Water. What is reverse osmosis?, 2018. URL <https://puretecwater.com/reverse-osmosis/what-is-reverse-osmosis>.
- [7] B.D. Freeman B. Marrot L.F Greenlee, D.F. Lawler and P. Moulin. Reverse osmosis desalination: Water sources, technology, and today's challenges. *Water Research*, 43:2317–2348, 2009. doi: 10.1016/S0921-4526(00)00753-5.
- [8] MultiMedia LLC. What is reverse osmosis?, 2017. URL <https://puretecwater.com/reverse-osmosis/what-is-reverse-osmosis>.
- [9] J Kucera. Reverse osmosis: Industrial processes and applications, 2015.
- [10] Craig Bartels, Rich Franks, Stefan Rybar, Manfred Schierach, and Mark Wilf. The effect of feed ionic strength on salt passage through reverse osmosis membranes. *Desalination*, 184(1-3):185–195, 2005.
- [11] Robert Bergman. *Reverse osmosis and nanofiltration*. American Water Works Association, 2007.
- [12] Lenntech BV. Reverse osmosis desalination process, 2017. URL <https://www.lenntech.com/processes/desalination/reverse-osmosis/general/reverse-osmosis-desalination-process.htm>.
- [13] Yue Wang, Shichang Wang, and Shichang Xu. Experimental studies on dynamic process of energy recovery device for ro desalination plants. *Desalination*, 160(2):187–193, 2004.
- [14] Baltasar Peñate and Lourdes García-Rodríguez. Energy optimisation of existing swro (seawater reverse osmosis) plants with ert (energy recovery turbines): Technical and thermoeconomic assessment. *Energy*, 36(1):613–626, 2011.
- [15] S. U. N. Jiayi, W. A. N. G. Yue, X. U. Shichang, and W. A. N. G. Shichang. Energy recovery device with a fluid switcher for seawater reverse osmosis system \*. *Chinese Journal of Chemical Engineering*, 16(2): 329–332, 2008. ISSN 1004-9541.
- [16] Mageed Jean Guirguis. Energy recovery devices in seawater reverse osmosis desalination plants with emphasis on efficiency and economical analysis of isobaric versus centrifugal devices. 2011.
- [17] Danfoss. Danfoss isave animation, 2018. URL <https://www.youtube.com/watch?v=J81mcTV7tUw>.
- [18] Danfoss. isave 21 plus. <https://www.danfoss.com/en/products/energy-recovery-devices/dcs/energy-recovery-devices-for-reverse-osmosis-applications/isave-21-plus/#tab-overview>, 2019.

- [19] Richard L Stover. Seawater reverse osmosis with isobaric energy recovery devices. *Desalination*, 203 (1-3):168–175, 2007.
- [20] N.F.B. Diepeveen. *On the application of fluid power transmission in offshore wind turbines*. PhD thesis, TU Delft, Delft University of Technology, 2013.
- [21] A. Jarquin Laguna. *Centralized electricity generation in offshore wind farms using hydraulic networks*. PhD thesis, TU Delft, Delft University of Technology, 2017.
- [22] Sebastiaan Mulders, Niels Diepeveen, and J. W. Wingerden. Control design, implementation and evaluation for an in-field 500 kw wind turbine with a fixed-displacement hydraulic drivetrain. *Wind Energy Science Discussions*, pages 1–37, 05 2018. doi: 10.5194/wes-2018-35.
- [23] A. R. Bartman, P. D. Christofides, and Y. Cohen. Nonlinear model-based control of an experimental reverse-osmosis water desalination system. *Industrial and Engineering Chemistry Research*, 48(13): 6126–6136, 2009. ISSN 0888-5885.
- [24] Richard L Stover and Andreas Gorenflo. Swro membrane design with isobaric energy recovery devices. In *Proceedings of the American Membrane Technology Association Conference and Exposition, Las Vegas, Nevada*, 2007.
- [25] Richard Stover and Bill Andrews. Isobaric energy-recovery devices: Past, present, and future. *IDA Journal of Desalination and Water Reuse*, 4:38–43, 01 2012. doi: 10.1179/ida.2012.4.1.38.
- [26] DOW Chemical. *DOW/ROSA Software, Version 9.1*. Midland, Michigan, United States, 2018. URL <http://media-library.dow.com/answer-center/water/ROSA-HTML5/Content/20161013UF+ROWAVE-Manual/TableofContents.htm>.
- [27] M.F. Supper. *Fluctuating flows on reverse osmosis membranes: An experimental approach for hydraulic drive train wind turbine applications*. Master's thesis, Delft University of Technology, 2017.
- [28] Yan-Yue Lu, Yang-Dong Hu, Xiu-Ling Zhang, Lian-Ying Wu, and Qing-Zhi Liu. Optimum design of reverse osmosis system under different feed concentration and product specification. *Journal of membrane science*, 287(2):219–229, 2007.
- [29] Alex R. Bartman, Aihua Zhu, Panagiotis D. Christofides, and Yoram Cohen. Minimizing energy consumption in reverse osmosis membrane desalination using optimization-based control. *Journal of Process Control*, 20(10):1261–1269, 2010. ISSN 0959-1524. URL <https://tudelft.on.worldcat.org/oclc/5900938762>.
- [30] S.P. Mulders, Stephane Jager, N.F.B. Diepeveen, and J.W. van Wingerden. Control design and optimization for the dot500 hydraulic wind turbine, 2017. URL <http://resolver.tudelft.nl/uuid:594f9180-ad47-4c7e-b0e8-e8686677afeb>.
- [31] John D. Sørensen and J. N. Sørensen. *Wind energy systems optimising design and construction for safe and reliable operation*, 2011. ISSN 9781613443804 (electronic bk.) 1613443803 (electronic bk.) 1845695801 (electronic bk.) 9781845695804 (electronic bk.) 9780857090638 (e-book) 0857090631 (e-book). URL <https://cornell-library.skillport.com/skillportfe/main.action?assetid=68320>.
- [32] F Greco and A Jarquin-Laguna. Simulation of a horizontal axis tidal turbine for direct driven reverse-osmosis desalination. In *Advances in Renewable Energies Offshore: Proceedings of the 3rd International Conference on Renewable Energies Offshore (RENEW 2018), October 8-10, 2018, Lisbon, Portugal*, page 181. CRC Press, 2018.
- [33] Energy Recovery. Turbochargers, 2018. URL <http://www.energyrecovery.com/water/turbochargers/>.
- [34] EagleRidge. What is a turbocharger and how does it work?, 2018. URL <https://www.eagleridgegm.com/what-is-a-turbocharger-and-how-does-it-work/>.
- [35] Flowserve. Flowserve releases new video showcasing its dweer energy recovery devices for swro desalination, 2018. URL <https://www.flowserve.com/en/more/about-company/news-events/flowserve-releases-new-video-showcasing-its-dweertm-energy-recovery-devices-for-swro-desalin>



# Hydraulic diagram and component list

In this Appendix, first the hydraulic diagram of the MicRODOT experimental test setup can be found. Second, the component list is listed in here. The components shown in the hydraulic diagram are labelled and can be identified using this list.

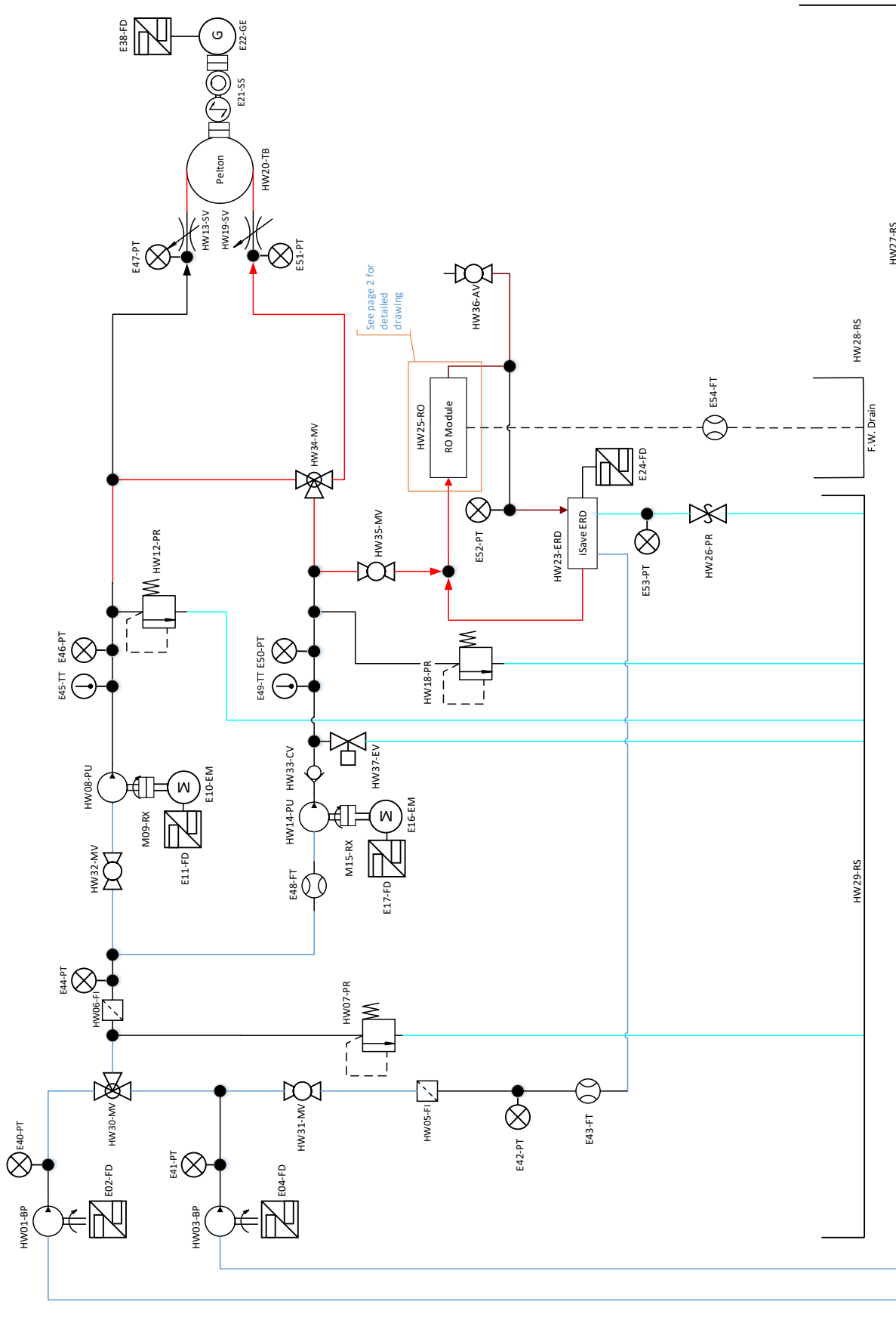


Figure A.1: Hydraulic Diagram of the MicRODOT experimental test setup (page 1)

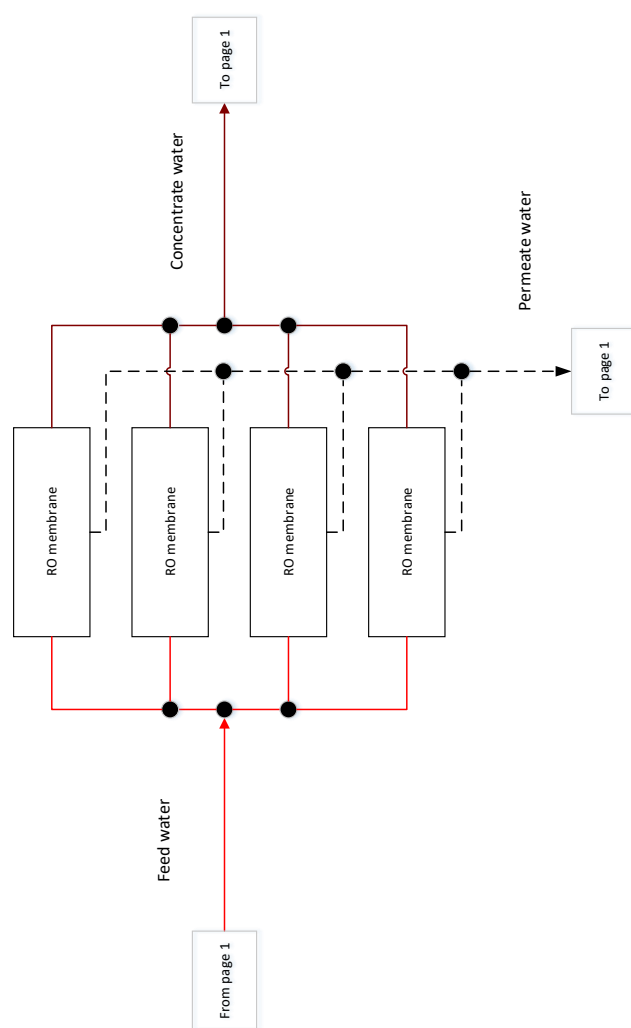


Figure A.2: Hydraulic Diagram of the MicRODOT experimental test setup, RO membrane arrangement (page 1)

Table A.1: Component list

Type	Labelling	Specification			
Family	Hydraulic diagram label	Supplier	Manufacturer	Function	details
Boost Pump	HW01-BP	Lenntech	Grundfos	Feedwater boost pump	Grundfos_CRN-3-11-A-FGJ-G-E-HQQE
Frequency Drive	E02-FD		Bonfiglioli	VFD	Bonfiglioli ActiveCube EtherCAT
Boost Pump	HW03-BP		Calpeda	Feedwater boost pump	Calpedaa_NGX6-22
Frequency Drive	E04-FD		Bonfiglioli	VFD	Bonfiglioli ActiveCube EtherCAT
Filter	HW05-FI	Lenntech	EW/USA	3 micron filter for ERD	HPCF-B-5DC2
Filter	HW06-FI		Cintropur	10 micron filter for HPP	Cintropur_NW500
Pressure Relief Valve	HW07-PR		Goetze	Pressure relief valve	Goetze 451bFK-20-f-f-20-20 PTFE
Pump	HW08-PU		The water Hydraulics	High Pressure Pump	Janus M30 35cc
Rotex Coupling	M09-RX			Rotex coupling	KTR Rotex 38 Standard
Electromotor	E10-EM	Elsto	Elsto	Electric motor	H3G-132M-4
Frequency Drive	E11-FD	Elsto	Bonfiglioli	VFD	Bonfiglioli ActiveCube EtherCAT
Pressure Relief Valve	HW12-PR		Goetze	Pressure relief valve	Goetze 451bFK-20-f-f-20-20 PTFE
Spear Valve	HW13-SV			Actuator Spear Valve	LVC24A-MP-TPC
Pump	HW14-PU		The water Hydraulics	High Pressure Pump	Janus M30
Rotex Coupling	M15-RX			Rotex coupling	KTR Rotex 38 Standard
Electromotor	E16-EM	Elsto	Elsto	Electric motor	H3G-132M-4
Frequency Drive	E17-FD	Elsto	Bonfiglioli	VFD	Bonfiglioli ActiveCube EtherCAT
Pressure Relief Valve	HW18-PR		Goetze	Pressure relief valve	Goetze 451bFK-20-f-f-20-20 PTFE
Spear Valve	HW19-SV			Actuator Spear Valve	LVC24A-MP-TPC
Pelton Turbine	HW20-TB				
Torque Sensor	E21-TS			Torque sensor Pelton	NCTE Series 3000
Generator	E22-GE		Elsto	Generator	H3G-160M2-2
Energy Recovery Device	HW23-ERD	Lenntech	Danfoss	Energy Recovery Device	iSave_21plus
Frequency Drive	E24-FD	Lenntech	Danfoss	VFD iSave 21plus	VLTAqua Drive FC 202
RD-membranes	HW25-RO	Lenntech		RD Pressure vessels and membranes	DOV Filmtec Sw30-4040 and H4E4G1 pressure vessel
Pressure Relief Valve	HW26-PR				
Reservoir	HW27-RS				
Reservoir	HW28-RS				
Reservoir	HW29-RS				
Manual valve	HW30-MV				
Manual valve	HW31-MV				
Manual valve	HW32-MV				
Check Valve	HW33-CV	Fluiconnecto	PH-Hydraulik	Check valve	RD-I-G3/4*
Manual valve	HW34-MV				
Manual valve	HW35-MV				
Air Relieve Valve	HW36-AV				
Electric valve	HW37-EV				
Frequency Drive	E38-FD				
	N/A				
Pressure transducer	E40-PT		Firstrate	Temperature sensor	FirstRate FST600-202
Pressure transducer	E41-PT		Firstrate	Temperature sensor	FirstRate FST600-202
Pressure transducer	E42-PT		Firstrate	Pressure sensor - low pressure lines	FirstRate FST800-211
Flow transducer	E43-FT	IFM		Magnetic inductive flow sensor	SM9000 SMR21XGXFRKG/US
Pressure transducer	E44-PT		Firstrate	Pressure sensor - low pressure lines	FirstRate FST800-211
Temperature transducer	E45-TT		Firstrate	Temperature sensor	FirstRate FST600-202
Pressure transducer	E46-PT		Firstrate	Pressure sensor - high pressure lines	FirstRate FST800-2000
Pressure transducer	E47-PT		Firstrate	Pressure sensor - high pressure lines	FirstRate FST800-2000
Flow transducer	E48-FT	IFM		Magnetic inductive flow sensor	SM7000 SMR34GGXFRKG/US-100
Temperature transducer	E49-TT		Firstrate	Temperature sensor	FirstRate FST600-202
Pressure transducer	E50-PT		Firstrate	Pressure sensor - high pressure lines	FirstRate FST800-2000
Pressure transducer	E51-PT		Firstrate	Pressure sensor - high pressure lines	FirstRate FST800-2000
Pressure transducer	E52-PT		Firstrate	Pressure sensor - high pressure lines	FirstRate FST800-2000
Pressure transducer	E53-PT		Firstrate	Pressure sensor - low pressure lines	FirstRate FST800-211
Flow transducer	E54-FT	IFM		Magnetic inductive flow sensor	SM7000 SMR34GGXFRKG/US-100

# B

## Wind driven Seawater Reverse Osmosis - Input parameters

In this appendix, the input parameters used for the wind driven seawater reverse osmosis model in Chapter 6 are given.

The input parameters used for the model are shown in Table B.1:

Table B.1: Input parameters for wind turbine design

Parameter	Value	Units
$\omega_{HPP}$	0 - 750	rpm
$V_p$	$3.5e^{-5}$	$m^3/rev$
$K_w$	$3.3e^{-9}$	s/m
$A_m$	7.34	$m^2$
$n_{mem}$	4	-
$\delta$	0.2641	$Pa/ppmK$
$R$	0.993	-
$a$	0.5	-
$Q_{ERD}$	10	$m^3/hr$
$T_{water}$	25	$^{\circ}C$
$C_f$	32000	ppm
$\eta_{hydr}$	0.8	-
$\eta_{mech}$	0.9	-
$U_{rated}$	12	m/s
$U_{in}$	3	m/s
$U_{out}$	23	m/s
$C_{p,max}$	0.35	-
$C_{t,max}$	0.086	-
$v_{tip,max}$	80	m/s
$\rho_{air}$	1.225	$kg/m^3$
$\rho_{water}$	1025	$kg/m^3$
$\gamma_{noERD}$	10	%



# C

## Experimental test setup - Main components

In this appendix, first more detail information regarding the used components is given. Next, the test plan, describing the steps taken before, during and after each tests, is elaborated on. Finally, the tests and tests results regarding the volumetric efficiency determination of the high pressure pump will be explained.

### C.1. MicRODOT Experimental setup - Components

In here, of each main component the main characteristics, limitations and specifications are given. Of some of the components, more detailed information from the manufacturer is given in Appendix E.

#### C.1.1. High Pressure Pump and Electric motor

The high pressure pump is a 'The Water Hydraulics, Janus M30 Bidirectional positive displacement pump'. It is coupled to an electric motor of Elsto. The characteristics of both are given below:

Table C.1: High pressure pump - Janus M30.

<b>Manufacturer</b>	The Water Hydraulics	
<b>Type</b>	Janus M30 MB160-M35	
Rotational Speed	4000	RPM
Displacement	34.6	$cm^3/rev$
Pressure (max)	160	bar
Temperature	2- 50	°C

Table C.2: Electric motor - Elsto.

<b>Manufacturer</b>	Elsto	
<b>Type</b>	H3G-160M-4	
Rotational Speed (max)	1500	RPM
Rated Power	7.5	kW
Voltage	3 x 400	V

### C.1.2. Reverse Osmosis system

For the Reverse Osmosis system, 4 RO membranes are used, each one placed in a pressure vessel. The 4 membranes are installed in a parallel configuration for maximum concentrate flow, needed to feed the ERD.

Table C.3: RO membranes - DOW FILMTEC

<b>Manufacturer Type</b>	DOW FILMTEC SW30-4040	
Active Area	7.4	$m^2$
Permeate flow rate	7.4	$m^3/d$
Feed flow rate (max)	3.6	$m^3/h$
Salt rejection	99.4	%
Pressure (max)	69	bar
Pressure drop (max)	1	bar
Temperature (max)	45	$^{\circ}C$

Table C.4: Pressure Vessel - Eurotrol.

<b>Manufacturer Type</b>	Eurotrol H4E4G1	
Pressure (max)	69	bar
Amount of membranes	1	-
Membrane size suitable	40	inch

### C.1.3. Energy Recovery Device

The Energy Recovery Device, used to recover energy from the high pressure concentrate flow, is the iSave 21 plus.

Table C.5: ERD - iSave-21 Plus.

<b>Manufacturer Type</b>	Danfoss iSave 21 Plus	
Rotational Speed	500-1500	RPM
Flow rate	6-21	$m^3/h$
Displacement	265.8	$cm^3/rev$
HP inlet pressure (min)	15	bar
HP inlet pressure (max)	83	bar
LP outlet pressure (min)	1	bar
Leakage (max)	2	%
Motor size (Power)	5.5	kW
Temperature	2-40	$^{\circ}C$

### C.1.4. Boost Pumps

The system makes use of two centrifugal boost pumps, one referred to as the large boost pump (largest flow) feeding the ERD, and one smaller boost pump feeding the high pressure pump. The large pump is the Calpeda pump, the smaller pump is the Grundfos pump.

Table C.6: Boost Pumps

(a)			(b)		
Manufacturer Type	Calpeda NGX 6/22		Manufacturer Type	Grundfos CRN3-11 A-FGJ-G-E-HQQE	
Flow rate	0.5 -8.4	$m^3/h$	Flow rate (max)	3	$m^3/h$
Rotational speed (max)	2800	RPM	Rotational speed (max)	2870	RPM
Pressure	2.5 -4.5	bar	Pressure (max)	25	bar
Temperature	0 - 35	°C	Temperature	-20 - 120	°C
Rated power	1.5	kW	Rated power	1.1	kW
Voltage	3 x 400	V	Voltage	3 x 400	V

### C.1.5. Filters

In the setup, two filter are installed. The filters are used necessary to avoid particles of a certain size to damage the high pressure pumps and the ERD. For the high pressure pump, the maximum allowed particle size is 10 micron, therefore a 10 micron filter is used in that line. The maximum particle size for the ERD is 3 micron hence a second filter was necessary.

Table C.7: Filters

(a)			(b)		
Manufacturer Type	Cintropur NW500		Manufacturer Type	EWP-USA HPCF-B-5DC2	
Particle size	10	$\mu m$	Particle size	3	$\mu m$
Flow rate (max)	28	$m^3/h$	Flow rate (max)	9	$m^3/h$
Pressure (max)	16	bar	Pressure (max)	6	bar
Temperature	0- 50	°C	Temperature (max)	45	°C

### C.1.6. Sensors

In the setup, flow, pressure and temperature sensors are installed. They are used for data logging as well as making sure the system is not operating at pressure or flow limits.

**Flow Sensor** Three flow sensors are installed, one in the feed flow line the high pressure pump, one in the permeate flow line and one in the feed flow line of the ERD. The SM7000 is used for the HPP and permeate flow lines, since there the flow rates are relatively small. The ERD feed flow rate is larger than the max flow of the SM7000, therefore the SM9000 is used in that flow line.

Table C.8: Flow sensors

(a)			(b)		
Manufacturer Type	IFM SM7000		Manufacturer Type	IFM SM9000	
Flow rate	0.01 - 3	$m^3/h$	Flow rate	0.3 - 18	$m^3/h$
Sampling time	20	ms	Sampling time	20	ms
Temperature	-20 - 70	°C	Temperature	-20 - 70	°C
Pressure (max)	16	bar	Pressure (max)	16	bar

**Pressure Sensors** For pressure sensors, a difference in low and high pressure pressure sensors is made. For the low pressure lines, the FST800-211 are used, for the high pressure lines, the FST800-2000 are used.

Table C.9: Pressure sensors

(a)			(b)		
<b>Manufacturer Type</b>	Firstrate FST800-211		<b>Manufacturer Type</b>	Firstrate FST800-2000	
Pressure	1 - 600	bar	Pressure	10 - 400	bar
Sampling time	20	ms	Sampling time	20	ms
Temperature	-20 - 125	°C	Temperature	-20 - 85	°C

**Temperature Sensor** Temperature sensors are used to for two purposes. The first is to log the temperature of the water, since this is an important parameters for i.e. the osmotic pressure term. Second, a sudden increase in water temperature could say something about the high pressure pump running dry.

Table C.10: Temperature sensor

<b>Manufacturer Type</b>	Firstrate FST600-202	
Pressure	0 - 300	bar
Sampling time	20	ms
Temperature	-50 - 200	°C

### C.1.7. Concentrate Valve

To be able to guarantee a constant pressure of at least 1 bar at the ERD low pressure outlet, a pressure relief valve is used. For the setup, a check valve is chosen which can be set to a fixed position at which it opens, for ranges between 1 to 1.5 bar. Since a minimum of 1 bar is necessary, such a valve is sufficient and is the easiest and less expensive solution to guarantee a constant pressure.

## C.2. Test Plan

The test plan is described in this section. This plan shows which steps to take before, during and after testing to assure safe and proper testing. The test plan is written and executed in Excel. Of this file, some direct copies of the test plan are given. The test plan makes use of the component names as can be found in the Hydraulic diagram in Appendix A. For the tests that focus on varying the rotational speed of the HPP, the test plan is given in Table C.11, for the tests covering a variation in rotational speed of the ERD, the plan is given in Table C.12. In these tables, it is referred to 'ROi tests' which stands for 'Reverse Osmosis integration tests'. The entire setup can be used for different tests, some focusing on water production and some on electricity production, and therefore each type of test is given a name. Note that the tests as stated in the tables have been conducted several times hence the test numbers 7 and 8.

Table C.11: Test plan for tests having constant rotational speed of the ERD while varying the rotational speed of the HPP

Test no.	Component	Action	Expected result
7	<i>Constant ERD - Varying HPP rpm test 2</i>		
7.01	Set valves	Set all manual valves in right direction to use for ROi tests	
7.02	Open valve HW35-MV	Open valve HW35-MV	Water will flow through valve when ERD is turned on
7.03	Inspect hydraulic lines	Check for loose hydraulic connections	
7.04	Check sensor signals		
7.05	Log signals	E43FT,E48FT, E54FT, E50PT,E52PT, E53PT, E49-TT, RPM ERD, RPM HW14PU	Log signals for water production and pressures in system
7.06	Turn on HW03BP	Slowly increase RPM of HW03BP	Flush ERD up to 7 m <sup>3</sup> /hr feed flow is realized
7.07	Turn on HW23ERD	Slowly increase RPM of HW23ERD to meet flowrate (min 500RPM)	ERD flowrate will increase, system will be filled with water, RPM will be 500rpm
7.08	HW26PR gives right back pressure	Check sensor E53-PT for at least 1bar pressure	Pressure is at least 1 bar
7.09	Close valve HW35-MV	Close valve HW35-MV	When air is relieved from system, close valve
7.10	Turn on HW01BP	Slowly increase RPM of HW01BP	HW14PU will be fed
7.11	Turn on and Control RPM of HW14PU	Increase RPM of HW14PU with 50 RPM every 15 secs up to 700 RPM, depending on permeate produced (max = 1.223 m <sup>3</sup> /hr). Decrease RPM at same with same stepsize per timestep	HP flow and pressure will slowly increase, permeate water will be produced up to determined amount and will most probably follow same step pattern. Check if system reaches steady state within 15 sec.
7.12	Turn of HW01BP	Slowly decrease RPM of HW01BP to complete standstill when HW14PU is turned off	Water stops feeding HW14PU
7.13	Turn off HW23ERD	Slowly decrease RPM of HW23ERD to complete standstill	Turn off HW23ERD when pressure at membranes is as desired
7.14	(Open HW37EV)	For faster depressurising of the system - Open HW37EV	Pressure will drop faster when HW37EV is opened
7.15	Turn off HW03BP	Slowly decrease RPM of HW03BP to complete standstill	Turn off HW03BP so it will no longer feed the ERD
7.16	Save and write log files		
7.17	Check log files		

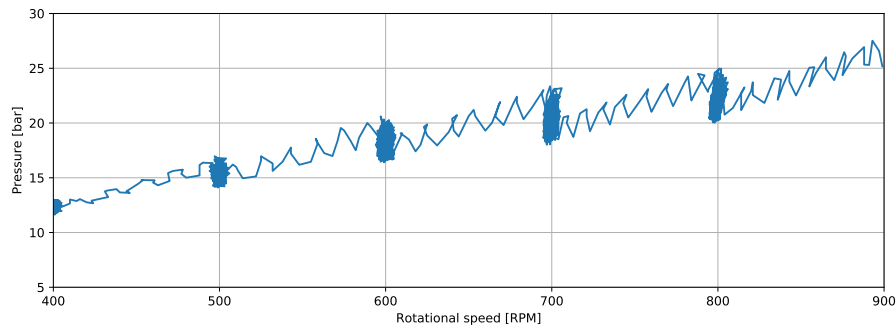
Table C.12: Test plan for tests having constant rotational speed of the HPP while varying the rotational speed of the ERD

Test No.	Component	Action	Expected result
<b>8</b>	<i>Constant HPP rpm - Varying ERD RPM test 2</i>		
<b>8.01</b>	Set valves	Set all manual valves in right direction to use for ROi tests	
<b>8.02</b>	Open valve HW35-MV	Open valve HW35-MV	Water will flow through valve when ERD is turned on
<b>8.03</b>	Inspect hydraulic lines	Check for loose hydraulic connections	
<b>8.04</b>	Check sensor signals		
<b>8.05</b>	Log signals	E43FT,E48FT, E54FT, E50PT,E52PT, E53PT, E49-TT, RPM ERD, RPM HW14PU	Log signals for water production and pressures in system
<b>8.06</b>	Turn on HW03BP	Slowly increase RPM of HW03BP	Flush ERD up to 7 m <sup>3</sup> /hr feed flow is realized
<b>8.07</b>	Turn on HW23ERD	Slowly increase RPM of HW23ERD to 450 rpm	ERD flowrate will increase, system will be filled with water
<b>8.08</b>	HW26PR gives right back pressure	Check sensor E53-PT for at least 1bar pressure	Pressure is at least 1 bar
<b>8.09</b>	Close valve HW35-MV	Close valve HW35-MV	When air is relieved from system, close valve
<b>8.10</b>	Turn on HW01BP	Slowly increase RPM of HW01BP	HW14PU will be fed
<b>8.11</b>	Turn on HW14PU	Slowly increase RPM of HW14PU up to +600 RPM until permeate production is around 1m <sup>3</sup> /hr.	HP flow and pressure will slowly increase, permeate water will be produced up to determined amount
<b>8.12</b>	Increase RPM of ERD and decrease with same steps	Increase RPM of ERD with 25rpm per 15 sec up to max 650 rpm and decrease back to 450 rpm	Pressures/flows vary?
<b>8.13</b>	Turn off HW14PU	Turn of HW14PU	Pressure will drop
<b>8.14</b>	Turn of HW01BP	Slowly decrease RPM of HW01BP to complete standstill when HW14PU is turned off	Water stops feeding HW14PU
<b>8.15</b>	Turn off HW23ERD	Slowly decrease RPM of HW23ERD to complete standstill	Turn off HW23ERD when pressure at membranes is as desired
<b>8.16</b>	(Open HW37EV)	For faster depressurizing of the system - Open HW37EV	Pressure will drop faster when HW37EV is opened
<b>8.17</b>	Turn off HW03BP	Slowly decrease RPM of HW03BP to complete standstill	Turn off HW03BP so it will no longer feed the ERD
<b>8.18</b>	Save and write log files		
<b>8.19</b>	Check log files		

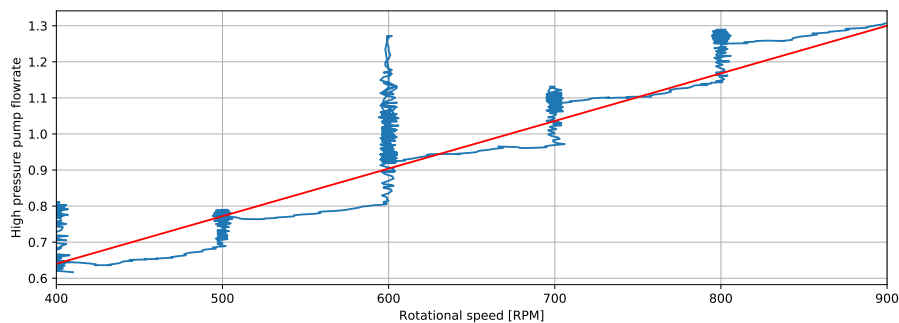
### C.3. Determination of Volumetric Efficiency

In this subsection, the determination of the volumetric efficiency of the high pressure pump is given. This efficiency depends on the pressure of the system and the rotational speed of the high pressure pump and is determined empirically for different pressures and speeds. To map the efficiency, one flow sensor is placed in the intake line of the high pressure pump, and one is located in the leakage line. The difference between these two flows is the output flow provided by the high pressure pump. A spear valve is located in the high pressure output line of the high pressure pump, to control the pressures. Several tests are done, for each tests the spear valves' position was set to a different fixed position, after which the rotational speed of the high pressure pump was increased step wise up to the maximum possible rotational speed. This resulted in a total mapping of pressures, flows and efficiencies.

The shown results are for the flow rates and pressures at which the tests have been conducted. However, for future usage of the setup, data at higher pressures and rotational speeds is obtained and stored as well. In Figure C.1, the pressure (Figure C.1a), flow rate (Figure C.1b) and efficiency (Figure C.1c) over the rotational speed of the high pressure pump are given. For the given pressure and flow range of the pump, the mean volumetric efficiency, as can be seen from Figure C.1c, is approximately 0.71. This mean value is used in the numerical model.

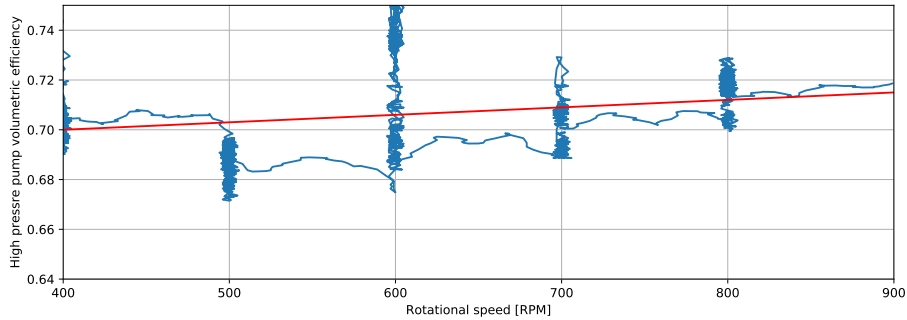


(a) Pressure over rotational speed



(b) Output flow over rotational speed

Figure C.1: Determination of the volumetric efficiency of the High Pressure pump for different flows and pressures



(c) Volumetric efficiency per rotational speed

Figure C.1: Determination of the volumetric efficiency of the High Pressure pump for different flows and pressures

#### C.4. Visualisation MicRODOT Test Setup

Some additional images of the MicRODOT test setup are given here. In Figure C.2, the three water tanks are shown. The feed water tank (white, right) contains approximately  $0.7m^3$  of water, from here the two boost pumps are provided with feed water. The black tank (middle) is the concentrate storage tank and the green tank (left) is the permeate storage tank. From both the concentrate and the permeate tank, water is pumped back into the feed water tank, so that it can be re-used. Above the water tank, the Pelton turbine with the generator and two spear valves can be seen. These are not used for this research, but for future research, they can be added to the desalination setup.



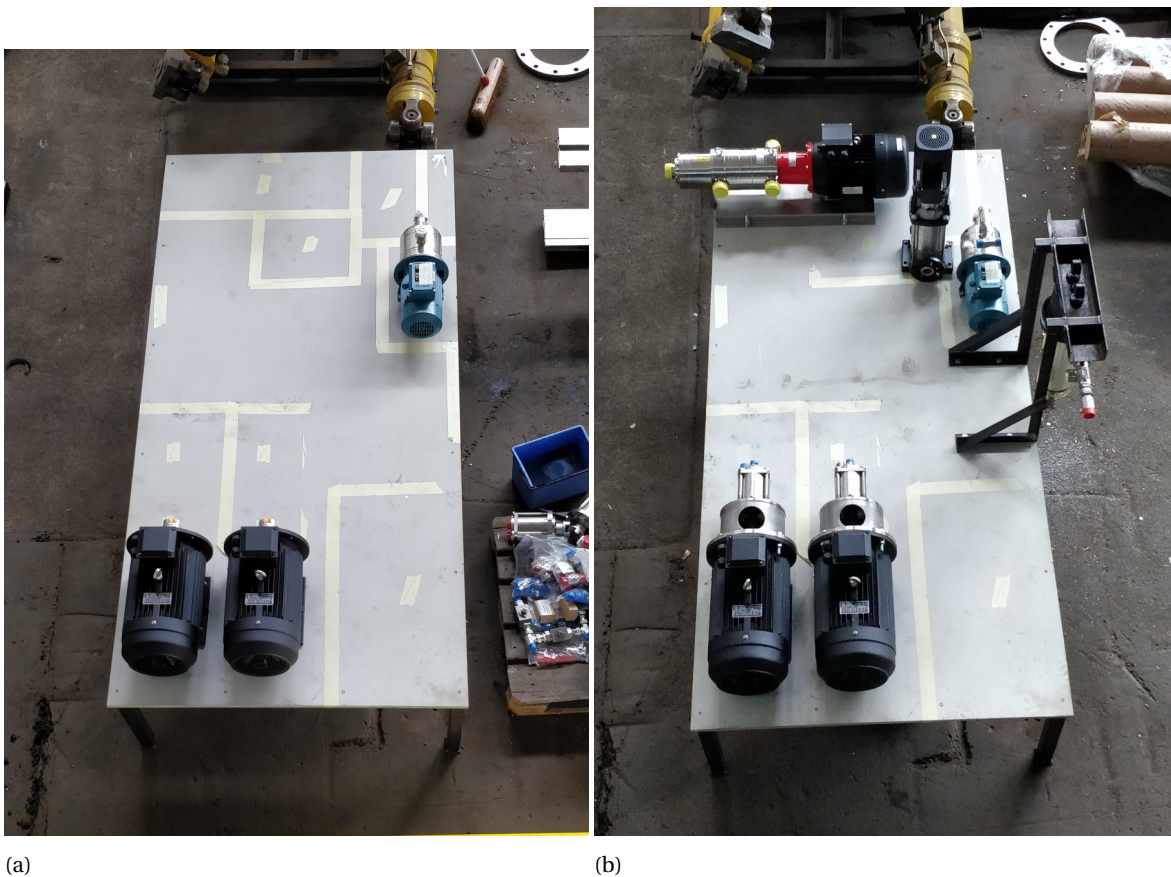
Figure C.2: The three water tanks shown in the figure are the permeate tank (green, left), the concentrate tank (black, middle) and the feed water tank (white, right).

In Figure C.3, a more zoomed-in picture of the test setup is shown. There, the two filters (denoted by Fi), the two boost pumps (BP) and the ERD can be distinguished. The iSave ERD actually consists of three components, on the left is the electric motor, in the middle the pressure exchanger is located and on the right (at the tip) the positive displacement recirculating pump is placed.



Figure C.3: A close up of the setup, clearly showing the filters, boost pumps and ERD

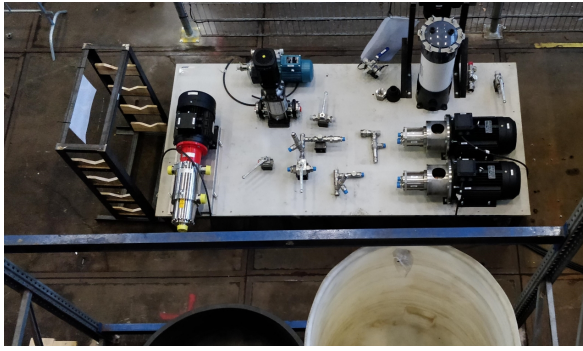
In the images given by Figure C.4, a progress overview is given during the design and construction phase of the MicRODOT test setup.



(a)

(b)

Figure C.4



(c)



(d)



(e)



(f)



(g)

Figure C.4

# D

## Energy Recovery Devices - Elaborate information

This appendix will provide information about the types of Energy Recovery Devices. A short description of each type is given.

### D.1. Francis Turbine

The Francis Turbine (Figure D.1), or reverse running pumps, are ERDs that transfer hydraulic energy to mechanical energy. It was the first type of ERD deployed in Seawater Reverse Osmosis (SWRO) desalination plants. However, the flow range and pressure required for getting maximum efficiency of operation was very narrow and limited, which was one of the main disadvantages [16]. Due to their low efficiency of around 50 to 60%, they were replaced by Pelton wheels in the 1980s [19].



Figure D.1: Francis turbine with Generator [16]

### D.2. Pelton Wheel

A Pelton wheel is similar to a water wheel. A high pressure feed water stream is directed into the buckets of the Pelton wheel via a nozzle, as can be seen in Figure D.2. In this way, the kinetic energy of the pressurised feed stream is converted into mechanical energy in the form of rotation. This mechanical energy can then

be used in two ways. It can be either used to produce electricity by adding a generator to the shaft of the Pelton wheel, which can then be converted into pumping power again or a pump can be directly connected to the shaft to boost up the inlet pressure of the RO membrane.

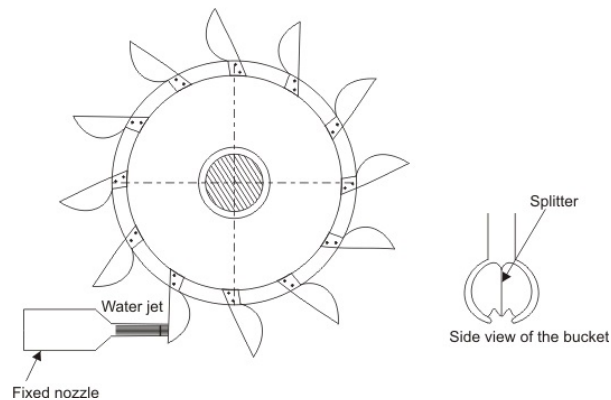


Figure D.2: Pelton wheel working principle

The overall efficiency of the Pelton wheel is higher than of the Francis Turbine. Its efficiency remains constantly high, also during variations in pressure and flow. The overall efficiency of a SWRO plant that uses a Pelton wheel is 80 to 85% [16].

### D.3. Turbocharger/Hydraulic Pressure Booster

When using a turbocharger, the high pressure concentrate stream coming out of the membranes is used to make a hydraulic turbine spin. This spinning motion means the turbine is driven by kinetic energy. A so called compressor wheel is attached to the same axis as the turbine. At the inlet of the compressor wheel, a low pressure feed stream comes in. The compressor wheel converts the kinetic energy of the compressor wheel back in hydraulic energy, creating a high pressure feed stream [33]. The working principle is visualised in Figure D.3. This figure is based on an existing figure which explained the working principle of a turbocharger for cars, however, the working principle is similar for energy recovery principles using hydraulic fluids.

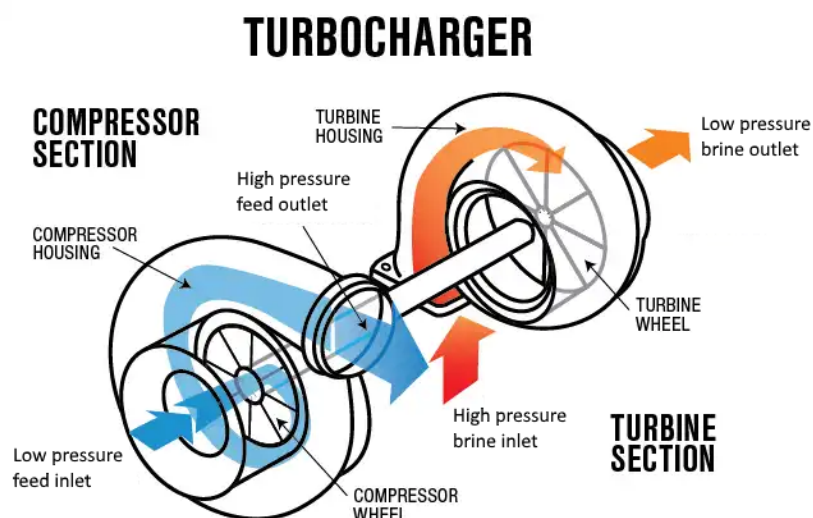


Figure D.3: Turbocharger working principle [34]

The efficiency of the Turbocharger has a maximum of around 89% to 90%, which is a little higher than the efficiency of the Pelton wheel. However, the highest transfer efficiency can be calculated by multiplying the efficiency of each part of the turbocharger. These parts are the nozzles, impellers and turbines, giving approximately  $90\% \cdot 90\% \cdot 99\%$ , which gives around 80% efficiency.

The Turbocharger can be adapted and used for small flow rates, meaning it can be used for small scale desalination plants. To increase flow rates, large scale hydraulic pumps need to be used, making it less attractive for larger implementations.

## D.4. DWEER

The DWEER Energy Recovery Device does not convert its hydraulic energy to mechanical energy. It directly converts hydraulic energy to hydraulic energy, from the brine stream to the feed stream. The main advantage is that direct energy transfer is more efficient. This is called a 'work exchanger'. The DWEER separates the reject(brine) and the feed stream by a piston via a simple design. It consists of two pressure vessels, four check valves and a so called LinX™ valve. A DWEER ERD can be used in large desalination plants, mostly due to its large size pressure vessels.

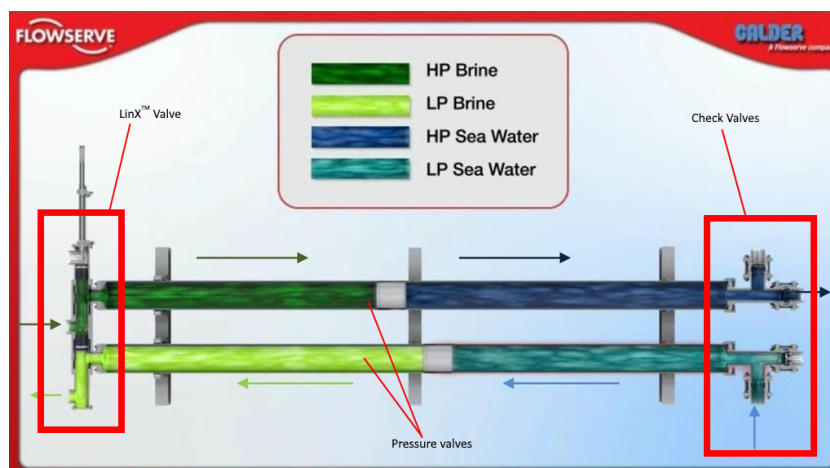


Figure D.4: DWEER working principle [35]

The working principle of the DWEER will be explained using image D.4. Low pressure seawater enters the DWEER via the check valves. In the LinX™ valve, the high pressure brine stream enters via the middle inlet. This high pressure brine stream enters the top vessel, which at that moment is already filled with low pressure seawater. The streams are separated by pistons. The pressure of the brine is transferred to the seawater, which then exit the DWEER via the check valves, now having a high pressure. At the same time, low pressure seawater enters the bottom vessel, pushing out the low pressure brine water that was already in place. This brine exits the DWEER via the bottom side of the LinX™ valve. After that, the LinX™ valve actuates, meaning it switches and the process repeats itself, but now the other way around since the top vessel now contains low pressure brine and the bottom vessel has low pressure seawater in place. When using a DWEER, a booster pump is still necessary to pressurize the feed stream up to the correct pressure.

## D.5. Pressure Exchanger (PX)

The most efficient and widely used ERD nowadays is the Pressure Exchanger Energy Recovery Device, also known as PX ERD. Just like the DWEER, the Pressure Exchanger (PX) converts hydraulic energy directly to hydraulic energy. This is done by the use of a rotating piston, firstly designed by Energy Recovery Inc [16]. The working principle is explained by the use of Figure D.5.

1. The rotor (depicted as the white cylinder) rotates in the direction as shown by the arrow. The rotor chamber is filled with low pressure feed water, provided by a boost pump. This replaces the low pressure brine water that was in place.

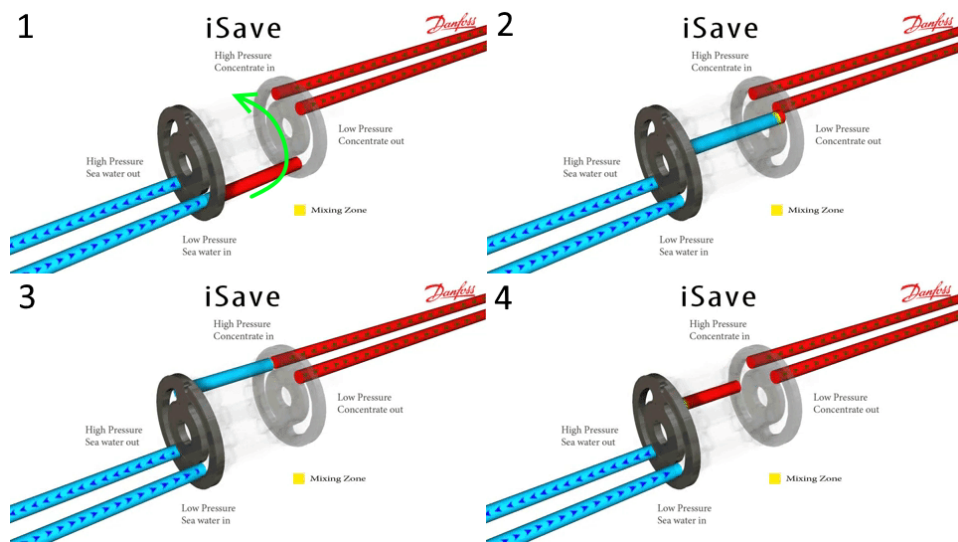


Figure D.5: Pressure exchanger (PX) working principle [17]

2. While rotating, the chamber is fully filled with low pressure feed water.
3. The high pressure concentrate pushes out the low pressure feed, directly converting the hydraulic energy of the concentrate water to the feed water. In this way, the low pressure feed becomes a high pressure feed stream. This feed stream will feed the reverse osmosis membranes.
4. All the feed water is pushed out of the chamber and the chamber now fully contains low pressure concentrate water. Now we are back to step one and the cycle repeats.

Since there is no physical barrier between the feed water and the concentrate, a small part of the concentrate will mix with the feed water, leading to a slight increase of the high pressure feed water stream. This mixing can be (mostly) accounted for by supplying more low pressure feed water than there is concentrate water. The performance of the pressure exchanger can be determined by its energy transfer efficiency and the degree of mixing. The efficiency of the PX can be seen as the ratio of the total energy output by the device to the total energy input (in a percentage). The rotational speed can be up to approximately 1500 rounds per minute (rpm), depending on the length of the rotor and the flow rate of the concentrate.

Pressure Exchanger ERDs are mostly used in medium to large scale desalination systems, since it is most efficient to use at high concentrate flows. Nowadays however, more and more small scale PX ERDs are being developed, meaning they can compete with, for example, turbocharger ERDs in small scale operations. A graph comparing the efficiencies of the isobaric, turbocharger and Pelton turbine ERDs can be found in Figure D.6.

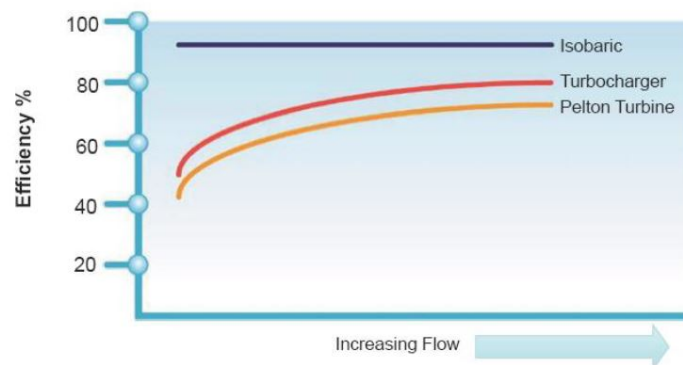
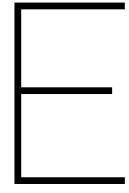


Figure D.6: Efficiencies of Energy Recovery Devices [16]



# Technical Data and Performance Sheets

This appendix includes the technical data of respectively the iSave 21 Plus and the Reverse Osmosis membranes (DOW Filmtec SW30-4040) used in the MicroDOT experimental setup. On top of that, the performance data of the used high pressure pump (Janus M30) and the two boost pumps is given.


**Data sheet | Energy Recovery Device | iSave 21 Plus and iSave 40**
**3. Technical data**
**3.1 iSave without motor**

iSave size		iSave 21 Plus	iSave 40
Code number		180F7015	180F7011
Geometric displacement	cm <sup>3</sup> /rev	273	626
	ln <sup>3</sup> /rev	16.7	38.2
Pressure			
Differential pressure HP in - HP out max. <sup>1)</sup>	bar	5	5
	psi	72.5	72.5
HP max. outlet pressure	barg	83	83
	psig	1200	1200
HP min. inlet pressure	barg	15	20
	psig	217	290
HP max. inlet pressure	barg	83	83
	psig	1200	1200
HP inlet min. pressure, intermittent <sup>2)3)</sup>	barg	3	3
	psig	44	44
LP inlet max. pressure	barg	5	5
	psig	72	72
LP inlet max. pressure intermittent <sup>3)</sup>	barg	10	10
	psig	145	145
LP outlet min. pressure	barg	1	1
	psig	14.5	14.5
LP differential LP in - out at HP max. flow	bar	0.9	1.2
	psi	13	17.5
Speed			
Min. speed	rpm	500	600
Max. speed	rpm	1500	1200
Typical flow			
HP outlet flow range <sup>4)</sup> at max. differential pressure	m <sup>3</sup> /h	6-22	21-41
	gpm	26-96	92-180.5
Lubrication flow at 60 barg (871 psig) max.	m <sup>3</sup> /h	0.4	0.8
	gpm	1.8	3.5
LP inlet max. flow	m <sup>3</sup> /h	33	67
	gpm	145	295
Torque			
Torque at max. differential pressure operation <sup>1)</sup>	Nm	49	102
	lbf-ft	36	75
Max. starting torque (stick/slip)	Nm	50	150
	lbf-ft	37	110
Media temperature <sup>5)</sup>	°C	2-40	2-40
	°F	36-122	36-122
Ambient temperature	°C	0-50	0-50
	°F	32-104	32-104
Filtration requirements (nominal) <sup>6)</sup>		3 micron melt-blow	
Salinity increase at membrane at 40% recovery rate		2-3 %	
Weight	kg	47	123
	lb	103	271

- <sup>1)</sup> Continuous torque above max. differential pressure will reduce the lifetime of the iSave.  
<sup>2)</sup> Pressure can reach this pressure level at start-up and permeate flush.  
<sup>3)</sup> Intermittent pressure is acceptable for less than 10

- minutes within a period of 6 hours.  
<sup>4)</sup> Typical average flow at 60 bar.  
<sup>5)</sup> Dependent on NaCl concentration.  
<sup>6)</sup> Please see section 7. filtration.



## Data sheet | Energy Recovery Device | iSave 21 Plus and iSave 40

### 3.2 iSave with IEC motor

iSave		iSave 21 Plus <sup>A)</sup>	iSave 21 Plus	iSave 40	
Code number horizontal		180F7016	180F7017	180F7001	180F7004
Code number vertical		180F7016	180F7017	180F7003	180F7005
Motor size IEC version IEC 400 V, 50 Hz <sup>1)</sup>	kW	5.5	7.5	11	15
	HP	7.5	10	15	20
Frame size	IEC	132 S	132 M	160 L	180 L
	pole	4	4	6	6
Motor data					
Nominal speed	rpm	1450	1450	970	970
Min. speed at 400 V	rpm	500	<sup>2)</sup> 500	600	600
Max. speed at 400 V	rpm	1500	1500	<sup>3)</sup> 1100	1200
Rated current at 400 V	A	11	15.2	22	30
Torque					
Motor torque at nominal speed <sup>3) 4)</sup>	Nm	36	49	<sup>5)</sup> 108	146
	lbf-ft	26.5	36	80	107.7
Motor torque at min. speed <sup>3)</sup>	Nm	27	36	95	129
	lbf-ft	20	27	70	95
Motor ambient temperature, max.	°C	40	40	40	40
	°F	122	122	122	122
Motor insulation	Class	B	B	B	B
Motor degrees of protection	IP	55	55	55	55
Sound pressure level max. <sup>6)</sup>	dB(A)	78	79	84	84
Weight	kg	105	116	254	305
	lb	231	255	560	672
Footprint (horizontal/vertical)	m <sup>2</sup>	0.31	0.32	0.5/0.16	0.54/0.17
	foot <sup>2</sup>	3.34	3.45	5.38/1.72	5.81/1.83

<sup>A)</sup> Differential pressure HP in - HP out max. is limited to 3 bar [44 psi]

- <sup>1)</sup> Three-phase-asynchronous-motor according to DIN-IEC and VDE 0530 standards.
- Voltage and frequency according to IEC 38
  - The motors are fitted with a rating plate in multi-tension: 380-420 V / 660-720 V, 50 Hz or 440-480 V, 60 Hz
  - Tolerance  $\pm 5\%$  according to VDE 0530
  - Standard coating according to IEC 60721-2-1

<sup>2)</sup> If voltage is below 400 V we recommend to use another size of electric motor. Please contact Danfoss High Pressure Pumps for further information.

<sup>3)</sup> Torque load for iSave and motor see diagram on page 23 and 25.

<sup>4)</sup> Due to inertia and stick-slip friction of the iSave, the torque may exceed the maximum allowable operation torque for the iSave when it is taken into use and/ or speed is ramped up from zero to maximum. A VFD or a soft starter must be used for ramp up.

<sup>5)</sup> The starting torque must not exceed the values stated under "Max. starting torque (stick/slip)". The VFD must be able to deliver 140% start torque. The Danfoss VFD type FC 301 and FC 302 can be used. For advice on VFD settings, please consult our relevant guideline or contact Danfoss.

<sup>6)</sup> A-weighted sound pressure level at 1 meter from the pump unit surfaces (reference box) acc. to EN ISO 20361 section 6.2. The noise measurements are performed acc. to EN ISO 3744:2010 on ERD with motor (motor-pump unit) at max. pressure and speed.



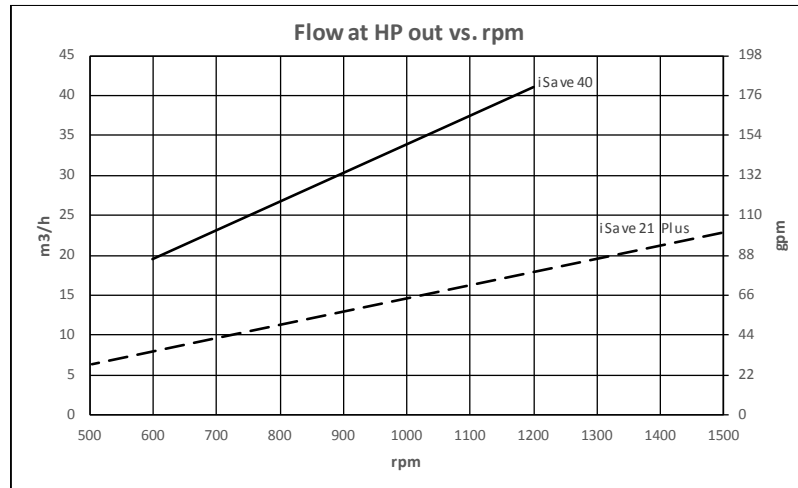
**Data sheet | Energy Recovery Device | iSave 21 Plus and iSave 40**

**4. Flow at different rpm**

The diagram shows that the HP flow can be changed by changing the rotation speed of the iSave. The flow/rpm ratio is constant, the required flow is obtainable by changing the rotation speed to a required value.

For accurate data please use our selection tool which is available on our website: [www.isave.danfoss.com](http://www.isave.danfoss.com)

The iSave is delivered with a 3.1 performance certificate according to EN10204.

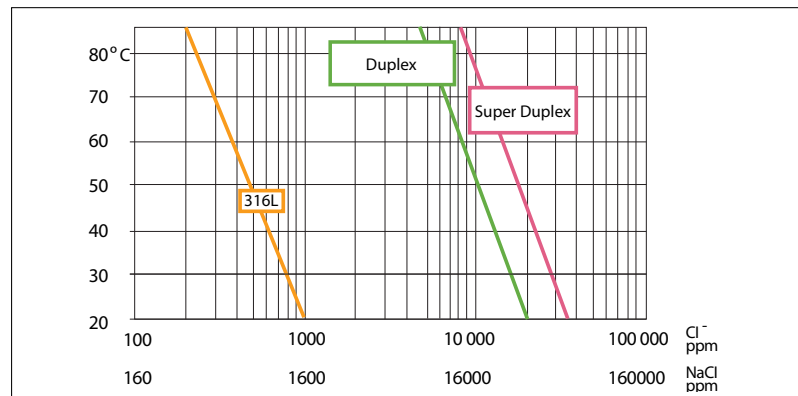


**5. Corrosion**

**5.1 Operation**

The chart below illustrates the corrosive resistance of different types of stainless steel related to NaCl concentration and temperature. All critical parts of the iSave is made of Super Duplex 1.4410/UNS 32 750 or Duplex 1.4462/UNS 32803.

Always flush the iSave with fresh water at operation stop in order to minimize the risk of crevice corrosion.

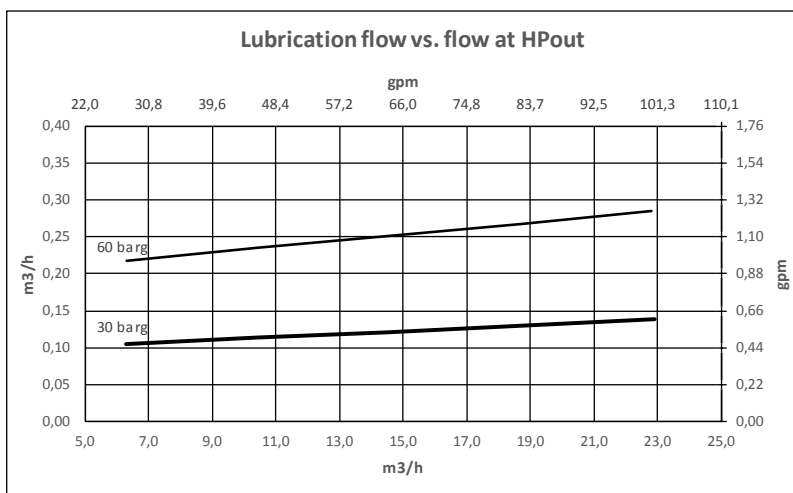
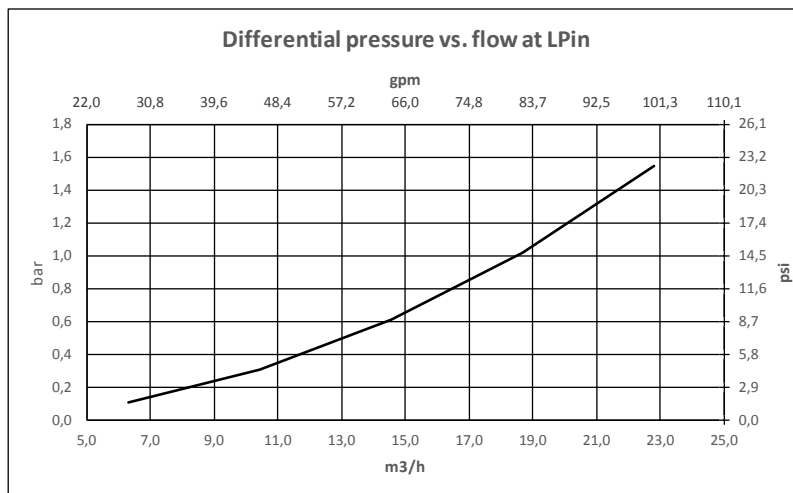




Data sheet | Energy Recovery Device | iSave 21 Plus and iSave 40

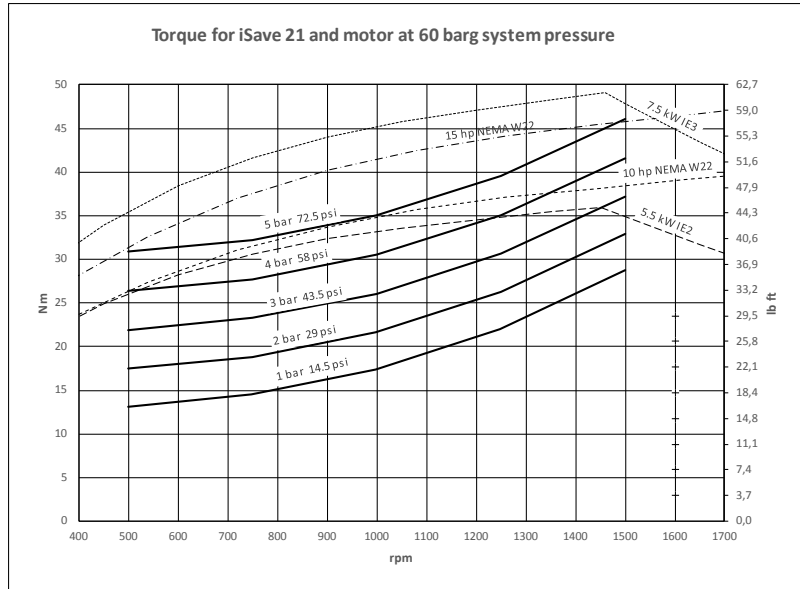
11. Performance curves

11.1 Performance and torque curves iSave 21 Plus





Data sheet | Energy Recovery Device | iSave 21 Plus and iSave 40





Product Information

**LENNTECH**

info@lenntech.com Tel. +31-152-610-900

www.lenntech.com Fax. +31-152-616-289

## FILMTEC™ SW30-4040 Membranes

### Features

Improved FILMTEC™ seawater reverse osmosis elements offer the highest productivity while maintaining excellent salt rejection.

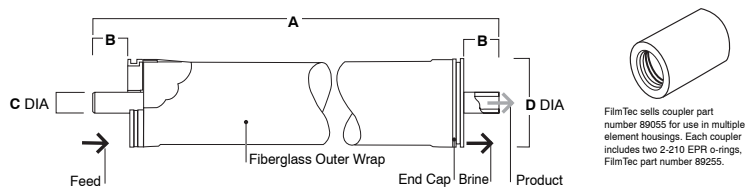
- FILMTEC SW30 membrane elements have the highest flow rates available to meet the water demands of both sea-based and land-based desalinators.
- FILMTEC SW30 elements may also be operated at lower pressure to reduce pump size, cost and operating expenses.
- Improved FILMTEC seawater membrane combined with automated, precision element fabrication result in the most consistent product performance available.

### Product Specifications

Product	Part Number	Active Area ft <sup>2</sup> (m <sup>2</sup> )	Applied Pressure psig (bar)	Permeate Flow Rate gpd (m <sup>3</sup> /d)	Stabilized Salt Rejection (%)
SW30-2514	80733	6.5 (0.6)	800 (55)	150 (0.6)	99.4
SW30-2521	80734	13 (1.2)	800 (55)	300 (1.1)	99.4
SW30-2540	80737	29 (2.8)	800 (55)	700 (2.6)	99.4
SW30-4021	80740	33 (3.1)	800 (55)	800 (3.0)	99.4
SW30-4040	80741	80 (7.4)	800 (55)	1,950 (7.4)	99.4

1. Permeate flow and salt rejection based on the following test conditions: 32,000 ppm NaCl, pressure specified above, 77°F (25°C) and the following recovery rates: SW30-2514 – 2%, SW30-2521 & SW30-4021 – 4%, SW30-2540 & SW30-4040 – 8%.
2. Permeate flows for individual elements may vary +/-20%.
3. For the purpose of improvement, specifications may be updated periodically.

**Figure 1**



Product	Maximum Feed Flow Rate gpm (m <sup>3</sup> /h)	Dimensions – Inches (mm)			
		A	B	C	D
SW30-2514	6 (1.4)	14.0 (356)	1.19 (30.2)	0.75 (19)	2.4 (61)
SW30-2521	6 (1.4)	21.0 (533)	1.19 (30.2)	0.75 (19)	2.4 (61)
SW30-2540	6 (1.4)	40.0 (1,016)	1.19 (30.2)	0.75 (19)	2.4 (61)
SW30-4021	16 (3.6)	21.0 (533)	1.05 (26.7)	0.75 (19)	3.9 (99)
SW30-4040	16 (3.6)	40.0 (1,016)	1.05 (26.7)	0.75 (19)	3.9 (99)

1. Refer to FilmTec Design Guidelines for multiple-element systems.
2. SW30-2514, SW30-2521 and SW30-2540 elements fit nominal 2.5-inch I.D. pressure vessels.  
SW30-4021 and SW30-4040 elements fit nominal 4-inch I.D. pressure vessel.

1 inch = 25.4 mm

**Operating Limits**

• Membrane Type	Polyamide Thin-Film Composite
• Maximum Operating Temperature	113°F (45°C)
• Maximum Operating Pressure	1,000 psi (69 bar)
• Maximum Pressure Drop	15 psig (1.0 bar)
• pH Range, Continuous Operation <sup>a</sup>	2 - 11
• pH Range, Short-Term Cleaning <sup>b</sup>	1 - 13
• Maximum Feed Silt Density Index	SDI 5
• Free Chlorine Tolerance <sup>c</sup>	<0.1 ppm

<sup>a</sup> Maximum temperature for continuous operation above pH 10 is 95°F (35°C).

<sup>b</sup> Refer to Cleaning Guidelines in specification sheet 609-23010.

<sup>c</sup> Under certain conditions, the presence of free chlorine and other oxidizing agents will cause premature membrane failure. Since oxidation damage is not covered under warranty, FilmTec recommends removing residual free chlorine by pretreatment prior to membrane exposure. Please refer to technical bulletin 609-22010 for more information.

**Important Information**

Proper start-up of reverse osmosis water treatment systems is essential to prepare the membranes for operating service and to prevent membrane damage due to overfeeding or hydraulic shock. Following the proper start-up sequence also helps ensure that system operating parameters conform to design specifications so that system water quality and productivity goals can be achieved.

Before initiating system start-up procedures, membrane pretreatment, loading of the membrane elements, instrument calibration and other system checks should be completed.

Please refer to the application information literature entitled "Start-Up Sequence" (Form No. 609-02077) for more information.

**Operation Guidelines**

Avoid any abrupt pressure or cross-flow variations on the spiral elements during start-up, shutdown, cleaning or other sequences to prevent possible membrane damage. During start-up, a gradual change from a standstill to operating state is recommended as follows:

- Feed pressure should be increased gradually over a 30-60 second time frame.
- Cross-flow velocity at set operating point should be achieved gradually over 15-20 seconds.
- Permeate obtained from first hour of operation should be discarded.

**General Information**

- Keep elements moist at all times after initial wetting.
- If operating limits and guidelines given in this bulletin are not strictly followed, the limited warranty will be null and void.
- To prevent biological growth during prolonged system shutdowns, it is recommended that membrane elements be immersed in a preservative solution.
- The customer is fully responsible for the effects of incompatible chemicals and lubricants on elements.
- Maximum pressure drop across an entire pressure vessel (housing) is 50 psi (3.4 bar).
- Avoid static permeate-side backpressure at all times.

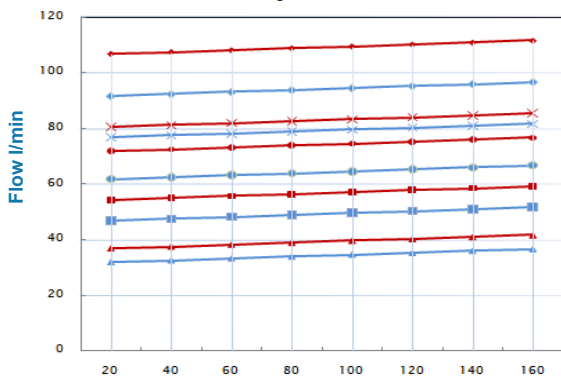
Notice: The use of this product in and of itself does not necessarily guarantee the removal of cysts and pathogens from water. Effective cyst and pathogen reduction is dependent on the complete system design and on the operation and maintenance of the system.

Notice: No freedom from any patent owned by Seller or others is to be inferred. Because use conditions and applicable laws may differ from one location to another and may change with time, Customer is responsible for determining whether products and the information in this document are appropriate for Customer's use and for ensuring that Customer's workplace and disposal practices are in compliance with applicable laws and other governmental enactments. Seller assumes no obligation or liability for the information in this document. NO WARRANTIES ARE GIVEN; ALL IMPLIED WARRANTIES OF MERCHANTABILITY OR FITNESS FOR A PARTICULAR PURPOSE ARE EXPRESSLY EXCLUDED.

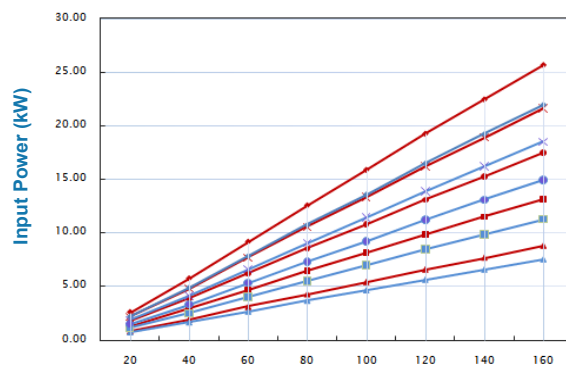




Input Flow



Output Power kW

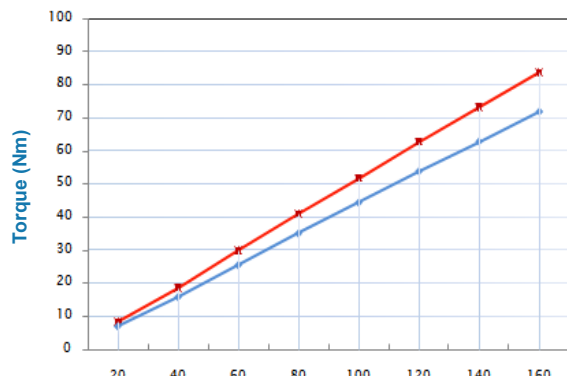


Pressure (bar)

Pressure (bar)

—▲— 35cc 1000rpm   
 —■— 35cc 1500rpm   
 —●— 35cc 2000rpm   
 —×— 35cc 2500rpm   
 —◆— 35cc 3000rpm  
—▲— 30cc 1000rpm   
 —■— 30cc 1500rpm   
 —●— 30cc 2000rpm   
 —×— 30cc 2500rpm   
 —◆— 30cc 3000rpm

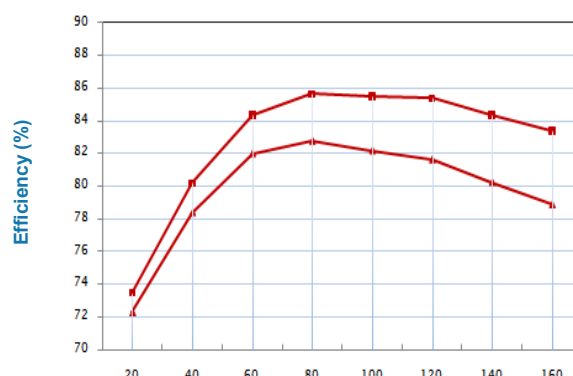
Output Torque



Pressure (bar)

—■— 35cc 1500rpm   
 —◆— 30cc 1500rpm

Overall Efficiency



Pressure (bar)

—▲— 35cc 1000rpm   
 —■— 35cc 1500rpm

Omschrijving	Specificatie
<b>Algemene informatie:</b>	
Productnaam::	CRN 3-11 A-FGJ-G-E-HQQE
Artikelnummer::	96516835
EAN nummer::	5700396750675
<b>Technisch:</b>	
Toerental voor pomgegevens:	2853 omw/min
Nominale flow:	3 m³/u
Rated head:	52.7 m
Stages:	11
Impellers:	11
Low NPSH:	N
Pump orientation:	Vertical
Shaft seal arrangement:	Single
Code for shaft seal:	HQQE
Approvals on nameplate:	CE, EAC, ACS
Curve tolerance:	ISO9906:2012 3B
Pump version:	A
Model:	A
<b>Materialen:</b>	
Base:	Stainless steel
	EN 1.4408
	AISI 316
Waaier:	Stainless steel
Impeller:	EN 1.4401
Waaier:	AISI 316
Material code:	G
Code for rubber:	E
Bearing:	SIC
<b>Installatie:</b>	
Maximum omgevingstemperatuur:	60 °C
Maximale bedrijfsdruk:	25 bar
Max. druk bij toegestane temp:	25 bar / 120 °C
	25 bar / -20 °C
Type of connection:	DIN / ANSI / JIS
Connect code:	FGJ
Size of inlet connection:	DN 25/32
Afmeting van de zuigaansluiting:	1 1/4 inch
Size of outlet connection:	DN 25/32
Afmeting van de persaansluiting:	1 1/4 inch
Pressure rating for pipe connection:	PN 25
Flange rating inlet:	300 lb
Flange size for motor:	FT100
<b>Vloeistof:</b>	
Te verpompen medium:	Water
Bereik vloeistoftemperatuur:	-20 .. 120 °C
Liquid temperature during operation:	20 °C
Dichtheid:	998.2 kg/m³
<b>Elektrische gegevens:</b>	
Motor standard:	IEC
Motortype:	80C
IE efficiëntieklasse:	IE3
Nominaal vermogen - P2:	1.1 kW
Vermogen (P2) benodigd voor pomp:	1.1 kW
Netfrequentie:	50 Hz
Nominale spanning:	3 x 220-240D/380-415Y V
Nominaalstroom:	4.35/2.50 A
Startstroom:	450-500 %
Cos phi - power factor:	0.83-0.76
Nominaal toerental:	2840-2870 omw/min
Efficiëntie:	IE3 82.7%
Motorrendement bij nominale belasting:	82.7 %

Grundfos Product Center [2018.02.043]

Omschrijving	Specificatie
Motor efficiëntie bij 3/4 vermogen:	84.6 %
Motor efficiëntie bij half vermogen:	85.4 %
Pooltal:	2
Dichtheidsklasse (IEC 34-5):	55 Dust/Jetting
Insolatie klasse (IEC 85):	F
Motorbeveiliging:	GEEN
Motor Nr.:	85U05105
Regeling:	
Frequency converter:	NONE
Overige:	
Minimum efficiency index, MEI $\geq$ :	0.7
Net weight:	29 kg
Gross weight:	31.8 kg
Shipping volume:	0.074 m <sup>3</sup>

Grundfos Product Center [2018.02.043]

# NGX 60 Hz



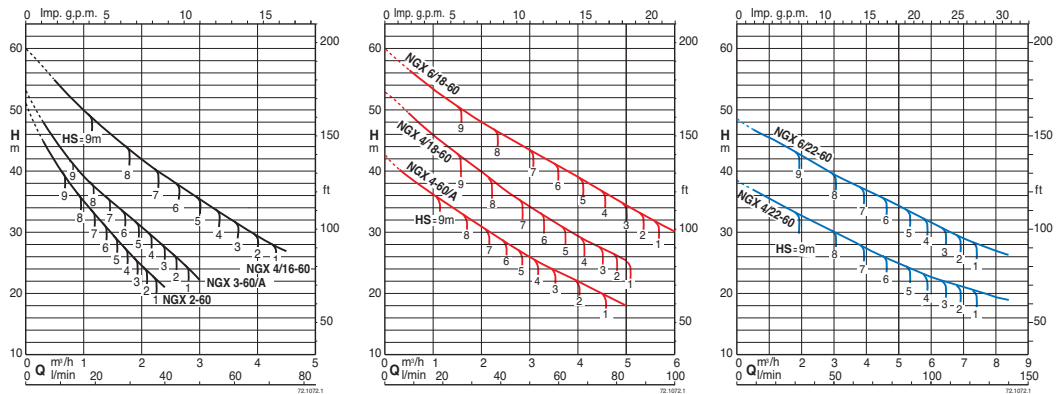
## Performance - Prestaciones

n ≈ 3450 rpm

3~	1~	P1 kW	P2		Q m³/h l/min	H																				
			kW	HP		0	0,3	1	2	2,4	3	4	4,5	5	5,5	6	6,5	7	8	8,4						
NGX 2-60	NGXM 2-60	0,8	0,45	0,6	0	5	16,6	33,3	40	50	66,6	75	83,3	91,6	100	108	116	133	140							
NGX 3-60/A	NGXM 3-60/A	0,95	0,55	0,75	51	45	35	24,5	21	53	48	39,5	31	28	22	42,5	40	36	31	29	26	22	20	18		
NGX 4-60/A	NGXM 4-60/A	1,1	0,75	1	60	57	50	42	39,3	35,5	29,5	27	60	57	50	42	39,3	35,5	29,5	27						
NGX 4/16-60	NGXM 4/16-60	1,6	1,1	1,5	53	51	46	40	37,5	34,3	29,5	27,5	25,5	53	51	46	40	37,5	34,3	29,5	27,5	25,5				
NGX 4/18-60	NGXM 4/18-60	1,6	1,1	1,5	38,5	37,5	35,5	32,5	31,5	30	27,5	26	24,5	23,5	22,5	21,8	21	19,7	19							
NGX 4/22-60	NGXM 4/22-60	1,6	1,1	1,5	59,5	56,5	53,5	48	46	43,5	39	36,7	34,5	32,5	30,3	59,5	56,5	53,5	48	46	43,5	39	36,7	34,5	32,5	30,3
NGX 6/18-60	NGXM 6/18-60	2,1	1,5	2	48,5	47,2	46	43	42	40,3	37,5	36	34,5	33	32	30	29	27	26,3							
NGX 6/22-60	NGXM 6/22-60	2,1	1,5	2																						

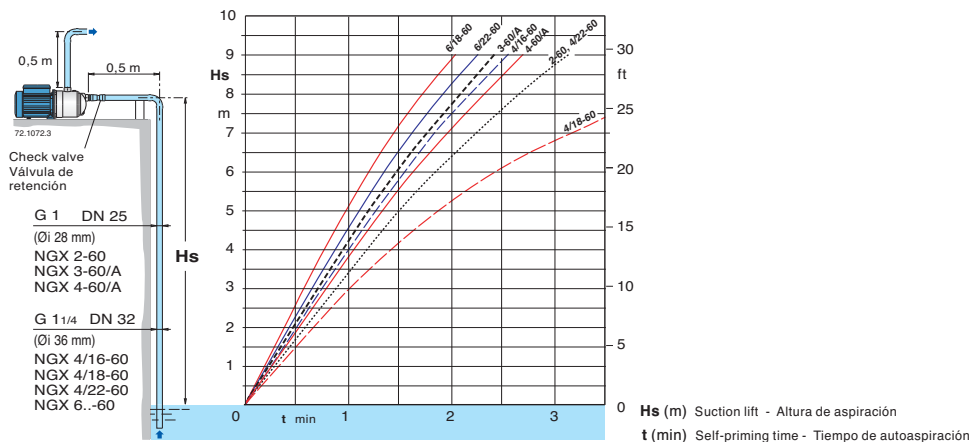
P2 Rated motor power output. H Total head in m. Tolerances according to UNI EN ISO 9906:2012.  
 Potencia nominal del motor. Altura total en m. Tolerancias según UNI EN ISO 9906:2012.

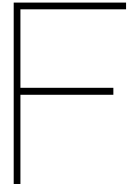
### Characteristic Curves for different suction lifts Hs - Curvas Características con distintas alturas de aspiración Hs



### Self-priming capability - Capacidad de autoaspiración

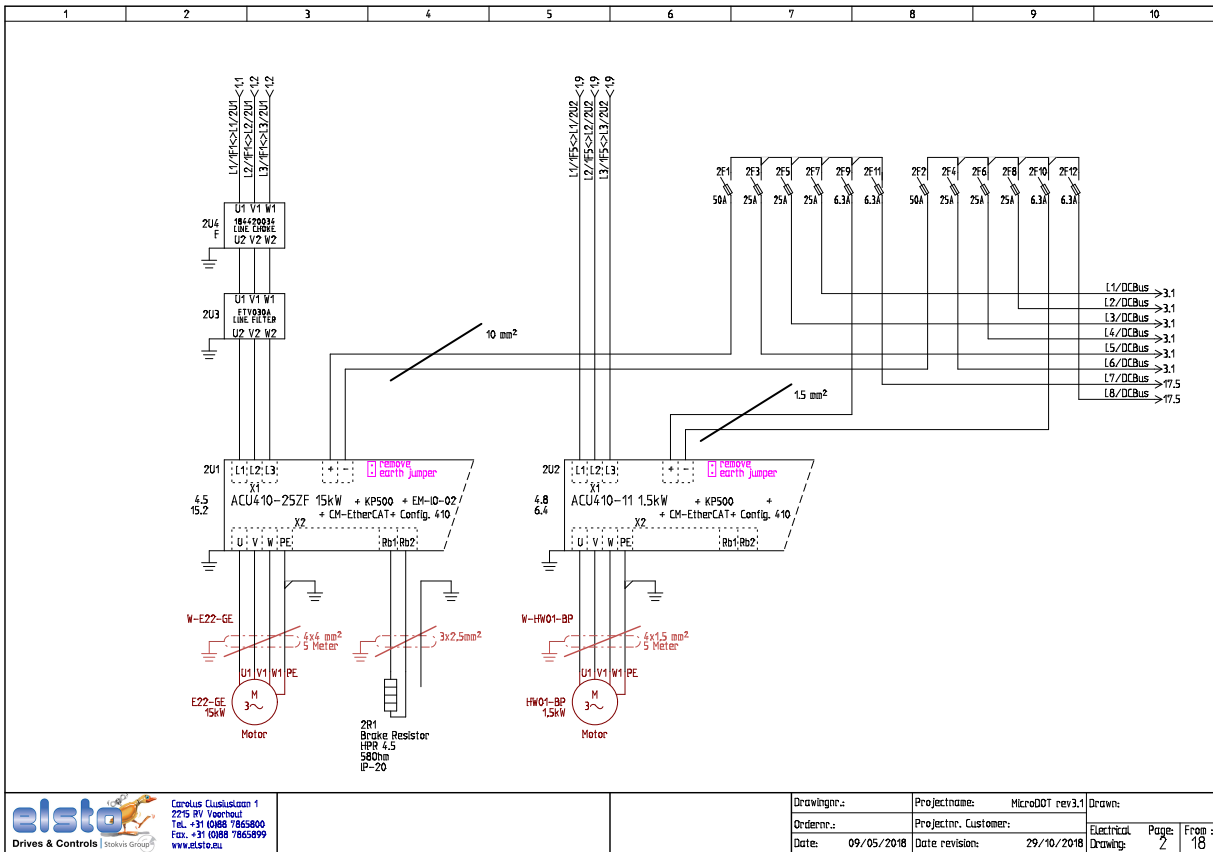
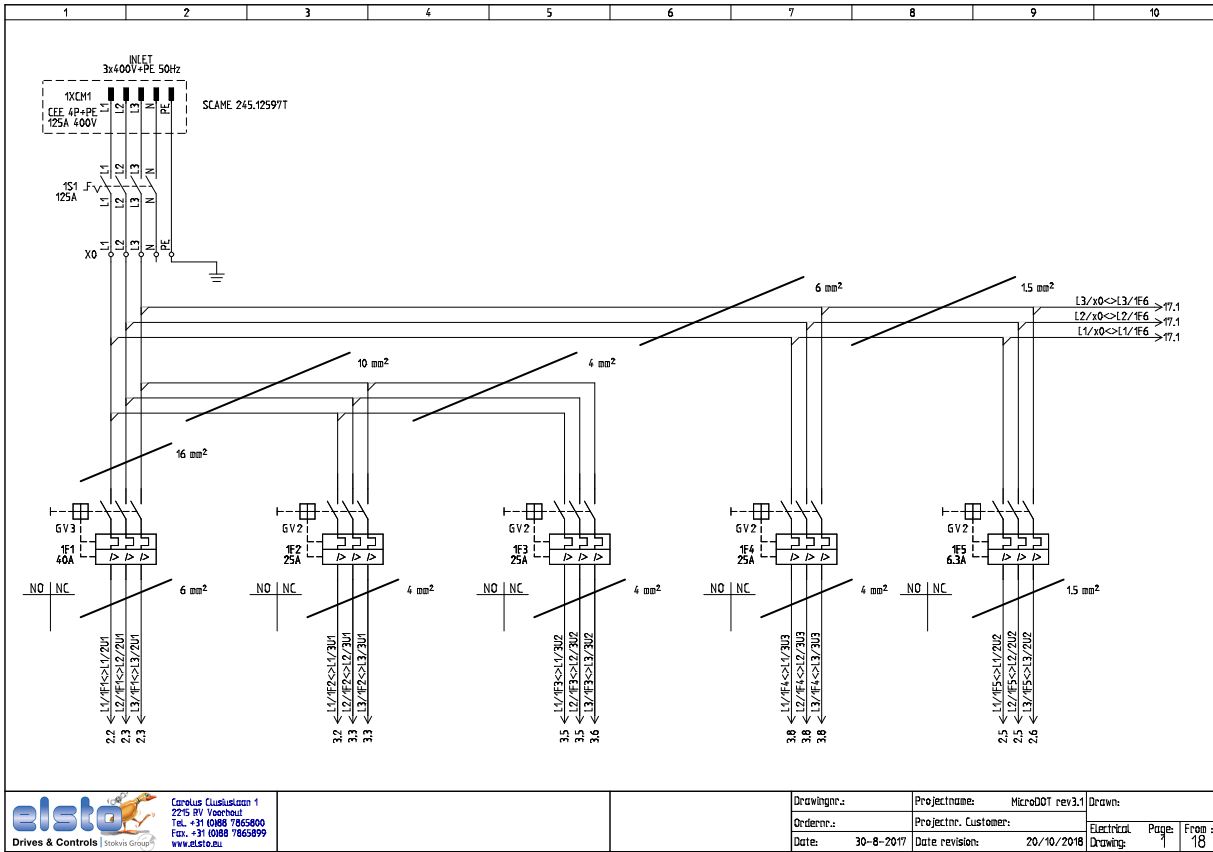
60 Hz (n ≈ 3450 1/min), H<sub>2</sub>O, T = 20°C, Pa = 1000 hPa (mbar)

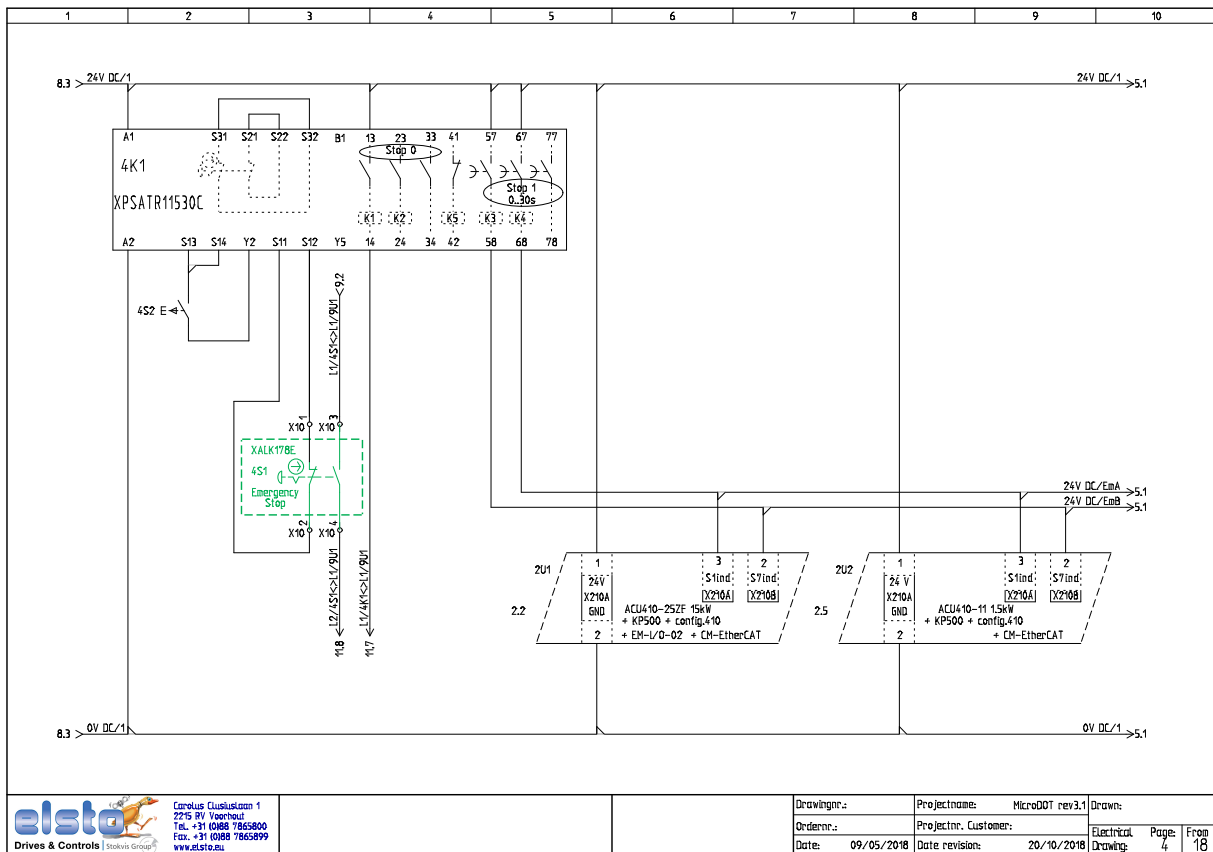
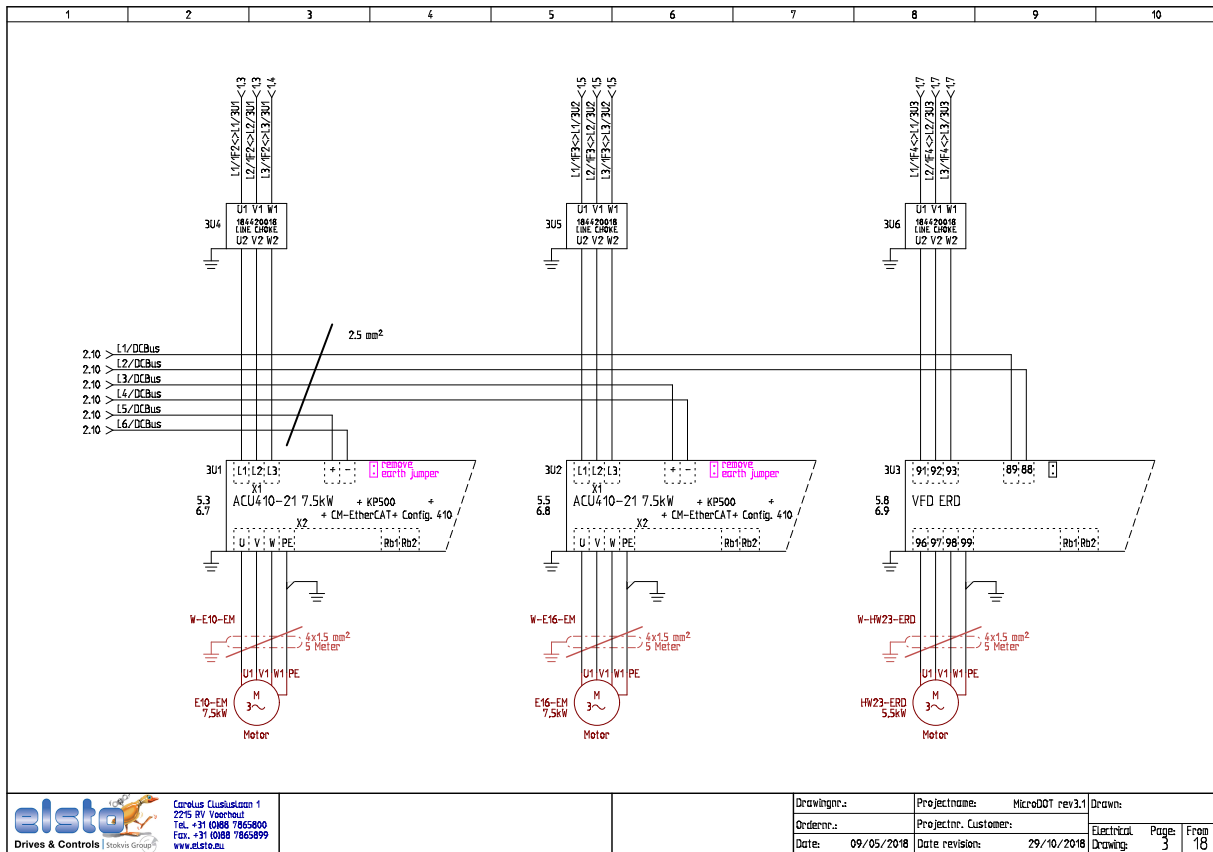


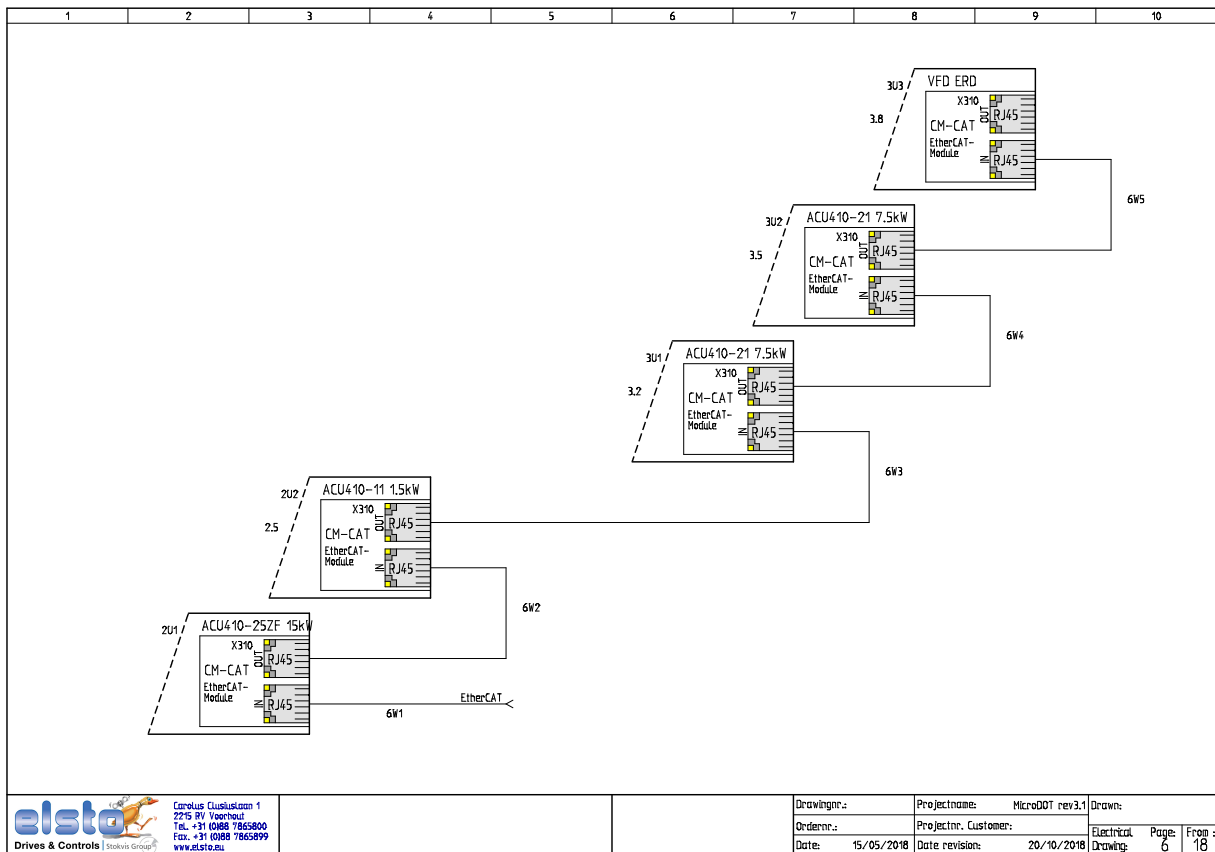
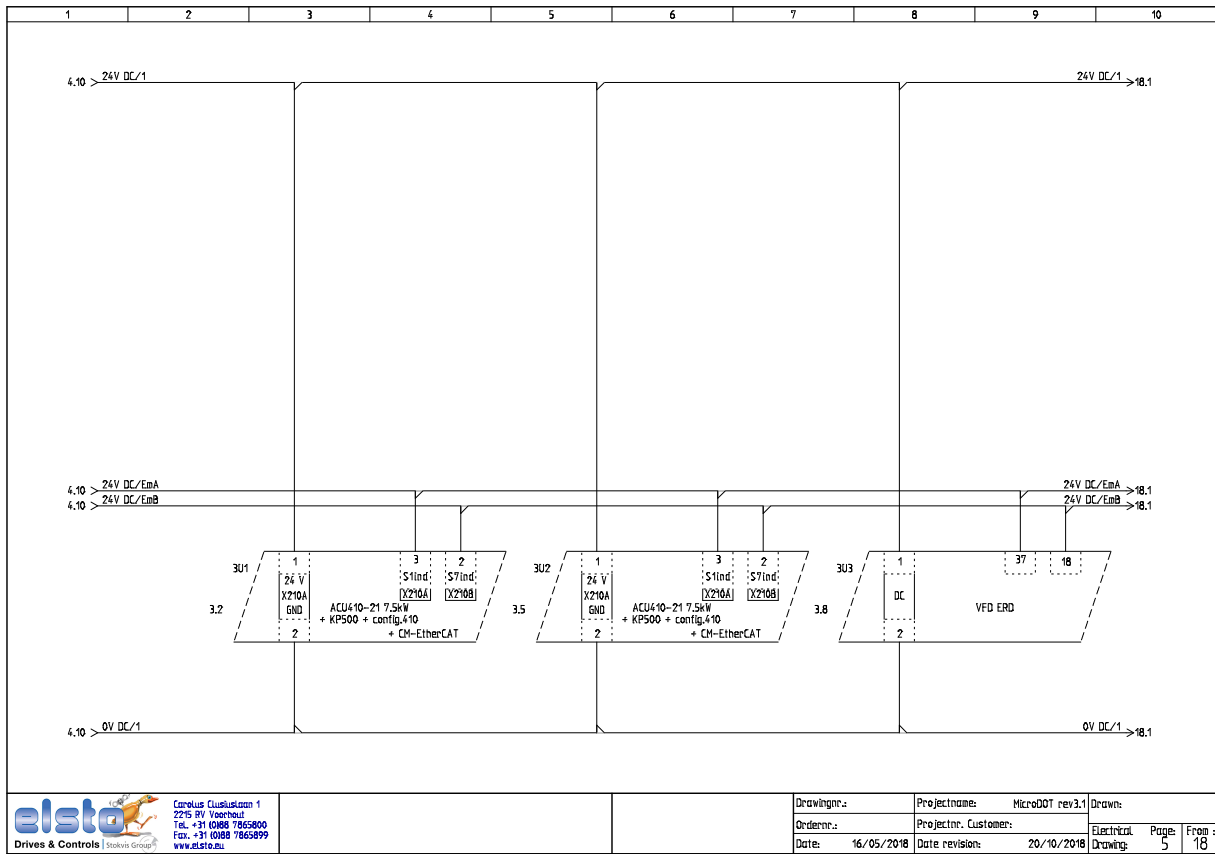


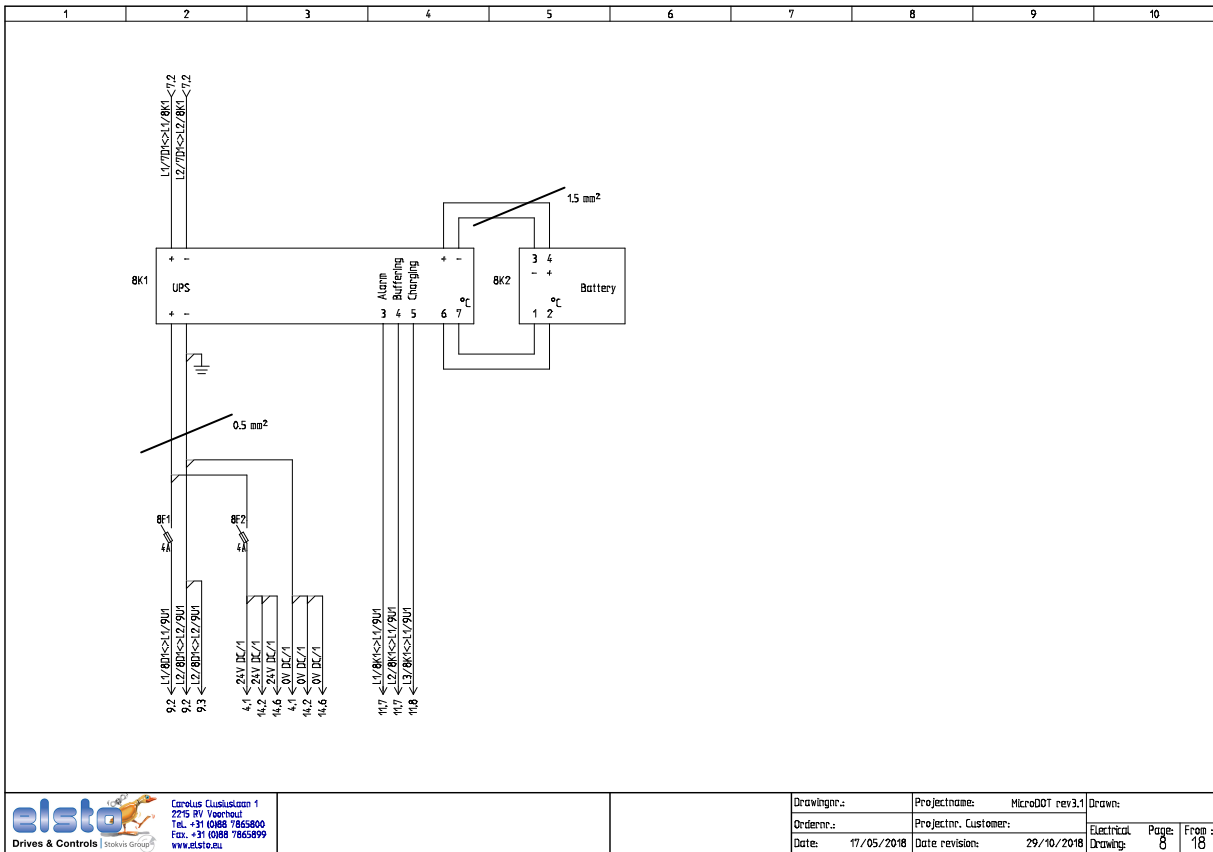
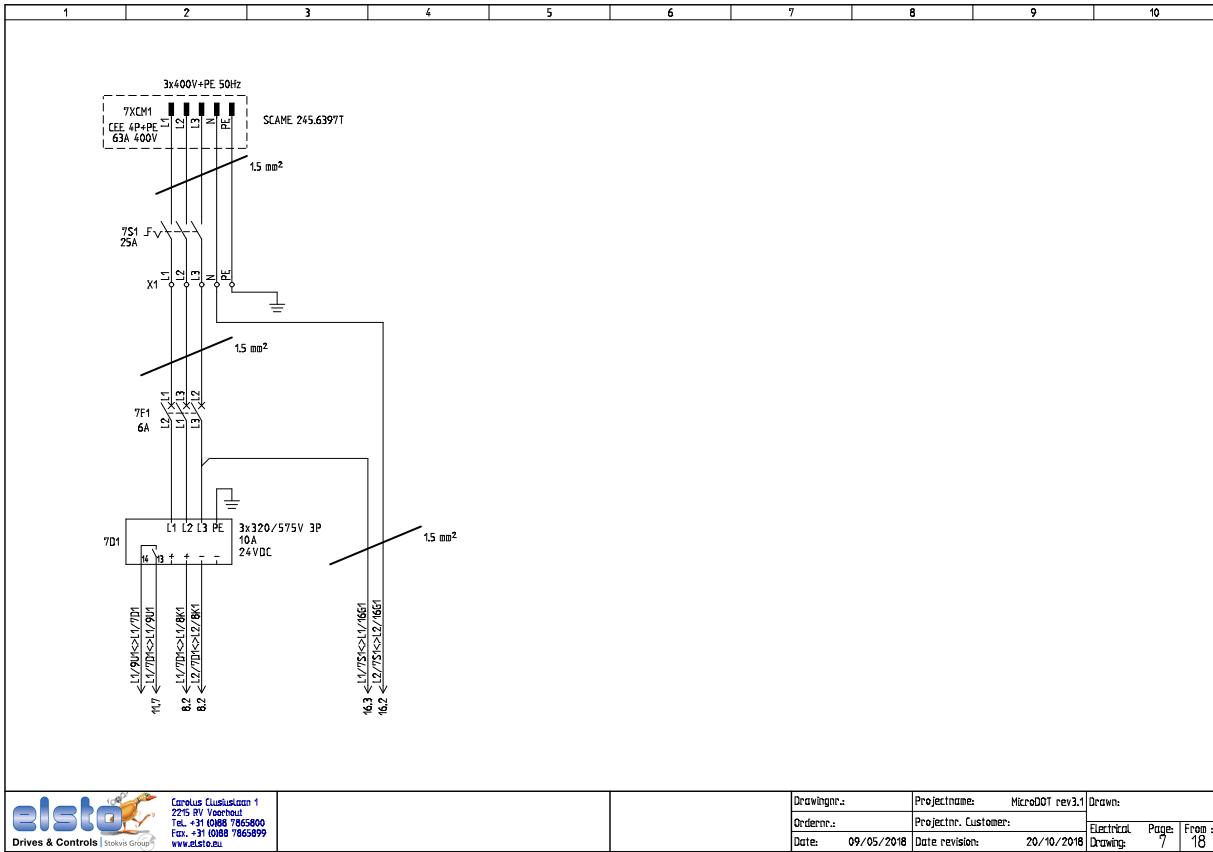
# Electrical Wiring Diagram

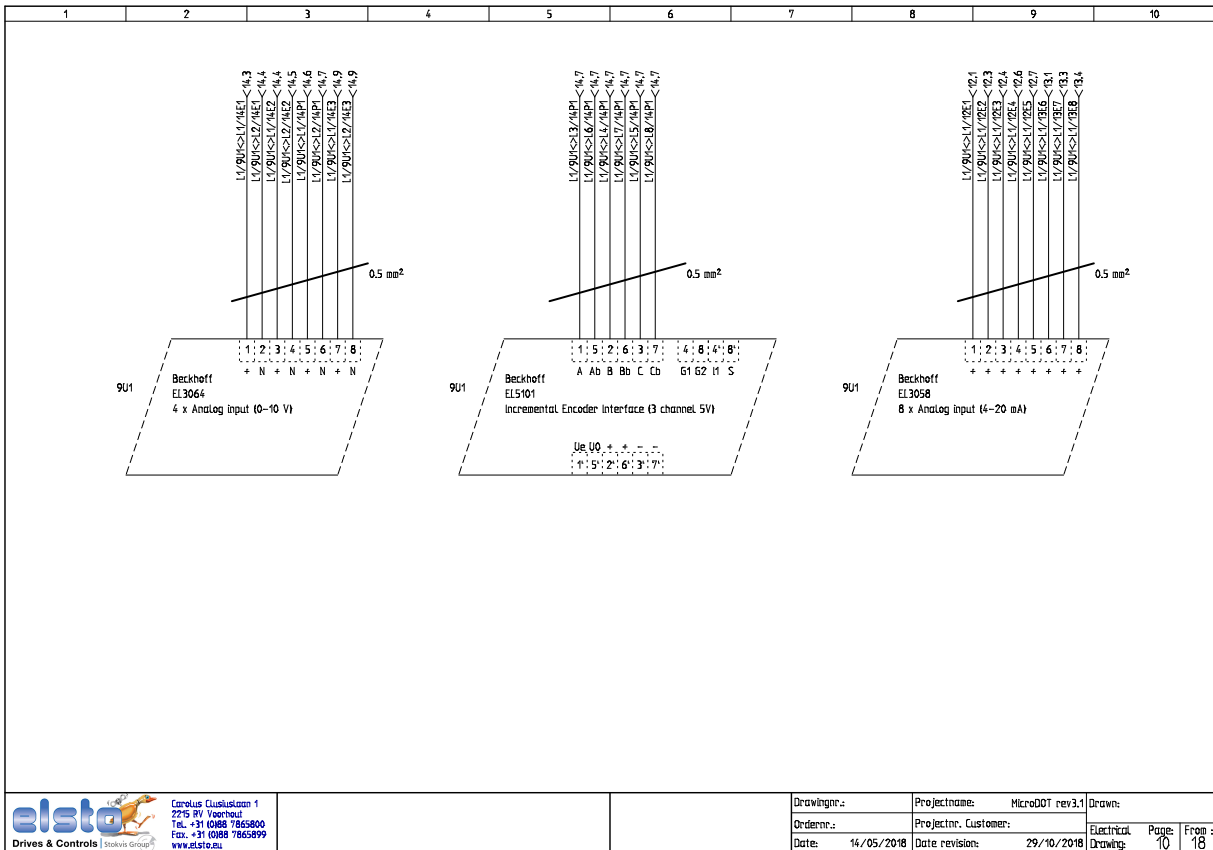
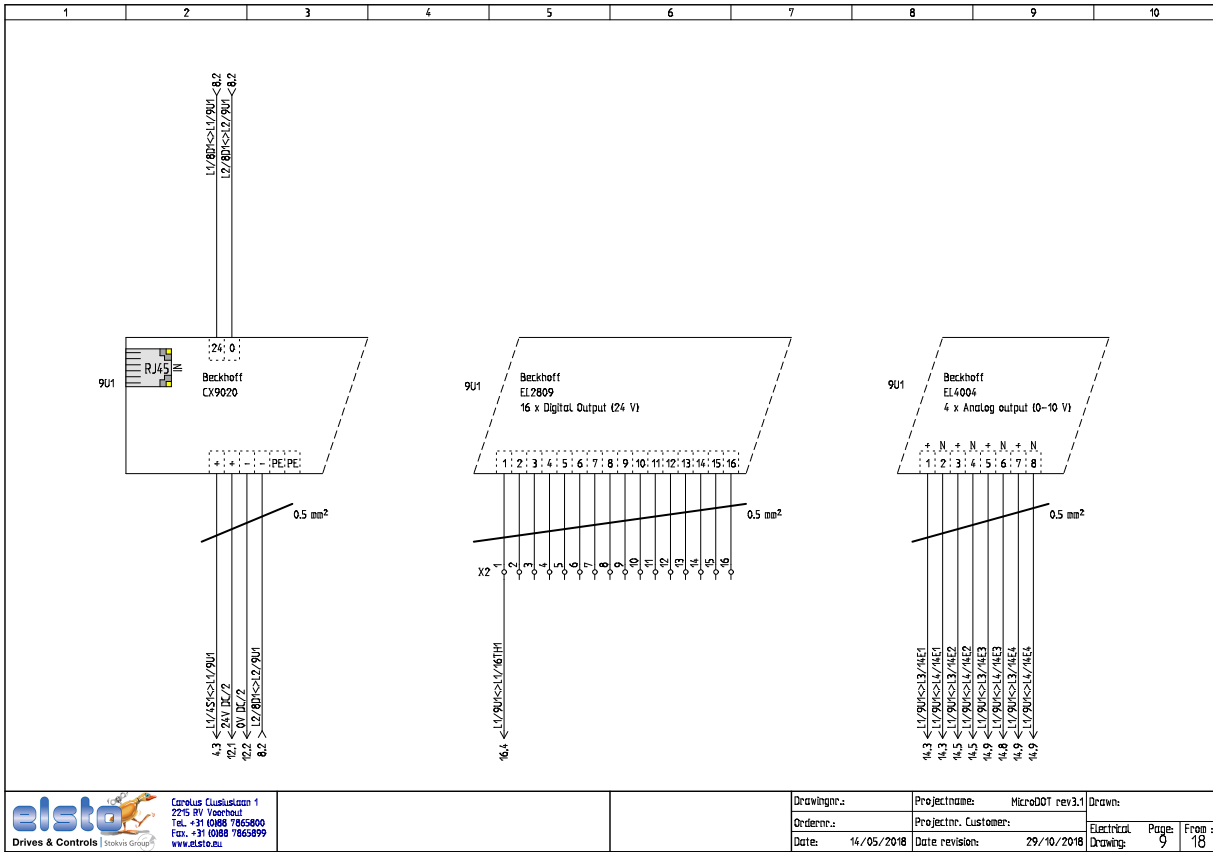
This appendix shows the electrical wiring diagram of the electrical control cabinet, designed to be able to control and power the MicRODOT experimental setup.

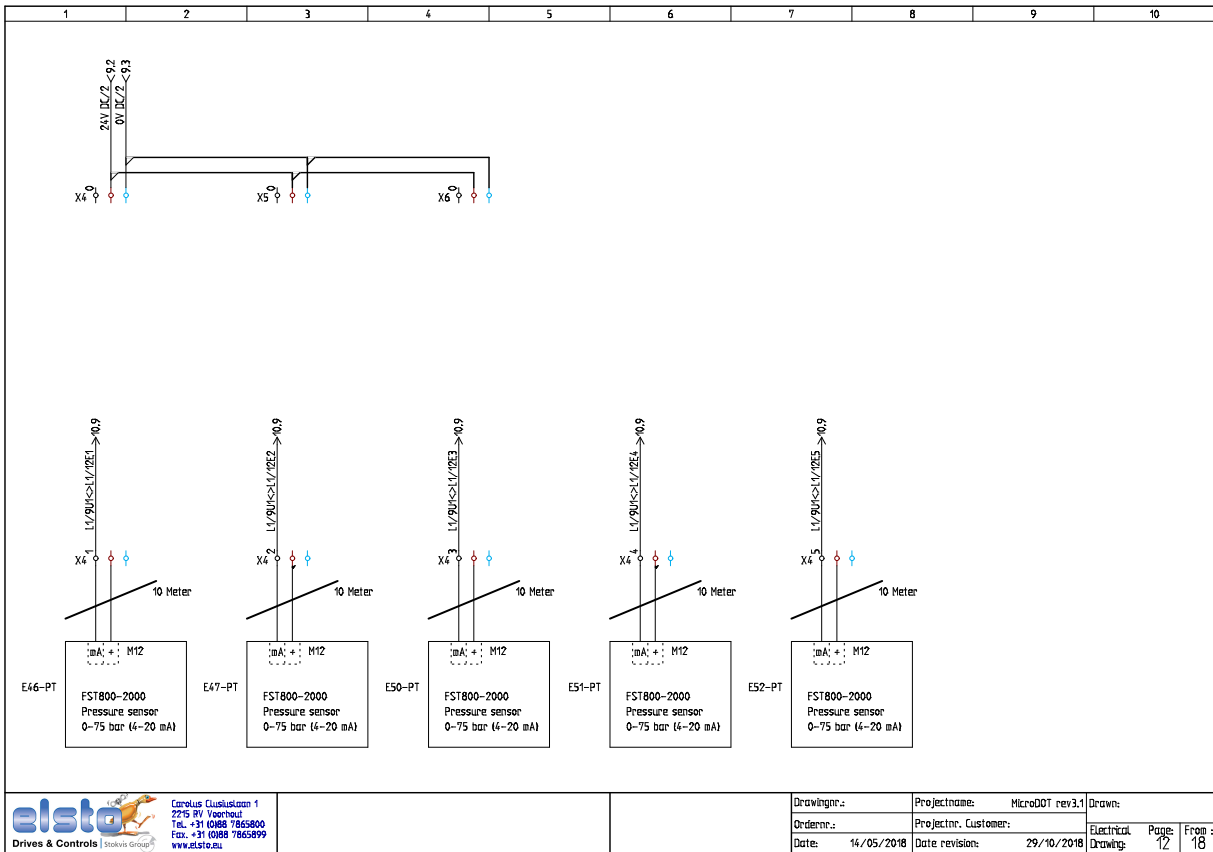
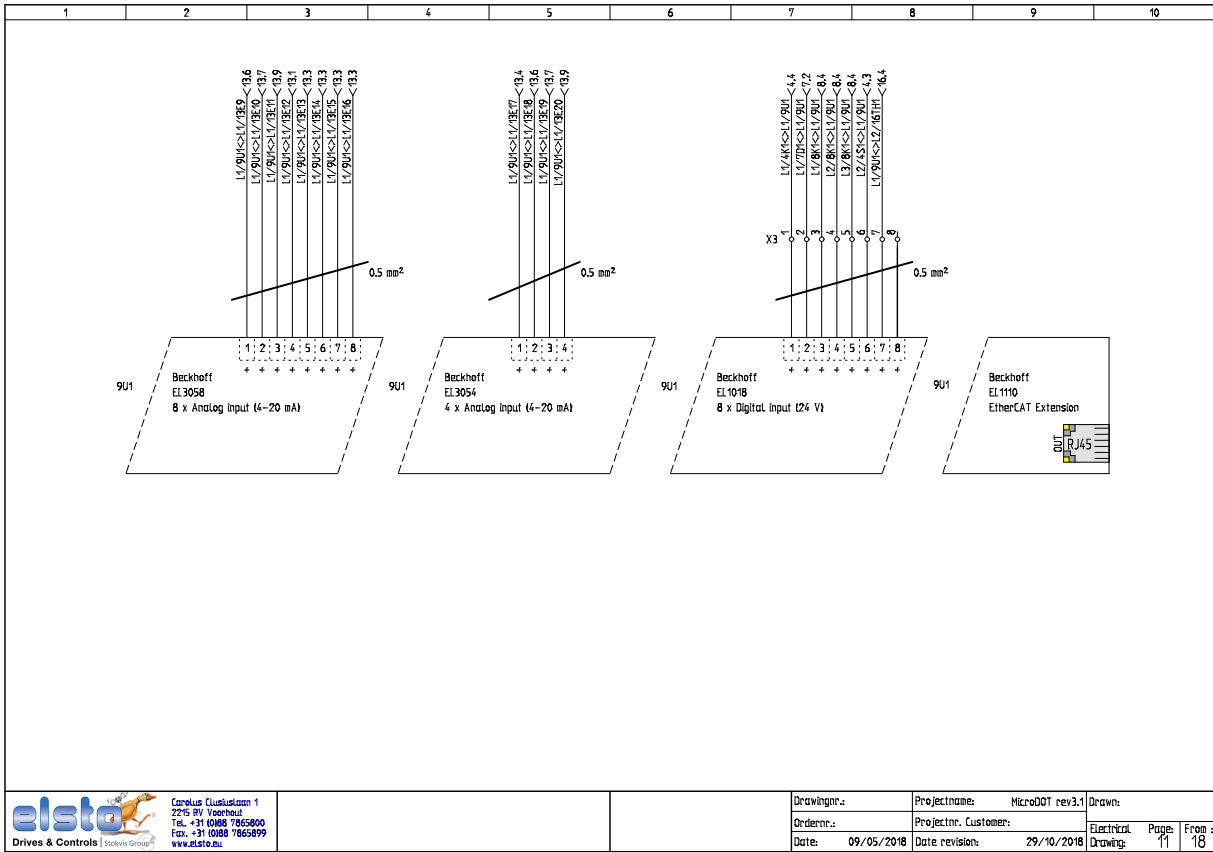


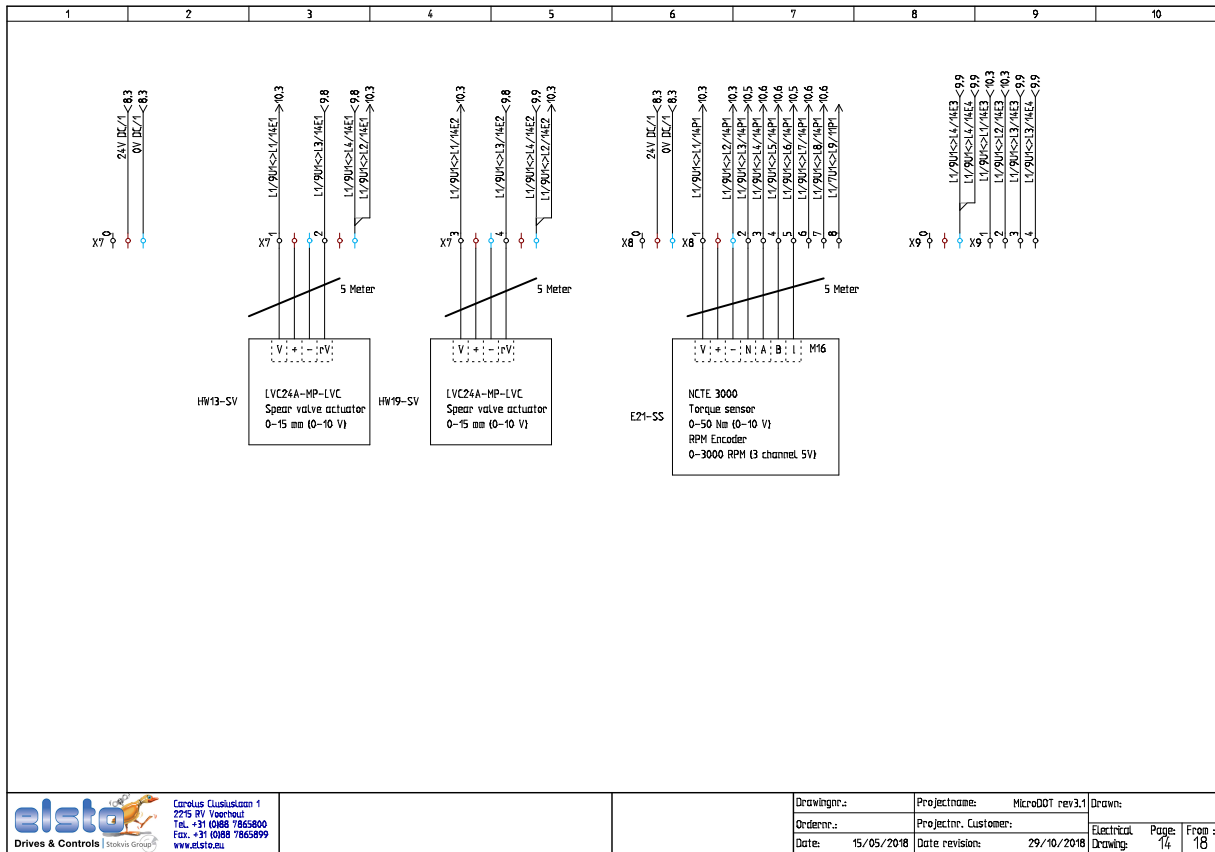
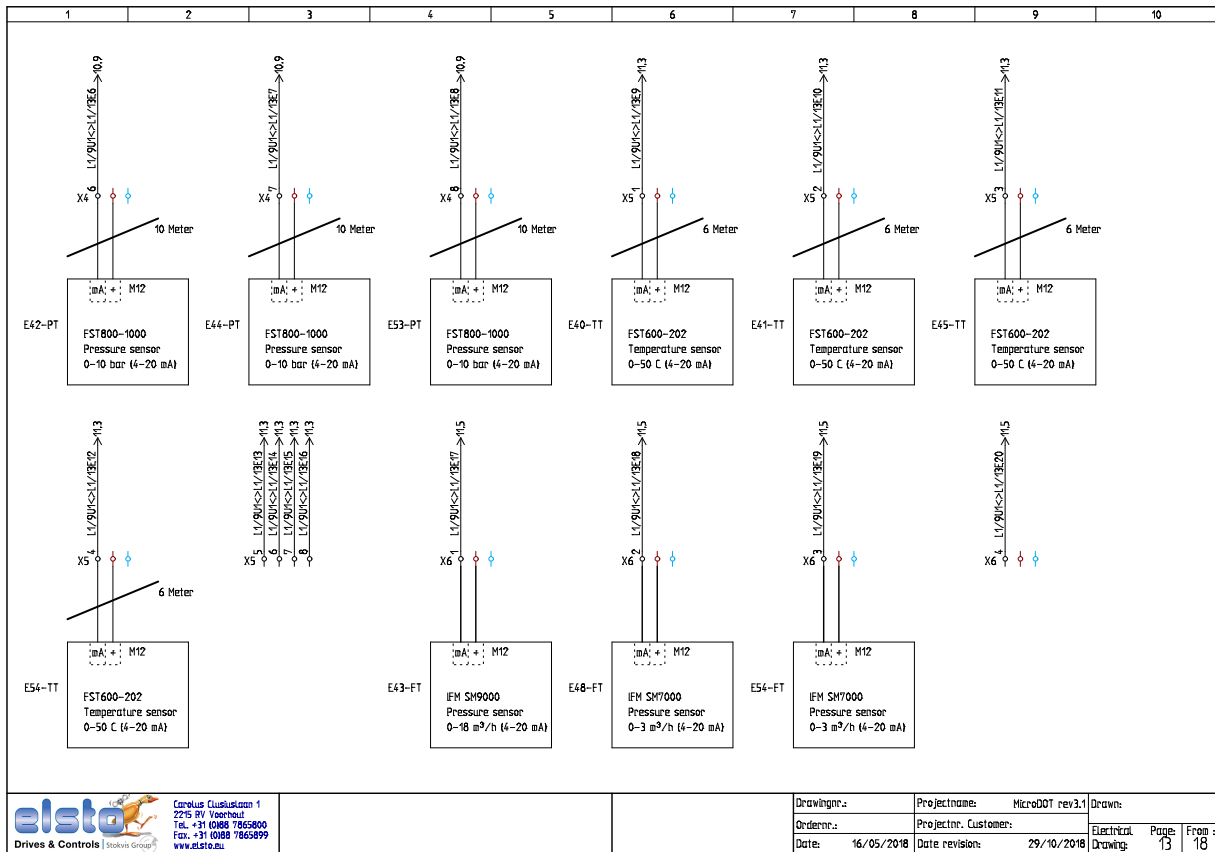


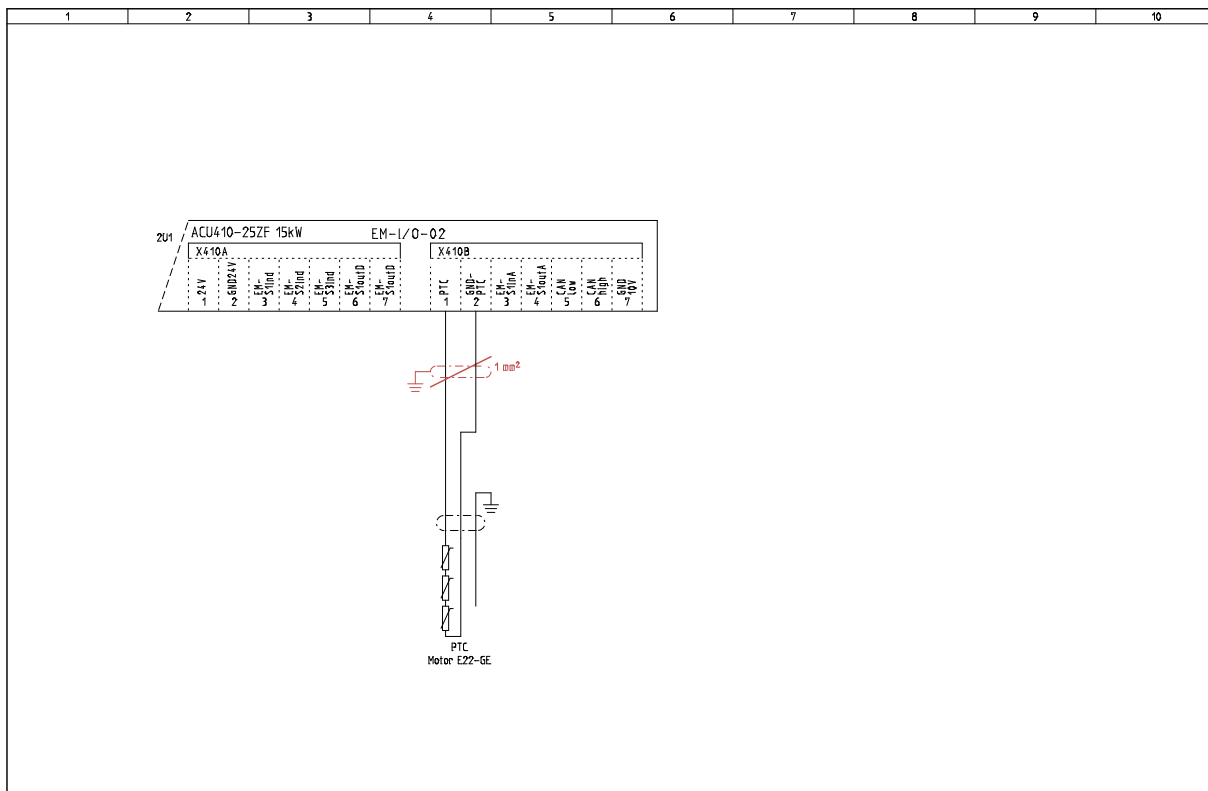




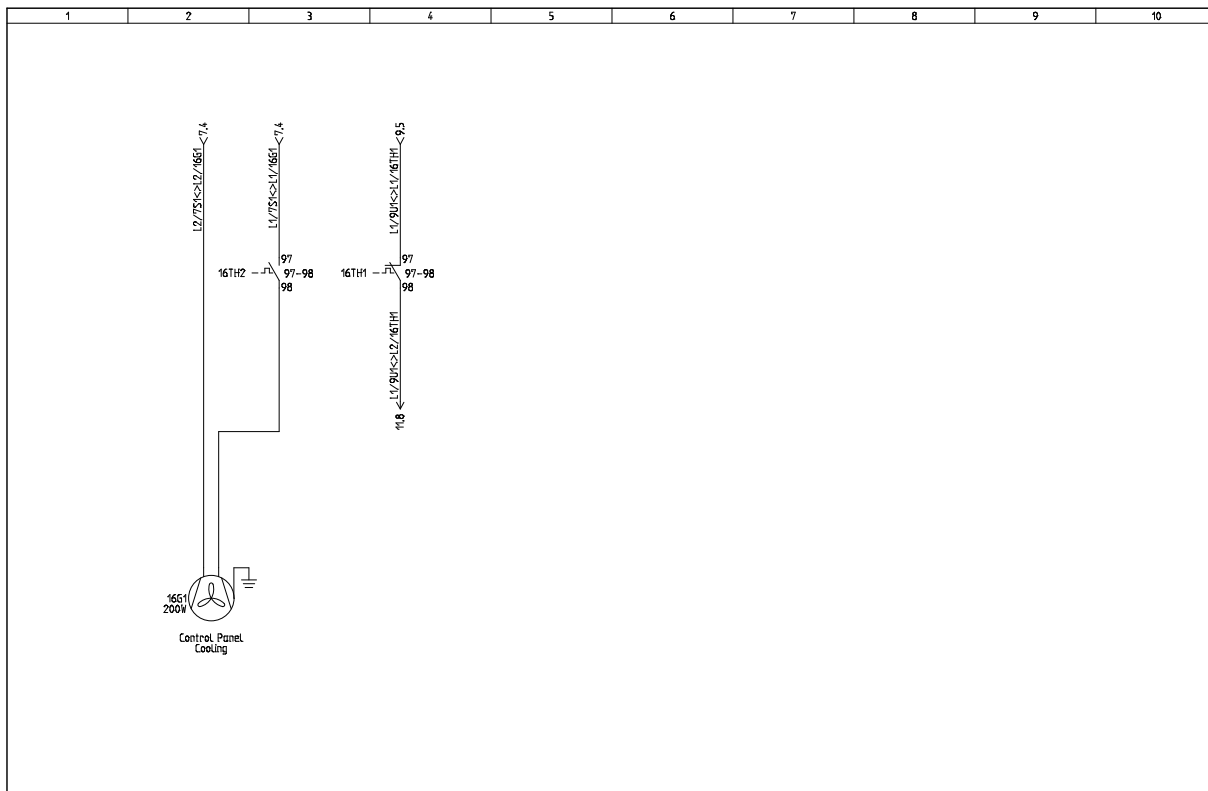








 Corneus Cuijckeman 1 2215 RV Veenhout Tel. +31 (0)88 7865800 Fax. +31 (0)88 7865899 www.elsta.eu		Drawing:	Projectname: MicroDOT rev3.1	Drawn:
		Ordernr.:	Projectnr. Customer:	Electrical Page:
	Date: 25/05/2018	Date revision: 29/10/2018	Drawing:	From: 15   18



 Corneus Cuijckeman 1 2215 RV Veenhout Tel. +31 (0)88 7865800 Fax. +31 (0)88 7865899 www.elsta.eu		Drawing:	Projectname: MicroDOT rev3.1	Drawn:
		Ordernr.:	Projectnr. Customer:	Electrical Page:
	Date: 06/06/2018	Date revision: 29/10/2018	Drawing:	From: 16   18

